A UNIFIED METHOD FOR THE ANALYSIS OF NONLINEAR VISCOELASTICITY AND FATIGUE CRACKING OF ASPHALT MIXTURES USING THE DYNAMIC MECHANICAL ANALYZER

A Dissertation

by

VERONICA TEIXEIRA FRANCO CASTELO BRANCO

Submitted to the Office of Graduate Studies of
Texas A&M University
in partial fulfillment of the requirements for the degree of

DOCTOR OF PHILOSOPHY

December 2008

Major Subject: Civil Engineering

A UNIFIED METHOD FOR THE ANALYSIS OF NONLINEAR VISCOELASTICITY AND FATIGUE CRACKING OF ASPHALT MIXTURES USING THE DYNAMIC MECHANICAL ANALYZER

A Dissertation

by

VERONICA TEIXEIRA FRANCO CASTELO BRANCO

Submitted to the Office of Graduate Studies of
Texas A&M University
in partial fulfillment of the requirements for the degree of

DOCTOR OF PHILOSOPHY

Approved by:

Chair of Committee,	Dallas N. Little
Committee Members,	Eyad Masad
	Robert L. Lytton
	Charles J. Glover
	Amit Bhasin
Head of Department,	David Rosowsky

December 2008

Major Subject: Civil Engineering

ABSTRACT

A Unified Method for the Analysis of Nonlinear Viscoelasticity and Fatigue Cracking of Asphalt Mixtures Using the Dynamic Mechanical Analyzer. (December 2008)
Veronica Teixeira Franco Castelo Branco, B.S., Federal University of Ceará, Brazil;
M.S., Federal University of Rio de Janeiro, Brazil
Chair of Advisory Committee: Dr. Dallas N. Little

Fatigue cracking is one of the primary modes of distress in asphalt pavements that has an important economic impact. Fatigue resistance characterization of an asphalt mixture is a complex issue due to: (i) composite nature of the material, (ii) gradation of aggregate particles, (iii) variation of asphalt film thickness, (iv) air voids distributions, (v) asphalt binder nonlinear viscoelastic behavior, (vi) effects of binder oxidative aging as a function of time, and (vii) micro crack healing during rest periods. Different methods to assess fatigue cracking in asphalt materials are available in the literature. However, there is no methodology to characterize fatigue cracking behavior of asphalt materials that is independent of the mode of loading (controlled-strain or controlled-stress). The objective of this research is to develop a new methodology to characterize fatigue cracking of the fine aggregate matrix (FAM) portion of asphalt mixtures using dynamic mechanical analyses (DMA). This is accomplished through different, but related, approaches. The first approach relies on identifying the various mechanisms of energy dissipation during fatigue cracking that are manifested in: (i) nonlinear viscoelastic deformation, (ii) fracture, and (iii) permanent deformation. Energy indices were derived to quantify each of these energy dissipation mechanisms and to quantify fatigue cracking irrespective of the mode of loading. The first outcome of the approach is a fatigue damage parameter (crack growth index) that provides comparable results for a given material even when tested under different modes of loading and different load (strain or stress) amplitudes.

The developed fatigue characterization method has a lower coefficient of variation when compared to conventional parameters (number of load cycles to failure or cumulative dissipated energy). The crack growth index parameter was also qualitatively and quantitatively compared to three dissipated energy methods available in the literature. The second outcome of this research is a constitutive model that can describe both asphalt mixtures' nonlinear viscoelastic response and fatigue damage in one formulation. Nonlinear viscoelastic as well as damage parameters were obtained for both modes of loading. This second approach has the advantage that the constitutive model can be implemented in a numerical framework to describe the response of asphalt mixtures under various boundary conditions.

DEDICATION

To the memory of my dad…The man who taught me that the only thing no one can take away from me is what I have learned…

ACKNOWLEDGEMENTS

When I came from Brazil, four years ago, to start in this Ph.D. program I had absolutely no idea how it would be…of course not… So many things happened during this time, in both my professional and personal lives, that I am afraid I will not be able to describe them with words. During these four years I was not worried about being better than anybody else, I was worried about being better than the person I was on August, 2004. Thinking about that, besides my weaknesses, my defects, and the things that I could have done better, I believe I achieved my objective.

I received a challenging research project to work with, much more challenging than what I expected it could be. It is interesting to note, now almost at the end, how this research was developed. So many things happened during this path, that now I understand why sometimes the trip itself could be more interesting than the final destination. I can not finish this dissertation without saying so many thanks. Although it is very dangerous to say names….I will take the risk because every single person involved in this process well deserves it.

Before starting, I would like to thank God for everything, even for the ones that I did not understand correctly during these four years. I am pretty sure that He looked for me and held my hands very strong every time that I needed, and the ones that I did not need also. I am sure He celebrated with me.

My sincere appreciation to my committee chair, Dr. Dallas N. Little, not only for giving me the support during this period, but also for trusting that I was able to conduct this project and giving me this excellent opportunity to learn. A special thanks to Dr. Eyad Masad for everything: for being much more than a professor, for sharing his knowledge, friendship and time with me, for being part of this research, celebrating and criticizing every time that I needed just to contribute to my development as an engineer and as a person. My gratitude! My appreciation also goes to Dr. Robert L. Lytton, Dr. Charles Glover, and Dr. Amit Bhasin for serving as committee members. I consider

myself fortunate to have you involved in this work. Thanks for the technical contributions and also for the permanent encouragement and motivation.

My gratitude is also extended to my family and friends in Brazil and in the U.S., in special to my parents, Mr. Francisco F. Cavalcante and Mrs. Aurilêda T.F. Cavalcante. Without their love, prayers, and encouragement I would not have been able to make this dream come true. My deepest gratitude goes to my husband, Cristiano R. Castelo Branco, and our son, Caio T.F. Castelo Branco. Without Cris' support during these four years I would never have been able to accomplish this objective. His love and patience were absolutely crucial and inspired me during this path. Both, Cris and Caio, were always my source of energy and the reason why I kept going and smiling.

I really appreciate the support of my colleagues: Allex Alvarez, Enad Mahmoud, Kamilla Vascocelos, and Syam Nair with whom I have shared personal and academic conversations. They made my time at Texas A&M much more enjoyable. Special gratitude goes to Kamilla Vasconcelos for being such a great friend and for filling my life with her happiness. My gratitude is also extended to Mrs. Barbara Hein and Mrs. Cathy Bryan for the necessary administrative support and friendship during this time.

I also thank the Federal Highway Administration (FHWA), the Texas Transportation Institute (TTI), the Asphalt Research Consortium (ARC), and Capes/Fulbright (funds for post secondary education – Brazil) for providing the necessary financial support for this research project. Thanks also to the Statistic Help Desk at TTI for developing the statistic algorithm used in Chapter VI and to the task force group that worked on the Standard Method for Preparing Dynamic Mechanical Analyzer (DMA) Specimens and Conducting Tests (Appendix A), and to my colleagues: Jonathan Howson, Kamilla Vasconcelos, and Silvia Caro.

TABLE OF CONTENTS

CHAPTER Page

CHAPTER Page

CHAPTER Page

LIST OF FIGURES

FIGURE Page

FIGURE Page

FIGURE Page

FIGURE Page

LIST OF TABLES

TABLE Page

TABLE Page

CHAPTER I

INTRODUCTION

OVERVIEW

The annual expenditure for maintenance and traffic services of pavements in the United States (U.S.) is in the order of $38 billion (*1*). There are four main forms of distresses in asphalt pavements: (i) thermal cracking, (ii) permanent deformation, (iii) fatigue cracking, and (iv) moisture induced damage. Fatigue cracking (micro and macro cracking formation and failure) due to repeated loading has been a subject of research since 1858 (*2*). In the context of asphalt pavements, repeated loads due to traffic and cyclic environmental conditions are the primary causes of fatigue cracking in asphalt mixtures. Fatigue cracking behavior is an important consideration for the material and pavement design process (*3*). Fatigue characterization of hot mix asphalt (HMA) is a challenging problem due to the: (i) composite nature of the material, (ii) gradation of aggregate particles, (iii) variation of asphalt film thickness within the mastic, (iv) distribution of air void sizes, (v) dependence of asphalt binder behavior on time and temperature, (vi) effects of binder oxidative aging as a function of time, and (vii) ability of the micro cracks in the bitumen or mastic to heal (close) during rest periods (*4, 5*).

There are numerous laboratory test methods to characterize fatigue cracking in HMA. Fatigue life measured in the laboratory is dependent on several factors including: (i) mode of loading (controlled-strain or controlled-stress), (ii) specimen geometry, (iii) loading configuration, (iv) loading frequency, and (v) mixture variables (*6*). Due to the influence of these factors, the results of the laboratory tests have led to the development of different definitions or criteria of failure (*7-9*), such as: (i) decrease in 50 percent or

---

This dissertation follows the style of the *Transportation Research Record.*

90 percent of the initial stiffness (for controlled-strain test), (ii) increase in 100 percent of the initial strain value (for controlled-stress test), (iii) achievement of an ultimate phase angle, (iv) attainment of a maximum value in the relationship between the actual dynamic modulus and the initial one, and (v) complete failure of the sample.

The current analysis of fatigue life depends on the type of test and data analysis method used. One of the current challenges in the characterization of fatigue resistance is that laboratory tests are conducted based on the anticipated strain or stress distribution in the pavement. Some researchers affirm that controlled-stress tests are more applicable to thick (greater than 150 mm) asphalt concrete layers, whereas controlled-strain tests are more applicable to thin (thinner than 50 mm) asphalt concrete layers. This rationale is based on field observations that for thick asphalt concrete layers the HMA is the main load-carrying component and loses stiffness during the load application process, while strain in thin asphalt concrete layers is controlled by the supporting layers and not by HMA stiffness (*3, 10*). However, the purpose of a laboratory test should be to determine fatigue cracking characteristics of the material for different stress states, while a structural model that incorporates these characteristics should account for the boundary conditions and pavement structure (*5*).

In general, there is a lack of consensus on the type of test, mode of loading, or method of analysis used to characterize fatigue cracking properties of asphalt materials. There are several approaches used to predict fatigue in HMA: (i) change in stiffness under repeated strain (or stress) application (*11*), (ii) dissipated energy (DE) approaches (*8, 12-14*), (iii) continuum mechanics approaches (*15*), and (iv) fracture mechanics approaches (*10, 16, 17*).

In an attempt to unify the results from different fatigue tests, a number of researchers utilized the concept of DE (area inside a stress-strain hysteresis loop) to formulate analytically based or empirical functions to evaluate the progress of damage and to determine the failure point (*5, 8, 12, 18-22*). There are several advantages in employing the DE based criterion to characterize fatigue cracking properties of asphalt materials because it can: (i) reconcile the differences in fatigue lives observed for the

same material subjected to different modes of loading, (ii) differentiate between viscoelastic energy dissipation and energy dissipation due to crack propagation or plastic damage, and (iii) reduce the high variability commonly associated with the number of cycles to failure from laboratory tests.

One of the challenges in the characterization of fatigue damage is separating the mixture response due to fatigue from the one due to nonlinear viscoelastic behavior. Bahia et al. (*23*), and Masad and Somadevan (*24*) reported the presence of high strain magnitudes within the asphalt binder in HMA when the mixture was subjected to a typical in-service stress state. Bahia et al. (*23*) reported that the localized strain in the binder film can be from 10 to 100 times the magnitude of the mixture bulk strain. The high strain amplitudes were attributed to the difference in the stiffness between asphalt binder and aggregate.

Schapery (*25*) developed a model for the nonlinear viscoelastic behavior that uses single integrals similar to the Boltzmann type in linear theory and characterizes the response of the material under a variety of stress states. Schapery's model presents some advantages because: (i) time-dependent creep or relaxation functions are obtained on the linear viscoelastic range, and (ii) different strain (or stress) amplitudes, environmental conditions, and modes of loading can be explored.

Masad et al. (*26*) used Schapery's approach and a dynamic shear rheometer (DSR) to analyze binder nonlinear viscoelastic response under different conditions (stress amplitude, temperature, frequency, and aging). They used a finite element subroutine to predict binder creep response. These authors concluded that binder long term performance can be predicted based on short term experiments under different stress amplitudes.

Fatigue damage characterization in HMA has been conducted using two scales: (i) the entire asphalt mixture (coarse and fine aggregates, filler – aggregate smaller than 75 μm, and asphalt binder), and (ii) fine aggregate matrix (FAM) (fine aggregate – aggregate smaller than 1.18 mm, filler and asphalt binder). Recent work at Texas A&M University proposed a fatigue testing that is conducted on FAM portion of the asphalt

mixture which has a relatively more uniform internal structure compared to the entire HMA. The FAM represents an important length scale that is intermediate between HMA and asphalt binder. The characterization of the fine portion was also motivated by the fact that this part of HMA influences crack formation and growth phenomena (*10*).

Kim et al. (*13*) used dynamic mechanical analyses (DMA) to characterize fatigue cracking and healing in FAM mixtures. These authors used Schapery's elastic-viscoelastic correspondence principle to transform viscoelastic state variables and boundary conditions to those in an equivalent elastic case. Instead of physical strain, they used pseudo strain variables (*27*). Controlled-strain tests were conducted at a frequency of 10 Hz and at 25ºC. The change in dynamic modulus, pseudo stiffness (slope of loops between physical stress and pseudo strain), and dissipated strain energy were monitored for tests performed at different strain amplitudes and the effect of rest periods was considered. Zollinger (*9*) used DMA tests to evaluate the susceptibility of asphalt mixtures to moisture damage. The ratio between the number of cycles to failure under wet and dry conditions was used as an indicator of the mixtures resistance to moisture damage. Arambula et al. (*28*) evaluated moisture susceptibility of HMA using results obtained from DMA and a fracture mechanics based crack growth model. This study demonstrated that both HMA (characterized using relaxation and uniaxial dynamic tension tests) and the corresponding FAM for each mixture (characterized using DMA tests) had similar moisture susceptibility.

OBJECTIVE AND SCOPE OF THE STUDY

The rate at which damage accumulates in a fatigue test depends among other factors on the mode of loading (controlled-strain or controlled-stress). This dependency has restricted the development of a comprehensive approach for characterizing fatigue damage. For a controlled-strain test, the applied strain amplitude is constant and the response stress amplitude decreases with each load cycle as the specimen accumulates damage. For a controlled-stress test, the applied stress amplitude is constant and the

response strain amplitude increases with each load cycle as the specimen accumulates damage. For both modes of loading, fatigue damage under dynamic loading is manifested as a decrease in the dynamic modulus and a simultaneous increase in the phase angle. For a controlled-strain test, the two manifestations of damage have opposite effects on the area of the stress-strain hysteresis loop. A decrease in the dynamic modulus causes the area of the hysteresis loop to decrease, whereas an increase in the phase angle causes the area of the hysteresis loop to increase. Typically, the net effect of these two changes is a decrease in the area of the hysteresis loop with the progression in the number of load cycles. On the other hand, in a controlled-stress test, both manifestations of damage (decrease in dynamic modulus and increase in phase angle) tend to increase the area of the hysteresis loop.

The objective of this research is to develop a fatigue cracking criterion that is independent of the mode of loading used on laboratory based fatigue tests. In other words, a failure criterion that can unify the fatigue characteristics obtained using a laboratory test in controlled-strain or controlled-stress modes of loading will be developed. Two approaches are implemented to achieve this objective. The first approach relies on quantifying the energy dissipated in viscoelastic deformation, fracture and permanent deformation. These energy components are then used to calculate an index for quantifying fatigue damage that is independent of the mode of loading. The second approach relies on using a constitutive relationship to model damage and nonlinear viscoelastic response under cyclic loading. The two approaches should give a similar outcome in terms of: (i) unify the results irrespective of the mode of loading, and (ii) rank the resistance of different mixtures to fatigue damage.

OUTLINE OF THE DISSERTATION

This dissertation is written according to Texas A&M University Thesis Manual for combining several papers into a dissertation and follows the style and format of the *Journal of the Transportation Research Record.* However, some of the content in this

dissertation was modified slightly from the papers to avoid unnecessary repetitions of information and to improve the dissertation flow. This document consists of eight chapters organized as follows:

Chapter I is an introduction. An overview, problem statement, objectives, scope of the study, and outline are presented.

Chapter II presents a literature review about fatigue cracking in asphalt pavements, controlled-strain and controlled-stress modes of loading, fatigue analysis using DMA, and nonlinear viscoelastic analysis.

Chapter III is a preprint of the article "A Unified Method for the Analysis of Controlled-Strain and Controlled-Stress Fatigue Testing" whose final and definitive form has been published in the *International Journal of Pavement Engineering*© [2008] [copyright Taylor & Francis]. The authors of this paper are: Eyad Masad, Veronica T.F. Castelo Branco, Dallas N. Little, and Robert L. Lytton. In this chapter, a new method to unify the DE calculations from both modes of loading was proposed.

Chapter IV was presented at the 87th Annual Meeting of the Transportation Research Board, January 15th, 2008, Washington, D.C., and accepted for publication in the 2008 series of the Transportation Research Record: *Journal of the Transportation Research Board* (forthcoming). This paper is reprinted with permission of the *Transportation Research Board*. The authors of this paper are: Veronica T.F. Castelo Branco, Eyad Masad, Amit Bhasin, and Dallas N. Little. In this chapter, the approach developed on Chapter III was validated for different strain and stress amplitudes.

Chapter V was accepted for publication in the *Journal of Materials in Civil Engineering* (ASCE). The authors of this paper are: Amit Bhasin, Veronica T.F. Castelo Branco, Eyad Masad, and Dallas N. Little. The paper "Quantitative Comparison of Energy Methods to Characterize Fatigue in Asphalt Materials" has been accepted for publication and is reprinted with permission from ASCE. Four DE methods to characterize fatigue in asphalt materials available in the current literature were analyzed using the same set of fatigue data.

Chapter VI presents an approach to determine the threshold or maximum load value (strain or stress) amplitude that differentiates nonlinear viscoelastic response from damage.

Chapter VII presents two approaches for the analysis of dynamic loading of asphalt mixtures exhibiting nonlinear and damage responses.

Chapter VIII presents an overall summary of the dissertation. Conclusions and recommendations for further studies are also presented in this chapter.

CHAPTER II

LITERATURE REVIEW

FATIGUE CRACKING IN ASPHALT PAVEMENTS

Fatigue cracking was studied by Wöhler in 1858 and can be defined by the material cracking caused by repeated load applications (*2*). Wöhler created the concept of the fatigue curve which relates the strain or stress amplitude to the number of load applications needed to cause failure. This curve is also used to characterize hot mix asphalt (HMA) fatigue behavior (Figure 2.1).

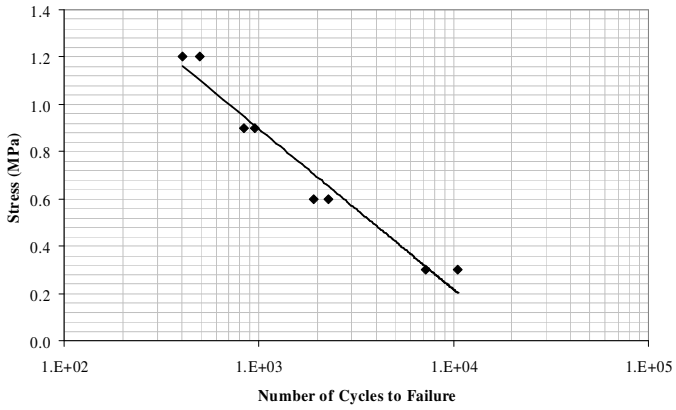

FIGURE 2.1 Fatigue Curve that Relates the Strain or Stress Amplitude to Number of Cycles to Failure.

It is necessary to develop fatigue cracking models that can be used in pavement design procedures such as those developed by the Asphalt Institute (AI), Shell, Illinois Department of Transportation, U.K. Transport and Road Research Laboratory, and Belgian Road Research Center, among others (*3*). The summary report on fatigue response of HMA published by the Strategic Highway Research Program (SHRP) (*6*) and the work of Matthews et al. (*20*) provide a thorough background on the fatigue

resistance of HMA and the factors that influence this resistance. These reports documented that HMA fatigue response is influenced by the method used to compact specimens, mixture variables (asphalt viscosity, asphalt content, aggregate gradation, air voids, and temperature), environmental variables (temperature and moisture), and mode of loading (controlled-strain or controlled-stress).

The SHRP report also presented load configurations, stress distributions, loading waveforms, frequencies, and states of stress used in existing fatigue test methods (*6*). These methods include third-point flexure, center-point flexure, cantilever, rotating cantilever, axial, diametral, and supported flexural beam tests. In terms of the analysis methods, the report recommended the dissipated energy (DE) approach for fatigue analysis, because it is capable of capturing the influences of mode of loading, temperature, frequency, and rest periods (*6*).

CONTROLLED-STRAIN VERSUS CONTROLLED-STRESS MODES OF LOADING

The SHRP review report on fatigue cracking documented that the controlled-stress test is recommended for thick asphalt concrete layers, whereas controlled-strain mode is recommended for thin asphalt concrete layers (*6*). For the same initial strain and stress amplitudes, controlled-stress tests yield a lower fatigue life in comparison with controlled-strain tests. This study also recommends stiffer asphalts and dense graded mixtures for thick asphalt concrete layers, whereas softer asphalts and open graded mixtures are recommended for thin asphalt concrete layers. The study reported that a decrease in temperature increases the fatigue life of thick asphalt concrete layers and decreases the fatigue life of thin asphalt concrete layers. The comparison between the two modes of loading is presented in Table 2.1.

TABLE 2.1 Comparison between Controlled-Strain and Controlled-Stress Modes of Loading (*6*)

Parameter	Mode of Loading	
	Controlled-Strain	Controlled-Stress
Asphalt concrete thickness	Thin	Thick
Failure criteria	Not well established	Complete failure
Fatigue life	Higher	Lower
Sensitivity for mixture variables	Lower	Higher
Rate of dissipated energy (DE)	Lower	Higher
Healing effect due to rest periods	Less beneficial	More beneficial

A number of studies have attempted to develop correlations between modes of loading and fatigue behavior of HMA. Kim et al. (*29*) used a mechanistic approach to predict fatigue resistance. These authors used tensile uniaxial tests for controlled-strain and controlled-stress modes of loading. They analyzed two different asphalt mixtures with Watsonville aggregate and asphalt binders AAD and AAM. Cylindrical samples were prepared, and the tests were conducted at 25ºC and at a frequency of 10 Hz. They first verified the correspondence principle (*27*) using constant-strain-rate monotonic tests with varied strain rates and then suggested a constitutive model to account for damage growth and micro damage healing. Stress (σ) was calculated using Equation 2.1.

$$\sigma = I(\varepsilon_e^R)[F + G + H] \tag{2.1}$$

where, I is the initial pseudo stiffness (ratio between the stress and the peak pseudo strain for the first cycle), ε_e^R is the effective pseudo strain ($\varepsilon^R - \varepsilon_s^R$), ε^R is the pseudo strain, ε_s^R is the shift in pseudo strain values for the controlled-stress mode, F is the damage function (change in the slope of the hysteresis loop for pseudo strain domain), G is the hysteresis function (difference between load and unload paths), and H is the microdamage healing function (how pseudo stiffness changes with rest periods).

Kim et al. (*29*) proposed models for the F, G, and H functions. Two different tests were conducted to validate these models: (i) cyclic loading tests (with different rest periods and strain/stress amplitudes), and (ii) constant-strain rate monotonic tests (with

different strain rates). For controlled-strain tests, the researchers were able to model stress reduction independent of strain amplitude with and without rest periods. However, for controlled-stress tests, the agreement between the predicted and the measured values was precarious comparative to controlled-strain tests. In the same study, Kim et al. (*29*) predicted the fatigue life of the mixtures. They adopted the point at which pseudo stiffness is reduced by 50 percent as a failure criterion. For both modes of loading, with and without rest periods, the proposed model showed good agreement with measured fatigue life. The mixture with the AAM binder showed greater fatigue life with rest periods for both modes of loading. The authors explained the superior healing properties of the mixture with the AAM binder based on chemical and micro structural properties of this asphalt (using surface energy concepts).

Lee and Kim (*30*) identified differences in hysteresis behavior resulting from the mode of loading using a haversine wave form (10 Hz frequency). Under controlled-strain, the secant pseudo stiffness (ratio of stress to a pseudo strain value at the peak pseudo strain of each cycle) decreases as damage accumulates during the test. On the other hand, under controlled-stress, the secant pseudo stiffness also decreases but the hysteresis loop shifts away from the origin during the test. The loop shift is attributed to the accumulation of permanent deformation. These authors calculated the damage parameter (S_p) (due to permanent deformation) as shown in Equation 2.2:

$$S_p = \left(\int_0^t \left| \sigma^{\frac{1}{N}} \right|^p dt \right)^{\frac{1}{p}} \tag{2.2}$$

where, N is the number of load cycles, and σ and p are defined using Equations 2.3 and 2.4, respectively.

$$\sigma = \left| \varepsilon^R \right|^N \tag{2.3}$$

$$p = (1+N)k \tag{2.4}$$

The k term is a function of the failure zone characteristics and is defined in different ways depending on the mode of loading. Values of k for controlled-stress and controlled-strain can be calculated using Equations 2.5 and 2.6. In order to do this, it is necessary to assume that the material's fracture energy (Γ) and failure stress are constants for the controlled-stress case, whereas Γ and the fracture process zone size are constants for the controlled-strain case.

$$k = \left(1+\frac{1}{m}\right) \rightarrow \text{controlled-stress} \tag{2.5}$$

$$k = \frac{1}{m} \rightarrow \text{controlled-strain} \tag{2.6}$$

where, m is the exponent of time in the power law equation of the relaxation modulus.

Lee and Kim used Schapery's approach to calculate crack growth rate and J-integral to predict stresses developed for both cases: (i) controlled-stress: only tensile stresses take place, and (ii) controlled-strain: tensile and compressive stresses take place (*27, 30*). They decided to normalize S_p values with respect to S_p at failure (S_f). For the controlled-strain mode, they assumed the failure criterion as 50 percent reduction in the initial secant pseudo stiffness. By plotting secant pseudo stiffness (S^R) divided by the initial pseudo stiffness (I) versus S_n (normalized damage parameter that is equal to S_p/S_f), the results of both modes of loading fell on the same curve.

In the same study, Lee and Kim developed equations to calculate stress (σ) for both modes of loading as follows (*30*):

$$\sigma = I(\hat{\varepsilon}^R)\left[\left(1+\frac{\varepsilon_S^R}{\hat{\varepsilon}_L^R}\right)F\left(S_n + G\left(\varepsilon_0^R, \frac{\varepsilon^R}{\varepsilon_L^R}\right)\right)\right] \rightarrow \text{controlled-stress} \tag{2.7}$$

$$\sigma = I(\hat{\varepsilon}^R)\left[F(S_p) + G\left(\varepsilon_0^R, \frac{\varepsilon^R}{\varepsilon_L^R}\right)\right] \rightarrow \text{controlled-strain} \quad (2.8)$$

where, $\hat{\varepsilon}^R$ is the pseudo strain (ε^R) minus the shift in the pseudo strain (ε_S^R), $\hat{\varepsilon}_L^R$ is the largest pseudo strain during its history up to that point (ε_L^R) minus the shift in the pseudo strain (ε_S^R), and ε_0^R is the initial pseudo strain. The model was verified using uniaxial tests at 25ºC with different strain and stress amplitudes. Again, the controlled-strain case was considered to be more accurate than the controlled-stress case.

Ghuzlan and Carpenter proposed a new failure criterion for both modes of loading based on beam fatigue tests at 20ºC (*8*). The criterion is based on calculating the change in the dissipated energy (*ΔDE*) between consecutives cycles (*a* and *a* + 1) divided by the DE in the first of the consecutives cycles (*a*). These authors defined failure as the number of load cycles (*N*) corresponding to a rapid increase in this energy ratio (Figure 2.2).

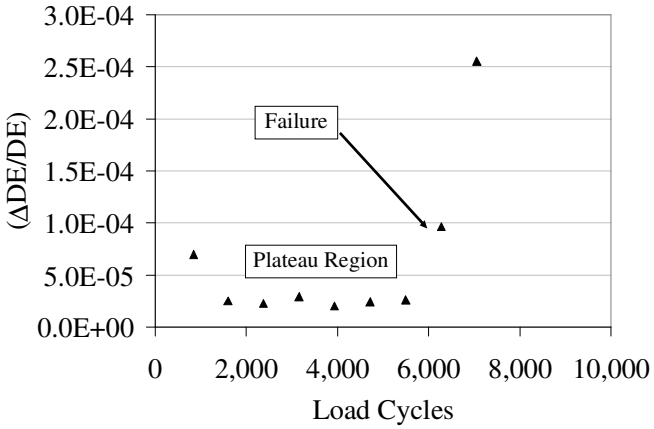

FIGURE 2.2 Dissipated Energy (DE) Ratio versus Number of Load Cycles (Controlled-Strain).

By plotting Δ*DE*/*DE* versus number of loading cycles, Ghuzlan and Carpenter (*8*) found that the energy ratio presents a plateau value – PV (value of Δ*DE*/*DE* which is

constant for different *N* values) during a sequence of loading cycles. By plotting the PV for both modes of loading versus the number of load cycles that caused the sample to fail (N_f), both controlled-strain and controlled-stress tests resulted in the same fatigue curve. Results indicated that higher fatigue life was associated with lower PV.

Benedetto et al. (*31*) published a summary of the work done by the International Union of Laboratories and Experts in Construction Materials, Systems and Structures (RILEM) about fatigue of bituminous mixtures (*31*). The work was performed on one HMA by 11 different research groups; each group testing involved:

- 11 different test methods,
- a temperature of 10ºC,
- a frequency of 10 Hz,
- different testing geometries, including type of load and strain/stress amplitudes, and
- both controlled-strain and controlled-stress modes of loading.

Analyses of the experimental measurements were conducted using classical (Wöhler curves) and continuum damage approaches. Results for this study were divided into three categories:

- linear viscoelastic properties (complex modulus and phase angle),
- fatigue life, and
- fatigue damage analyses.

Linear viscoelastic properties were approximately constant independent of the type of test and mode of loading used. For the fatigue life analysis, the authors defined failure as 50 percent reduction in the initial stiffness. The authors reported no correlation between results for different modes of loading. The authors found that, using empirical analyses, fatigue life test results were influenced by test type, mode of loading, and sample geometry.

For the fatigue damage analysis, the stiffness versus the number of cycles curve was divided into three phases: (i) phase I, or adaptation phase, where a rapid decrease in stiffness occurred; (ii) phase II, or quasi-stationary phase, during which a slow decrease

in stiffness occurred; and (iii) phase III, or failure phase, during which the decrease in stiffness was rapid once again. Benedetto et al. established a damage parameter - D_{exp} (Equation 2.9), and an experimental damage slope - a_T (Equation 2.10) for phase II (*31*).

$$D_{\exp} = \frac{(E_0 - E_N)}{E_0} \tag{2.9}$$

$$a_T = D_{\exp} \times \frac{E_0}{E_{00i}} \tag{2.10}$$

where, E_0 is the initial modulus for a given interval, E_N is the current modulus, and E_{00i} is the initial stiffness for the interval *i*. The term a_T is defined using Equation 2.11, where a_F is the "true" fatigue slope for a given interval (Equation 2.12) and a_B is the stiffness variation due to artifacts or biased effects (thermal heating and thixotropy).

$$a_T = a_F + a_B \tag{2.11}$$

$$a_F = a_T + a_w \frac{C_i(E_0 - E_{00i})}{E_{00i}} \tag{2.12}$$

where, a_w is the slope of the DE per cycle for a given interval, and C_i accounts for the nonlinear damage evolution law.

Benedetto et al. concluded that plotting a_T and a_F versus strain amplitude showed similar behavior for both modes of loading (controlled-strain and controlled-stress), even when different tests and sample sizes were used (*31*). Also, predicted a_F values agreed well with experimental results for the four-point bending test values when strains between 50 and 200 μm were used.

FATIGUE ANALYSIS USING DYNAMIC MECHANICAL ANALYSIS (DMA)

As discussed by Kim and Little, DMA has been used to characterize polymers for many years (*32*). Since 1988, DMA has been used to determine binder rheological properties (*33*). The pioneering work of Goodrich in 1988 used two different rheometers (rheometer mechanical spectrometer and a Rheometrics dynamic analyzer) to characterize binders and to attempt to relate their rheologic properties to mixture behavior in terms of low-temperature creep, flexural fatigue life at 25ºC, permanent deformation, and creep at 40ºC. Goodrich used controlled-strain tests at different frequencies, two aging processes (rolling thin film oven, RTFO, and long-term durability, LTD), two different disk diameters, different test temperatures, and five different asphalts (three conventional and two modified) (*33*). The goal of his work was to analyze the aging process and binder dynamic viscosity at different temperatures. Some of the conclusions for Goodrich's study were:

- aging effects (change in loss and storage modulus) are more visible at higher temperatures (above 0ºC),
- the ratio between storage and loss modulus (loss tangent) is lower for LTD residues, and
- LTD residue loss tangent curves present bigger transition zones (change in the slope of log loss tangent versus temperature curve) if compared to those from RTFO. The explanation for this is that LTD residues present higher polar constituents, higher degrees of molecular association, and higher elastic behavior.

Goodrich published results from a second study in which he attempted to investigate the influence of binder and aggregates on mixture properties at different temperatures (*34*). The difference between the 1991 study and the 1988 study was in the test methodology and materials used. In the 1991 study, two different tests were performed: parallel disk and rectangular bar. Both binders and mastics were analyzed in this study. Tests were performed under controlled-strain loading (oscillatory shear strain)

at different frequencies, temperatures, strain amplitudes, and asphalt film thicknesses. Some of the conclusions for this study were:

- loss and storage modulus change with aggregate addition (the larger the aggregates, the greater the effect),
- the peak value of storage modulus changes with temperature (dependent on binder film thickness and binder type),
- at low temperatures (below 10ºC) the asphalt itself, not the polymer, dominates the binder rheology. Peak dynamic loss modulus temperature and low temperature loss tangent are governed by asphalt stiffness rather than the type of polymer added,
- for medium temperatures (between 10 and 50ºC) mixture rheology is affected by binder properties, and
- for higher temperatures (above 50ºC) mixture rheology is affected by aggregate properties.

Gubler used two rheometers (RMA 800 Rheometrics DSR, and Bohlin CS-2 rheometer) to analyze filler effects on rheological properties of asphalt binders and mastics (*35*). They used a parallel plate test in controlled-strain mode with different strain amplitudes at two temperatures (34 and 52ºC), and three different frequencies. The tests were performed in the following sequence: low strain, high strain, and low strain amplitude. The purpose was to evaluate how the complex modulus changes with high strain amplitude and then how it recovers when low strain amplitude is imposed again. Two binders, three fillers, two free binder volumes (the binder in excess of that required to fill the void space among the particles), and two aging procedures were considered.

Gubler results were based on (*35*):

- change in complex modulus,
- aging index (relation between unaged and aged complex modulus),
- catalytic effect (percent increased in the aging index), and
- change in the phase angle during the test.

These authors concluded that: (i) catalytic effect is independent of filler concentration, (ii) modulus changes are not affected by the binder or filler type for the same free binder volume, (iii) aged systems possess a higher initial complex modulus and also demonstrate a higher decrease in the modulus during the test, and (iv) as the free binder volume increases the complex modulus for most of the tested samples decreases.

Smith and Hesp conducted a study to analyze the crack pinning effect due to filler addition (*36*). According to these authors, crack pinning is the mechanism by which inclusions in a composite material interact with and slow down crack's progression. They tested six mastic systems with one binder and three different fillers (artificial and natural). In their study a Rheometrics rheometer (RDA II) was used to run the controlled-strain tests (torsional load) at 10ºC, a frequency of 40 Hz, and different strain amplitudes. The failure criterion adopted in this study was 50 percent reduction in the initial stiffness.

Some of Smith and Hesp's conclusions were: (i) for artificial filler (glass spheres): sphere size has no significant impact on fatigue life for the same free binder volume, and (ii) for natural filler (limestone): the smaller the grain size, the higher the fatigue life. This last conclusion was explained by the crack pinning effect. Smaller grain size results in smaller distances between particles, which in turn force the crack to overcome a greater obstacle in order to propagate. The filler increases the toughness of the brittle matrices; this effect is more evident for the controlled-strain tests due to the slow propagation of microcracks and the decrease in stress during the test.

Kim et al. were the first authors to propose DMA torsional shear tests under controlled-strain loading for cylindrical (50 mm × 12 mm) mastic samples (*13*). Each mastic sample was composed of binder (AAD or AAM), Ottawa sand, and fillers. These authors used eight percent of binder (by weight) to produce a binder film thickness of approximately 10 μm in the system. Tests were performed at three different temperatures and three different frequencies, and the samples were compacted using a

prefabricated mold at static pressure (Figure 2.3). In this study, Kim et al. used three different test methods:

- dynamic strain sweep test to find the strain amplitude required to determine the linear viscoelastic properties,
- dynamic frequency sweep test to predict relaxation behavior, and
- torsional controlled-strain cyclic loading to induce fatigue damage in the specimens (*13*).

FIGURE 2.3 Prefabricated Mold for Dynamic Mechanical Analysis (DMA) Samples Compaction.

Kim et al. proposed three damage indicators (pseudo stiffness, dynamic modulus, and dissipated strain energy,) and used the transition point, that coincides with the maximum of the product of the number of cycles and shear modulus and the peak of the plot of phase angle, to identify fatigue failure (Figure 2.4) (*13*).

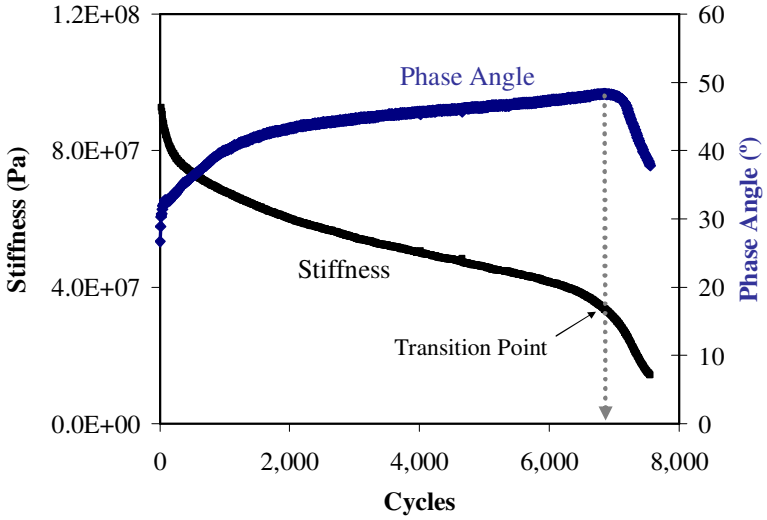

FIGURE 2.4 Stiffness and Phase Angle versus Number of Loading Cycles.

Kim et al. proposed a mechanical fatigue prediction model shown in Equations 2.13 and 2.14. The damage parameter (S_f) included in Equation 2.13 can be calculated using Equation 2.15 (*37*).

$$N_f = \frac{f(S_f)^k}{k(0.5IC_1C_2)^\alpha}\left|G^*\right|^{-2\alpha}(\gamma_0)^{-2\alpha} \tag{2.13}$$

$$k = 1+(1-C_2)\alpha \tag{2.14}$$

$$S_f \cong \sum_{i=1}^{N}\left[\frac{I}{2}\left(\gamma_{m,i}^R\right)^2\left(C_{i-1}-C_i\right)\right]^{\frac{\alpha}{1+\alpha}}(t_i-t_{i-1})^{\frac{1}{1+\alpha}} \tag{2.15}$$

where, N_f is the number of cycles at failure, f is the loading frequency, I is the initial pseudo stiffness, C_1 and C_2 are regression constants, G^* is the linear viscoelastic dynamic modulus, γ_0 is the strain amplitude applied, α is a material parameter related to creep or relaxation properties, N is the number of load cycles, $\gamma_{m,i}^R$ is the maximum pseudo strain for the i loading time, and C is the pseudo stiffness.

Some of the conclusions of this study were: (i) AAM binder mastic systems show higher shear stress and fatigue life, (ii) the model is able to predict fatigue life, and (iii) the inclusion of rest periods (two minutes) increased fatigue life by 8.7 percent for the mastic system prepared using AAD binder and by 23.9 percent for the mastic system with AAM binder, indicating that AAM binder has better healing potential.

Kim and Little used the same analysis method presented by Kim et al. (*13*) but for a larger range of materials and aging procedures (*32*). This study used two aging procedures (three and six months), two fillers (limestone and hydrated lime with different particle distribution), one type of fine aggregate (Ottawa sand), different frequencies, temperatures, and strain amplitudes, and eight different binders (natural and modified). In terms of the effect of polymer modification and aging on fatigue life, Kim and Little concluded that the longer the aging process, the lower the healing potential of the binder (*32*). They also found that high cure rubber (HCR) binder presented higher healing potential (approximately 70 percent of the dynamic modulus was recovered), and polymer modified binder presented higher fatigue life and lower rate of damage evolution. Kim and Little also concluded that the addition of filler assists in increasing resistance to microcracking (*32*). Also, mastics with hydrated lime presented 28 percent more cumulative dissipated pseudo strain energy (DPSE) prior to failure, and higher fatigue life, compared with the limestone mastics.

The study by Kim and Little used two models to investigate the influence of fillers on mastic fatigue resistance: continuum damage fatigue model and rheological particulate composite model (*32*). For the continuum damage fatigue model they used the dynamic modulus, the damage parameter (S), and DPSE to represent damage accumulation and fatigue life of the material. For the rheological analyses, they used Nielsen's model and the stiffening ratio (ratio between the shear modulus of the mastic and the shear modulus of the binder). Some of the most important conclusions of the study by Kim and Little were that cumulative DPSE is higher with filler addition (AAD-1 binder plus hydrated lime presented 588 percent more accumulation of pseudo strain energy compared with the other systems), and hydrated lime systems present higher

stiffening ratios for higher filler volume fractions. They explained the success of the hydrated lime systems based on the fact that this filler has higher physico-chemical interaction with the binder (especially AAD-1) (*32*).

Zollinger used DMA (CVOR 200 Bohlin) under controlled-strain (torsional load) to analyze moisture damage (*9*). He studied six fine aggregate matrix (FAM) composed of fine aggregate, filler, and binder using a new DMA sample fabrication method. In this method, DMA samples were obtained from a Superpave gyratory compactor (SGC) sample (152 mm). The standard procedure for a SGC was followed and then the DMA samples were cored This procedure promises better control of sample air voids and takes less time (Figure 2.5).

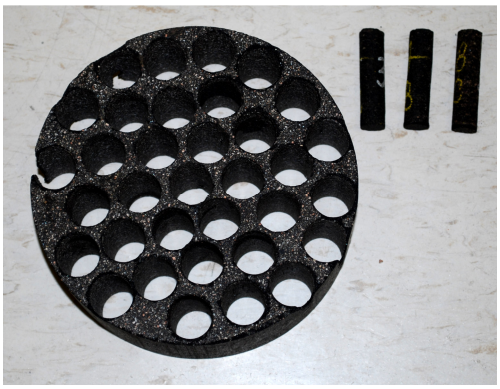

FIGURE 2.5 Dynamic Mechanical Analysis (DMA) Samples Cored from Superpave Gyratory Compactor (SGC) Sample.

Zollinger conducted two different tests: (i) time sweep tests using low strain amplitude (0.0065%) to determine the linear viscoelastic material properties, and (ii) time sweep tests using high strain amplitude (0.2% and 0.3%) to analyze fatigue damage with and without moisture damage (*9*). In this study, the DPSE was divided by the ratio of the complex modulus (G^*) to the initial complex modulus (G_0) in order to calculate the DE per unit volume of the intact part of the material (Equation 2.16):

$$W_R = \frac{DPSE}{\frac{G^*}{G_0}} \tag{2.16}$$

Zollinger also used a crack radius index ($R(N)$) to compare the resistance of the different FAM to fracture as follows (*9*):

$$R(N) = \left[(2n+1)^{n+1} \left(\frac{E_R b}{4\pi E_1 \Delta G_f} \right)^n N \right]^{\frac{1}{2n+1}} \tag{2.17}$$

$$n = \frac{1}{m} \rightarrow \text{controlled-strain} \tag{2.18}$$

where, E_R is the reference modulus, b is the slope of the W_R versus log(N) plot, E_1 is the intercept of the log(relaxation modulus)-log(time) relationship, ΔG_f is the adhesive bond energy, N is the number of load cycles, and m is the exponent of time in the power law equation of the relaxation modulus. Zollinger concluded that the common assumption of 50 percent reduction in stiffness as a good failure point is not true for all mixtures. The $R(N)$ analysis captured the influence of moisture on fatigue damage and was also successful in ranking the mixtures according to known field performance in terms of resistance to moisture damage (*9*).

Arambula et al. (*28*) evaluated moisture susceptibility of HMA and correspondent mastics using dynamic analysis and crack growth model. These authors evaluated three asphalt mixtures (and correspondent mastics). Results from this study showed similar results (in terms of moisture sensibility) for both HMA (characterized using relaxation and uniaxial dynamic tension) and correspondent FAM (characterized using DMA). The crack growth index showed potential in terms of presenting results that rank mixtures according to field performance and also differentiating between the wet and the dry behavior.

NONLINEAR VISCOELASTIC ANALYSIS

Material's behavior can be linear or nonlinear depending on a combination of factors (stress/strain amplitudes, temperature, and rate of loading). There are several studies in the literature that focus on nonlinear viscoelastic behavior characterization for a variety of materials, such as: wood, composites, polymers, and asphalt materials.

The study performed by Straganac et al. (*38*) presented a method for nonlinear viscoelastic behavior characterization using high-altitude scientific balloons materials. The method is based on Schapery's theory (*39*) extended to incorporate dynamic oscillatory test results. These authors used Schapery's work to extend the approach used for time-temperature superposition and developed a time-stress superposition principle identifying stress-dependent shift factors. According to Schapery's theory (*39*), nonlinear viscoelastic strain response can be described as:

$$\varepsilon(t) = g_0 D_0 \sigma(t) + g_1 \int_0^t \Delta D(\psi - \psi') \frac{\partial g_2 \sigma}{\partial \tau} \partial \tau \tag{2.19}$$

where, ε and σ are the uniaxial strain and stress, respectively. g_0, g_1 and g_2 are nonlinear stress-dependent material parameters, D_0 and ΔD are the initial and the transient components of the creep compliance, respectively, and ψ and ψ' are reduced time variables defined using Equations 2.20 and 2.21.

$$\psi = \psi(t) = \int_0^t \frac{dt}{a_\sigma} \tag{2.20}$$

$$\psi' = \psi'(\tau) = \int_0^\tau \frac{dt}{a_\sigma} \tag{2.21}$$

where, a_σ is the stress-dependent shift factor, and t and τ are the present time and the time elapsed since load application, respectively.

Equations for stress response (using strain as an independent variable) were also derived in a similar manner as in Equations 2.19 through 2.21.

Straganac et al. (*38*) used dynamic oscillatory frequency sweep tests for oscillatory strain at a constant temperature and preload (percentage of the yield of the material, used to maintain a tensile load on the specimen). The main objective of this study was to evaluate the preload magnitude effect on the nonlinear viscoelastic material behavior. The dynamic modulus was measured for different preload (stress) magnitudes using a frequency range ($0.1 \leq w \leq 100$ rad/s) and creating stress-dependent dynamic modulus curves for a constant temperature. Stress-dependent shift factors were then calculated as a result of data shifting and superposition. Similar to the time-temperature superposition principle, using the time-stress superposition principle the property measured at a specific preload and frequency corresponds to the property at another preload and frequency. Transforming properties found in the frequency domain into the ones on the time domain, allowed the authors to conduct the analysis in a much shorter time. Two thin-film polyethylenes (Stratofilm® and Astrofilm) used in the high-altitude scientific balloons were analyzed during this study. Using linear analysis, the dynamic oscillatory test results deteriorated when compared to traditional creep results for preloads higher than 0.690 MPa. On the other hand, nonlinear viscoelastic analysis presented good agreement if compared to traditional creep results (even for different stresses' magnitudes).

Golden et al. (*40*) validated two approaches for nonlinear viscoelastic characterization using dynamic mechanical tests results: (i) hybrid approach (using linear dynamic mechanical analyses and constant applied stress tests), and (ii) nonlinear approach for oscillatory load conditions (using nonlinear dynamic mechanical tests).

For the first approach, Equation 2.19 was simplified resulting in Equation 2.22.

$$\varepsilon = g_0 D_0 \sigma + \left(\frac{g_1 g_2}{a_\sigma^{\,n}} \right) D_1 \sigma t^n \tag{2.22}$$

where, D_0 and $D_1 t^n$ are the elastic and transient components of creep compliance, respectively.

For the second approach, the authors derived an equation for the oscillatory component of the strain response ($\Delta\varepsilon$) from Equation 2.19.

$$\Delta\varepsilon = D_0 g_{0t} \Delta\sigma + \left(g_{1t} \frac{d\hat{g}_{2t}}{d\sigma} \left| \hat{D}^* \right| e^{i\hat{\delta}} + \hat{g}_{2t} \frac{dg_{1t}}{d\sigma} \frac{D_1}{a_{\sigma_t}^n} t^n \right) \Delta\sigma \tag{2.23}$$

where,

$$\hat{D}' = D_1 \Gamma(1+n) \cos\left(\frac{n\pi}{2}\right) (\hat{w})^{-n} \tag{2.24}$$

$$\hat{D}'' = D_1 \Gamma(1+n) \sin\left(\frac{n\pi}{2}\right) (\hat{w})^{-n} \tag{2.25}$$

$$\hat{w} = w a_{\sigma_t} \tag{2.26}$$

$$\hat{g}_2 = g_2 \sigma \tag{2.27}$$

$$\Delta\hat{g}_2 = \left(\frac{d\hat{g}_2}{d\sigma} \right) \Delta\sigma \tag{2.28}$$

$$\hat{\delta} = \tan^{-1}\left(\frac{\hat{D}''}{\hat{D}'} \right) \tag{2.29}$$

where, subscript $(\ )_t$ means that the parameter was evaluated at a constant stress σ_t (applied at $t=0$), and Γ is the gamma function.

Finally, the terms associated with the nonlinear complex compliance (D_{NL}) could be identified using Equations 2.30 and 2.31.

$$D'_{NL} = D_0 g_{0t} + g_{1t} \frac{d\hat{g}_{2t}}{d\sigma} \frac{D_1 \Gamma(1+n)}{(wa_{\sigma_t})^n} cos\hat{\delta} + \hat{g}_{2t} \frac{dg_{1t}}{d\sigma} \frac{D_1}{a_{a_t}^n} t^n \tag{2.30}$$

$$D''_{NL} = g_{1t} \frac{d\hat{g}_{2t}}{d\sigma} \frac{D_1 \Gamma(1+n)}{(wa_{\sigma_t})^n} sin\hat{\delta} \tag{2.31}$$

Details about the mathematical derivations can be found in the original document (*40*).

For the first approach, dynamic mechanical frequency sweep tests were performed using a constant temperature. Two sets of tests were conducted: (i) linear dynamic mechanical tests for five frequencies (swept from 0.4 to 100 rad/sec) at a constant temperature, oscillatory strain equal to 0.06 percent, and prestress from 0.69 to 1.03MPa (depending on the temperature used), and (ii) creep tests over two hours period for prestress from 1.5 to 4.5 MPa at 23ºC.

For the second approach, dynamic mechanical tests were adapted to measure the nonlinear viscoelastic properties. The tests were performed using constant prestress, frequency and temperature for a range of prestress values. The complete test response (linear and nonlinear) was obtained using the theory developed during this study (*40*).

The results for the thin film polyethylene (Stratofilm®) showed that:

- for the applied constant stress with linear dynamic mechanical tests: the predictions of material response using both, linear (creep compliance derived from the dynamic oscillatory measurements), and nonlinear (creep compliance derived from the dynamic oscillatory measurements using stress dependent shift factors derived from creep tests), responses could be compared to traditional creep test results. For higher prestress magnitudes (6.21 MPa), properties prediction deteriorated,
- for the applied oscillatory stress with nonlinear dynamic mechanical tests: the nonlinear viscoelastic parameters (g_1, g_2, and a_σ) were found using the transient and oscillatory displacements due to an input oscillatory load and

different amplitudes of prestress. The strain response was separated in transient and oscillatory parts.

Golden et al. (*41*) validated the nonlinear viscoelastic approach developed by Strganac et al. (*38*). These authors used a linear low density polyethylene film under dynamic oscillatory loading conditions and different loading histories: (i) series of discrete step load inputs, (ii) large-amplitude saw tooth oscillation, and (iii) large-amplitude sinusoidal oscillation. For the three loading cases, linear and nonlinear predictions were compared to direct measurements. The predicted response using the linear model was considered poor, but the response predicted using the nonlinear viscoelastic model was very good.

Shields et al. (*42*) investigated the nonlinear viscoelastic behavior of asphalt concrete mixtures using Schapery's theory (*25*). One dense-graded HMA was tested under uniaxial-stress condition (direct tension stress relaxation test) at different temperatures (from 40ºC to -40ºC) and strain amplitudes (from 0.01 to 0.8 percent). These authors used Schapery's theory considering reduced time induced by both: strain (ε), and temperature (T). The combined strain and temperature reduced time (ρ) was expressed using Equation 2.32.

$$\rho(t) = \int_0^t \frac{dt'}{a_\varepsilon[\varepsilon(t')]a_T[T(t')]} \tag{2.32}$$

where, a_ε is the strain-dependent nonlinear parameter, a_T is the temperature-dependent nonlinear parameter, and *t'* is an integral variable.

During this study, Shields et al. used three strain histories and temperatures to analyze HMA nonlinear viscoelastic effects on stress predictions: (i) constant-strain-rate, (ii) thermal stress restrained specimen test (TSRST), and (iii) sinusoidal temperature variation case.

Constant-strain-rate isothermal test results showed that the stress predicted using the relaxation modulus test is a function of the strain amplitude used. Good agreement was found between the predicted and the observed stress when the nonlinear viscoelastic

approach was used. The same agreement was considered poor when linear theory was applied for strain values higher than 0.1 percent. Similar conclusions were found for the TSRST anisothermal test results.

The authors also evaluated the nonlinear effects using a sinusoidal temperature variation. Strain caused by the temperature change was in the order of 0.37 percent and the resulting maximum stress was predicted using Schapery's nonlinear viscoelastic theory. For this case, the linear assumption overestimated the stress value in 250 percent comparative to the nonlinear viscoelastic predictions.

Bahia et al. (*23*) investigated the strain distribution within the binder domains of an asphalt mixture. They sliced a sample that was tested in the Superpave shear tester and use the surface image to generate a finite element (FE) mesh. Results showed that the strains within the binder films can be from 10 to 100 times (0.3 to 32 percent) of the asphalt mixture bulk strains. These strain values were explained to be due to the stiffness difference between aggregates and binders, especially for thin binder film thickness.

To evaluate the nonlinear viscoelastic effects in asphalt mixture responses, these authors used oscillatory shear tests (parallel plate geometry) with the following variables:

- eight binder types (modified and unmodified);
- five strain levels (1, 4, 10, 20 and 30 percent);
- five temperatures (10, 22, 34, 46, and 58ºC), selected to reach complex modulus (G^*) values of 2, 20, 200 and 2,000 kPa;
- three frequencies (0.15, 1.5 and 15 Hz);
- two maximum number of cycles (5,000 and 11,000 cycles);
- three rest periods intervals (0.5, 3 and 12 hours).

The conclusions from this study were separated in respect to the effect of the factor on the material behavior as follows:

- Temperature and frequency effects: binder's strain dependence showed to be highly related to temperature and frequency. Strain sweep tests results showed that by changing strain from 1 to 50 percent, G^* values dropped more than an

order of magnitude. More damage (decrease in G^* values) was observed at lower temperatures (around 10 to 22ºC). In respect to frequency, the results showed that the strain effect is more visible at higher frequencies (15 Hz) than at lower ones (0.15 Hz),

- Binder composition: different modified binders (elastometer, plastometer, oxidized) demonstrated different strain dependencies. The differences are mainly related to: magnitude of the drop in the rigidity (G^*) for strain sweep tests, trend of the rigidity change (plateau regions versus sudden drops), and strain temperature sensitivity (the higher the temperature, the lower was the sensitivity of the binders to strain amplitude),
- Rest periods and binder healing: the strain sweep tests' results for different healing periods showed that healing is a phenomenon that depends on binder composition (modified asphalts showed faster recovery when compared to neat asphalts),
- Fatigue: results can be separated in the following way: (i) effect of strain amplitude – both (modified and unmodified) asphalts presented significant G^* reduction (more than an order of magnitude) within 5,000 cycles when higher strains (20 percent) were used. Phase angle (δ) presented to be less sensitive to fatigue damage, comparative to G^*, (ii) effect of loading rate: the effect of frequency on G^* behavior was observed for tests performed using 20 percent strain. These results indicated that, after 4,000 cycles, the reduction in G^* (1,000 percent) was equivalent to change asphalt grade by at least three temperature intervals, (iii) effect of binder type and modifier: different compositions (level of asphaltenes) had profound effect on fatigue behavior (decrease in G^*), tests results using binder PAV aging showed that aging increased fatigue damage (faster decrease in G^*) for the two strain amplitudes (10 and 20 percent), asphalt modification (SBS, SB, EVA, PE unstabilized and EMA) results demonstrated that the polymer modification reinforces the asphalt fatigue resistance (modified asphalts presented lower rate of G^* decrease for tests performed at 20 percent

strain), (iv) rest periods: results from 20 percent strain tests showed that for both (modified and unmodified) asphalts the healing phenomena (manifested as fatigue damage recovery) is time dependent (the longer the rest period, more recovery on G^* was observed). Modified asphalt (PE unstabilize) presented faster recovery when compared to unmodified asphalt. This binder behavior indicated that no permanent deformation happened during the fatigue test (after 12 hours of rest period, the fatigue curve was similar to the initial one).

Airey et al. (*43*) used dynamic shear rheometer (DSR) strain and stress sweep tests to investigate the linear viscoelastic limits for different asphalt binders (unaged, short term aged, base and modified). They also plotted master curves using properties (G^* and δ) inside the linear viscoelastic (LVE) region and investigated the effects of aging using base and elastomeric PMB modified binder.

Five binders were used in this study: (i) conventional 50-pen bitumen, (ii) process modified multigrade bitumen (35/50), (iii) Styrene-Butadiene-Styrene (SBS) linear PMB, (iv) SBS radial PMB, and (v) Ethylene-Vivyl-Acetate (EVA) PMB. These binders were subjected to RTFO short-term aging before they were tested. These authors first conducted stress (strain) sweep tests to determine the LVE range using: (i) six temperatures (10, 20, 30, 40, 60, and 70ºC), (ii) four frequencies (0.1, 1, 5, and 10 Hz), and (iii) stress amplitudes from the minimum torque value to either maximum torque value or 30 percent reduction in G^*. LVE limit was select at the point where G^* reached 95 percent of its initial value. Once the LVE limits were selected, rheological properties (G^* and δ) were obtained and master curves were plotted.

From the master curves' results for the different combinations of frequencies and temperatures, the author's findings were: (i) G^* values for 50-pen bitumen and EVA PMB were identical at high frequencies, but EVA PMB G^* values were lower when lower frequencies were considered, the same happening for δ values, (ii) for SBS PMB binder, G^* values were higher at lower frequencies (higher temperatures) when compared to 50-pen bitumen, δ plots for SBS PMB binder presented a plateau region at intermediate frequency and lower values at low frequencies, and (iii) results for the

modified multigrade bitumen presented improved temperature susceptibility (lower stiffness at high frequencies and higher stiffness at low frequencies) when compared to 50-pen bitumen. δ results presented an increased elastic response comparative to 50-pen bitumen.

From the LVE limits study, Airey et al. (*43*) found that: (i) plots of G^* versus strain limits showed that all five binders presented similar behavior with a general increase in the strain limit with the decrease in binder stiffness, (ii) plots of G^* versus stress limit presented again similar behavior for all five binders with the multigrade bitumen presenting a slightly lower stress limit, (iii) plots of δ versus strain and stress limits indicated that there was a difference between SBS PMBs binder's behavior when compared to the other three binders investigated. The elastomeric polymer behavior became more dominant at high temperatures (low frequencies).

In order to present LVE limits for G^* and δ, the binders used in this study were separated in two groups: (i) process modified, plastomeric, and conventional binders, and (ii) thermoplastic rubber SBS PMPs. For the first group, the strain dependent LVE criteria was between 2 and 6 percent at low temperature (for $G^* > 1$ MPa and $\delta < 55°$), and the stress dependent LVE criteria was between 1.5 and 7 kPa at high temperatures (for $G^* < 10$kPa). The second group (thermoplastic rubber PMPs) presented no high temperature stress dependent LVE criterion and a second high temperature strain criterion between 50 and 200 percent.

The effects of aging on the rheological properties as well as on the linear limits were also investigated. 50-pen bitumen and radial SBS PMB were also tested in their unaged condition. The findings were: (i) rheological properties changed with the aging process (G^* increased and δ decreased), but the radial SBS PMB showed to be more resistant to aging (very similar master curves were found before and after aging), and (ii) linear behavior was not affected by the aging process (very similar strain and stress dependent LVE limits were found before and after aging).

Abbas et al. (*44*) proposed and implemented (into a FEM model) a convolution integral-based approach to describe binder stress-strain behavior. The model can be used

to simulate HMA viscoelastic behavior considering aggregate microstructure and binder nonlinear viscoelastic behavior. During this study, the authors modified Prony series approach and incorporated it into a user-defined material subroutine (UMAT). The purpose of doing this was to allow specifying strain-dependent binder model constants and to be able to model binder nonlinearity in an efficient computational approach. The complete formulation can be found in the original document (*44*).

In order to check the formulation efficiency, this approach was implemented into an ABAQUS subroutine. Results were compared to DSR measurements at one percent shear strain. G^* estimated for different radial frequencies presented excellent fit with both: DSR measurements and predictions using a LVE algorithm. The proposed formulation was also tested using a 10×10 rectangular plane-strain elements model subjected to one percent simple shear strain with different boundary restrains. Comparisons between the estimated and the input G^* showed that: (i) modulus estimation was affected by elements' position (predictions for elements near the sample center were closer to input values), (ii) the larger the area (FEM model mesh) of the sample results, the lower the binder G^* prediction tended to be.

The viscoelastic model proposed by Abbas et al. (*44*) was also implemented into a HMA microstructure model developed by Papagiannakis et al. (*45*). G^* predictions from the HMA model were compared to simple shear tester (SST) results obtained using 0.01 percent dynamic shear strain. G^* predictions were very close to measured values, even for different frequencies. The same HMA model was used to evaluate the relationship between axial (SST measurements) and shear (uniaxial dynamic measurements) modulus. Unreasonably high Poisson's ratio values were found. The authors attributed this finding to: (i) material nonlinearity, (ii) difference in the direction of the principal stresses for both tests, and (iii) non uniform deformation caused by boundary conditions and specimen dimensions in the shear test.

Huang et al. (*46*) used Schapery's model to characterize HMA nonlinear viscoelastic behavior. SST tests were performed at multiple frequencies (0.01, 0.02,

0.05, 0.1, 0.2, 0.5, 1.0, 2.0, 5.0, 10.0, 30.0 Hz), temperatures (52, 46, 40, 27ºC), and strain amplitudes (0.01, 0.04, 0.07, 0.1 percent) for two HMA with different gradations.

Dynamic compliance was determined as a function of frequency for each strain amplitude and temperature. Prony series coefficients in the frequency domain were used to formulate compliance as a function of time. For the analysis: (i) the master curve for each strain amplitude was plotted using time-temperature shifting factors, (ii) the nonlinear viscoelastic parameters ($g_1 g_2$) were obtained by vertical shifting curves for different strain amplitudes to a reference strain amplitude, (iii) the strain/stress shift factor (a_s) values were determined shifting the master curves at different strain amplitudes in the horizontal direction, and (iv) the long-term linear viscoelastic Prony series coefficients were obtained horizontally fitting the data to the lower strain amplitude data (0.01 percent).

Huang et al. (*46*) also performed model verification in two stages comparing: (i) FE predictions and closed form solution of the modified superposition principle (MSP), and (ii) numerical results (FE model with input parameters) with the experimental measurements. Findings from this model verification showed that FE results with the nonlinear material subroutine agreed with MSP calculated results and also that the numerical results showed good agreement with the experimental results.

Masad et al. (*26*) used DSR stress sweep tests to obtain binder G^* as a function of stress amplitude (for different frequencies, temperatures and aging conditioning). In order to have the same range of stress amplitudes for all tests, the stress amplitudes were normalized by the ultimate stress amplitude for each test. Four normalized stress amplitudes (0.01, 0.6, 0.8 and 1.0) were used during this analysis.

Masad et al. (*26*) implemented the recursive-iterative integration approach developed by Haj-Ali and Muliana (*47*) in the Schapery's nonlinear model. Schapery's integral form, Equation 2.19, was used, but temperature and aging shift factors were included in the reduced time equation, Equation 2.20 became Equation 2.33.

$$\Psi = \int_0^t \frac{dt}{a_T a_S a_g} \tag{2.33}$$

where, a_T is the temperature shift factor, a_s is the strain or stress shift factor, and a_g is the aging shift factor.

They also represented transient creep compliance (ΔD) using Prony series.

$$\Delta D^{\Psi} = \sum_{n=1}^{N} D_n (1 - exp(-\lambda_n \Psi^t)) \tag{2.34}$$

where, D_n is the n^{th} coefficient of Prony series and λ_n is the n^{th} retardation time.

The temperature shift factor (a_T) was calculated for different stress amplitudes using 30ºC as the reference temperature. Results from this analysis showed that a_T is independent of stress amplitude.

The nonlinear viscoelastic parameters ($g_1 g_2$) were also found by shifting the higher stress master curve to the linear stress amplitude (assumed as the lowest normalized stress amplitude). Results from this analysis showed that the higher the stress amplitude, the higher the nonlinear parameters ($g_1 g_2$) tended to be. Nonlinear viscoelastic parameters ($g_1 g_2$), stress shift factor (a_s) at normalized stress amplitudes, and linear viscoelastic coefficients of the Prony series were used to develop master curves at different stress amplitudes and predict binder's long term behavior.

Aging shift factors (a_g) were obtained by horizontal shifting the aged binder data to the unaged binder data (for each temperature and stress amplitude). Results from this part of the study showed that the a_g is mostly a function of temperature and almost independent of normalized stress amplitudes.

In the last part of this study, Masad et al. (*26*) input the unaged binder parameters to a FE subroutine. Binder's creep response for each temperature and normalized stress amplitudes were predicted. Model and DSR experimental results presented good agreement, for linear and nonlinear stresses.

CHAPTER III

A UNIFIED METHOD FOR THE ANALYSIS OF CONTROLLED-STRAIN AND CONTROLLED-STRESS FATIGUE TESTING*

OVERVIEW

Fatigue cracking is one of the primary distresses in asphalt pavements. This study presents a method to characterize fatigue resistance of the fine portion of the asphalt mixture using the dynamic mechanical analyzer (DMA). Three mixtures were characterized in controlled-strain and controlled-stress modes of loading. The new method has several advantages as it requires reasonable testing time, uses a small amount of material, utilizes fundamental properties of the mixture, and is able to unify the results from controlled-strain and controlled-stress modes of loading. The unified method relies on identifying the different mechanisms of energy dissipation during fatigue cracking that are related to changes in the phase angle, changes in stiffness, and development of permanent deformation during the fatigue damage process. Two fatigue damage parameters are derived in this chapter. The parameters are shown to have reasonable and lower coefficients of variation than conventional parameters such as number of loading cycles to failure and cumulative dissipated energy.

BACKGROUND

Fatigue cracking is one of the most common distresses in asphalt pavements. An accurate characterization of the fatigue resistance of hot mix asphalt (HMA) will result in a more reliable pavement design and a more accurate assessment of the performance of asphalt pavements.

---

*This is a preprint of an article whose final and definitive form has been published in the International Journal of Pavement Engineering© [2008] copyright Taylor & Francis.

In general, fatigue refers to damage and fracture under repeated loading. The fatigue process is a complex phenomenon because crack initiation and propagation processes evolve under different physical laws (*48*). It is particularly difficult to characterize fatigue in HMA due to the composite nature of the material, the different constitutive laws that govern the asphalt mixture constituents, the gradation of aggregate particle size, asphalt film thickness variation within the mastic, air void size distribution, and the dependency of asphalt binder behavior on time and temperature.

Most of the studies on fatigue rely on testing the full asphalt mixture under cyclic loading. However, recent work at Texas A&M University has shown that the full mixture results are highly influenced by the complexity and heterogeneity of the internal structure, which could hinder the efforts to link properties of mixture constituents to fatigue resistance. Therefore, a new approach has been adopted in which fatigue testing is conducted first on the fine portion of the mixture, which has a more uniform (or less heterogeneous) internal structure (*10*). Once the constituents of the fine portion are selected to achieve a desirable behavior, the full mixture can be tested in order to evaluate the effect of mixture design on performance. The fine portion of the mixture is tested using the DMA which has also been used for evaluating asphalt binders and mastics (binder and mineral filler smaller than 75 μm) rheological and fatigue properties (*13, 32-36*). These studies have shown that DMA is a powerful tool for material characterization under different loading conditions (frequency, temperature, modes of loading, etc), and material conditions (dry versus wet).

The testing of the mastic or the fine portion of the mixture is also motivated by findings that these phases influence crack formation and growth phenomena (*37*). According to Lytton (*49*), adhesive fracture occurs in thin mastic films and cohesive fracture occurs in thick mastic films. In addition, several studies have reported the significant influence that fillers properties have on HMA behavior. Gubler et al. (*35*) analyzed changes in the dynamic modulus and phase angle as a function of strain amplitude after aging using different methods. They showed that the filler acts in two paradoxical ways in HMA: (i) as a catalyst promoting binder aging, and (ii) as a

hindrance retarding binder aging. Kim et al. (*37*) tested mastic samples in a controlled-strain torsional loading mode and analyzed the results using both a continuum damage fatigue model and a rheological particulate composite model. The first analysis showed that filled systems had lower rates of damage evolution than pure binder or unfilled systems. The rheological model validated the physicochemical interaction between hydrated lime and asphalt binder and was used to quantify its impact on damage resistance. In a follow up study, Kim and Little (*50*) studied the effect of two different fillers (limestone and hydrated lime) on the mastic behavior using micromechanics models. The results showed that due to physicochemical interactions, the mechanical behavior of the hydrated lime – filled system is different than that of the limestone – filled system. Abbas et al. (*51*) analyzed mastic rheological properties using the discrete element method (DEM) and demonstrated the influence of different fillers on the stiffening behavior of the mastic at a wide range of temperatures and filler contents.

The results of laboratory fatigue testing of asphalt mastics and mixtures are affected by boundary and loading conditions (*31*). Defining the influence of the loading condition in terms of controlled-strain versus controlled-stress tests has been a challenge that hindered the development of a comprehensive fatigue performance model. Conventional analysis methods yield contradictory findings in terms of the fatigue life measured using controlled-strain versus controlled-stress testing. Some researchers affirm that controlled-stress tests are more applicable to thick asphalt concrete layers while the controlled-strain mode is more applicable to thin asphalt concrete layers (*3*). The failure criterion for the controlled-stress mode is typically the complete rupture of the sample, while rupture might not take place during the controlled-strain experiment. Therefore, some researchers adopt a 50 percent reduction in stiffness as the failure point in controlled-strain tests.

Van Dijk et al. (*52*) and Van Dijk (*12*), using dynamic bending tests, were the first to suggest the use of the dissipated energy (DE) concept to analyze HMA fatigue behavior. During the fatigue process the material is damaged (material structure changes and stiffness decreases) and energy is dissipated. Ghuzlan and Carpenter (*8*) attempted

to unify the results from controlled-strain and controlled-stress beam fatigue tests by using the ratio of the change in DE between consecutives cycles (i and $i+1$) to the DE in the first of the consecutives cycles (i). After plotting this ratio versus the number of load cycles, test results showed a constant plateau value (period during which the accumulation of damage is constant), which was independent of the mode of loading. Kim et al. (*29*) used the elastic viscoelastic correspondence principle proposed by Schapery (*27*) to derive damage functions and strain-stress relationships for controlled-strain and controlled-stress loadings under cyclic loading conditions.

STUDY SIGNIFICANCE AND OBJECTIVES

The common practice in fatigue analysis is to employ the controlled-strain mode for mixtures that are used in thin asphalt concrete layers and controlled-stress loading for mixtures used in thick asphalt concrete layers. This approach has been motivated by the observation that the strain amplitude remains almost constant in the bottom of a thin asphalt concrete layer, while stress amplitudes remains almost constant in the bottom of a thick asphalt concrete layer over a wide range of mixture stiffnesses. Recently, however, changes in the structural design of pavements, and the realization that multiple fatigue mechanisms may occur (bottom-up versus top-down cracking) make it difficult to identify pavement systems that adhere strictly to either controlled-strain or controlled-stress conditions.

This study is aimed at developing an analysis method that is capable of unifying the results from both modes of loading. This method is developed based on understanding the basic differences between the two modes of loading in terms of the energy supplied, separation of energy associated with fatigue damage from that due to the viscoelastic (linear or nonlinear) response, and crack growth rate. The efficacy of the new method is demonstrated through testing the fine portion of asphalt mixtures using the DMA. The following tasks support this objective:

- Conduct controlled-strain and controlled-stress DMA testing on specimens representing different mixtures,
- Use principles of dissipated pseudo strain energy (DPSE) to calculate the energy associated with the mixture fatigue damage,
- Illustrate the influence of mode of loading on the energy supplied during dynamic fatigue loading,
- Propose a new method to unify the DE calculations from both modes of loading,
- Derive a crack growth index that accounts for the DE, viscoelastic properties of the undamaged materials, and the bond energy in the mixture,
- Demonstrate the importance of separating the energy associated with the nonlinear viscoelastic response from the energy associated with damage in the unification of crack growth index values from the two modes of loading, and
- Investigate the variability in the calculation of the crack growth index and compare it to other commonly used indices to characterize fatigue damage.

MATERIALS AND TESTING

Specimens that represent three different asphalt mixtures were tested. The details on these mixtures are provided by Zollinger (*9*). Mixture A was reported to perform well in terms of resistance to cracking, mixture B performed fairly well to poorly, and mixture C performed poorly. The DMA specimens consisted of fine aggregate (smaller than 1.18 mm – No. 16 sieve), filler (smaller than 0.075 mm – No. 200 sieve), and binder. Compositions of the fine aggregate matrix (FAM) used in this study are presented in Table 3.1. As an example, the full HMA and FAM gradations for mixture A are presented in Figure 3.1.

TABLE 3.1 Compositions of Fine Aggregate Matrix (FAM) Used in This Study

Mixture ID	Material	% of Total Aggregate Weight	Binder PG
A	Sandstone Screenings	57	76-22
	Granite	38	
	Hydrated Lime	5	
B	Limestone	28	64-22
	Natural Sand	72	
C	Limestone	50	64-28
	Natural Sand	50	

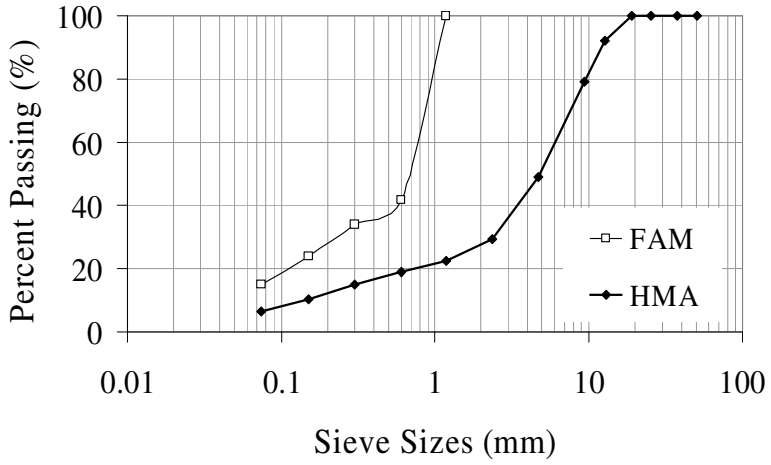

FIGURE 3.1 Hot Mixture Asphalt (HMA) and Fine Aggregate Matrix (FAM) Gradation Curves for Mixture A.

Two methods are described in the literature to prepare DMA specimens with dimensions of about 50 mm height and 12 mm diameter. The first method by Kim and Little (*50*) focused on testing the mastic (filler and binder) mixed with Ottawa sand. In this method, the filler volume to binder volume proportion was fixed at 10 percent. The binder was mixed with Ottawa sand such that the binder weight divided by the weight of Ottawa sand was eight percent. The total weight of mixture was 15 grams. Specimens were prepared individually using a mold with dimensions similar to the DMA specimen. A small tapping rod was used to compact the specimens in the mold. The second method proposed by Zollinger (*9*) and used in this chapter, was developed to test the fine

portion of asphalt mixtures. The DMA specimens were prepared using the fine aggregates from the full mixture instead of Ottawa sand. The proportions of the different sizes of fine aggregates in the DMA specimens were similar to their proportions in the full mixture. The asphalt mastic (binder plus filler) was mixed with the fine aggregates using a mechanical mixer, and the mixture was then aged for two hours at the mixing temperature. The Superpave gyratory compactor (SGC) was used to compact the fine portion of the mixture and prepare gyratory specimens with 152 mm in diameter and 85 mm in height. The target percent air void was 11 percent. SGC specimens were then cored from the top and bottom to obtain DMA specimens. 32 DMA samples were extracted from a SGC specimen using a special coring machine fabricated for this purpose. Figure 3.2(a) shows a gyratory specimen after coring DMA specimens. Prior to test execution, all specimens were glued to sample holders. The details on the design of the mixture for DMA testing and specimen preparation are provided by Zollinger (*9*).

The rheometer used on this study is CVOR-200-050 from Bohlin Instruments. The rheometer is able to apply a torque from 0.1 μN.m to 200 mN.m, a frequency from 10^{-6} to 150 Hz, and to control temperature from -150 to 550ºC. The DMA equipment is shown in Figure 3.2(b).

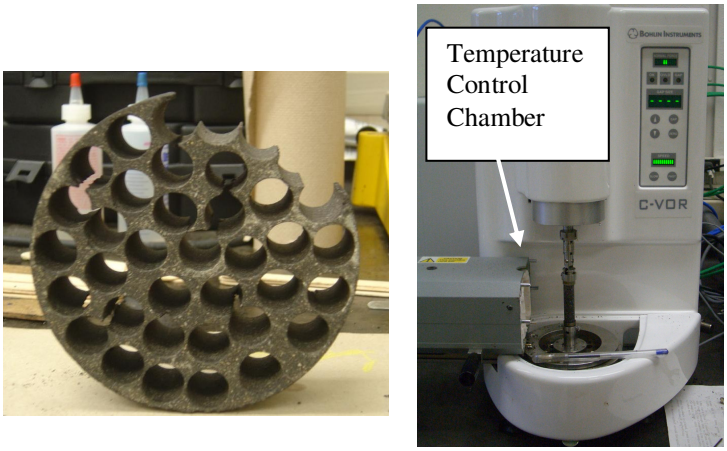

(a) (b)

FIGURE 3.2 (a) Superpave Gyratory Compactor (SGC) Sample (after Dynamic Mechanical Analyzer - DMA Samples Had Been Cored), and (b) Dynamic Mechanical Analyzer - DMA (Bohlin Instruments, CVOR-200-050).

The time sweep mode was used for both the controlled-strain and controlled-stress tests. This specific mode applies a fixed frequency (in this case 10 Hz) with a fixed value of either shear strain or shear stress. During the tests, the DMA sample was subjected to sinusoidal torsional loading. All tests were conducted at 25ºC. Both the controlled-strain and controlled-stress tests were performed in two different stages: (i) using low strain or stress amplitude to obtain material properties in the linear viscoelastic range, and (ii) using high strain or stress amplitude to determine the nonlinear viscoelastic material properties and induce fatigue damage. The testing parameters are shown in Table 3.2. The stresses used in the low amplitude testing were selected to correspond to a strain of 0.0065 percent. The strain used in the high amplitude loading was 0.2 percent. The stresses used in the high amplitude loading in controlled-stress testing corresponded to the stresses measured at 50 percent of the fatigue life in the controlled-strain tests. Data were collected every five cycles, and 128 points per cycle were recorded. Relaxation tests were also performed to determine relaxation moduli as a function of time ($G(t)=\frac{\tau(t)}{\gamma_0}=G_\infty+G_1 t^{-m}$). At least five specimens and a maximum of eight specimens were tested from each mixture in each mode of loading.

The Wilhelmy plate was used to measure the binder surface energy, while the universal sorption device was used to measure the aggregate surface energy using the testing protocols described by Bhasin et al. (*53*). Consequently, the adhesive bond energy between the binder and aggregates was calculated using the measured surface energy components. As shown later, the adhesive bond energy is an input to the model used to predict fatigue resistance.

TABLE 3.2 Dynamic Mechanical Analyzer (DMA) Testing Parameters

Type of Loading	Mixture ID	Test Mode	
		Controlled-Strain (Strain, %)	Controlled-Stress (Stress, Pa)
Low Amplitude Testing (Determine Linear Viscoelastic Properties)	A	0.0065	8,430
	B		3,200
	C		9,310
High Amplitude Testing (Determine Nonlinear Viscoelastic Behavior and Damage Characterization)	A	0.2	105,000
	B		91,400
	C		107,000

THEORY AND ANALYSIS METHODS

Basics of Controlled-Strain versus Controlled-Stress Loading

DMA measurements can be conducted in either the controlled-strain or controlled-stress mode of loading. In the controlled-strain test, the applied stress amplitude is adjusted throughout the test such that the resulting strain remains constant. This condition requires that the stress amplitude is reduced as the material damage increases. The stiffness of the undamaged portion of the material and the amount of damage play an important role in determining the value of the applied stress. For example, a material that has a low undamaged stiffness will require less stress to achieve the same strain compared with another material that has high stiffness. Therefore, it is usually noticed that fatigue life increases as mixture stiffness decreases due to reduction in applied stress

in controlled-strain tests. In the controlled-stress mode, the specimen is subjected to the same stress function throughout the test, and the strain response is a function of the mixture stiffness and the amount of induced damage.

The difference between controlled-strain and controlled-stress testing can be explained with the aid of the Paris crack propagation law for an elastic material. Paris' law can be written in the following form (*54*):

$$\frac{da}{dN} = c\left(\Delta k\right)^{d} \tag{3.1}$$

where, a is the crack length; N is the number of load cycles; $\Delta k = k_{max} - k_{min}$, k_{max} is the maximum value of the stress intensity factor; and k_{min} is the minimum value of the stress intensity factor in the load cycle. c and d are material constants that can be determined experimentally. The stress intensity factor can be defined as follows:

$$k = f(a)\sigma\sqrt{\pi a} \tag{3.2}$$

where, $f(a)$ is a function that depends on the crack and specimen geometry. The increase in the crack length leads to a rapid increase in the stress intensity factor until it reaches the fracture toughness (k_c) of the material and unstable crack propagation takes place. In a controlled-strain test, however, the strain amplitude is constant and the stress difference ($\Delta\sigma$) decreases as the crack propagates. The reduction in stress makes the crack propagation under controlled-strain loading less rapid than in the controlled-stress mode when both tests start at the same $\Delta\sigma$ value. In a controlled-strain test, the stress magnitude might decrease to a value below an amplitude at which the material can support very high or infinity number of load cycles without failure. At this level, which is typically referred to as the endurance limit, the stress intensity factor does not reach the material fracture toughness. This is consistent with experimental observations that: (i) complete failure or rupture of specimens is less likely to occur in controlled-strain tests compared with controlled-stress tests, and (ii) controlled-strain test requires more loading cycles than controlled-stress test to cause the same level of damage when both tests begin at the same stress amplitude.

Dissipated Pseudo Strain Energy (DPSE)

The stress-pseudo strain relationship within the framework of continuum damage mechanics has been used for the characterization of damage in asphalt mixtures. The underlying concept in this approach is based on separating the energy that is dissipated due to damage from the viscoelastic energy. Two tests are needed to develop the stress-pseudo strain relationship. The first test is conducted at small strain or stress values that are used to determine the linear viscoelastic properties. Then, a fatigue test is conduced at a higher strain or stress values in order to induce damage and characterize the asphalt mixture's fatigue resistance. In principle, it is possible to induce damage by conducting long term fatigue loading at the same strain or stress values that are used to determine the linear viscoelastic properties. However, this approach is time consuming and it might even prohibit characterization of fatigue damage if the applied strain or stress magnitudes are within the asphalt mixture endurance limit.

Under sinusoidal stress loading, the stress (τ) and strain (γ) functions for an undamaged viscoelastic material are described using Equations 3.3 and 3.4, respectively.

$$\tau = \tau_0 \sin(wt) \tag{3.3}$$

$$\gamma = \gamma_{0VE} \sin(wt - \delta_{VE}) \tag{3.4}$$

where, τ_0 and γ_{0VE} are the stress and strain amplitudes respectively, w is the angular frequency, t is the time, and δ_{VE} is the viscoelastic phase angle between the strain and stress responses. The subscript "VE" refers to viscoelastic properties that the material would attain if it did not exhibit damage at the strain and stress amplitudes used in the fatigue test. As it will be discussed later, "VE" can refer to either linear or nonlinear viscoelastic responses or properties. The "0" subscript refers to the amplitude of the strain sinusoidal function.

The pseudo energy can be calculated using a pseudo stress-strain relationship or using a stress-pseudo strain relationship. The latter relationship is formulated here in

order to allow direct comparison between the results from the controlled-strain and controlled-stress tests. Under controlled-strain fatigue loading, the applied strain (γ) and the stress (τ) response will have the forms in Equations 3.5 and 3.6, respectively.

$$\gamma = \gamma_{0F} \sin(wt) \tag{3.5}$$

$$\tau = \tau_{0NF} \sin(wt + \delta_{NF}) \tag{3.6}$$

where, the "F" subscript indicates that the labeled quantities (strain, stress, material properties) are associated with the fatigue test. The "N" subscript is used to indicate that the parameter changes as a function of the number of loading cycles. The pseudo strain (γ^R) is given by:

$$\gamma^R = \frac{G^*_{VE} \gamma_{0F} \sin(wt + \delta_{VE})}{G_R} \tag{3.7}$$

where, G^*_{VE} is the dynamic modulus, G_R is the reference modulus (its selection is discussed later). Basically, the pseudo strain is the viscoelastic stress response of the material divided by G_R assuming that the material is not damaged under the applied strain function shown in Equation 3.5.

Under controlled-stress fatigue loading, the applied stress (τ) and the strain (γ) response will have the forms in Equations 3.8 and 3.9, respectively.

$$\tau = \tau_{0F} \sin(wt) \tag{3.8}$$

$$\gamma = \gamma_{0NF} \sin(wt - \delta_{NF}) \tag{3.9}$$

If the material is undamaged and subjected to the strain function in Equation 3.9, then the corresponding undamaged stress for this strain is shown in Equation 3.10:

$$\tau = G_{VE}^{*}\gamma_{0NF}\sin(wt - \delta_{NF} + \delta_{VE}) \tag{3.10}$$

The pseudo strain under controlled-stress loading is the function in Equation 3.10 divided by the reference modulus:

$$\gamma^{R} = \frac{G_{VE}^{*}\gamma_{0NF}\sin(wt - \delta_{NF} + \delta_{VE})}{G_{R}} \tag{3.11}$$

The various stress-pseudo strain behaviors are illustrated in Figure 3.3 for different material conditions (linear viscoelastic, nonlinear viscoelastic, and damage). Consider the case where the linear viscoelastic condition is taken as the reference undamaged state (the linear viscoelastic properties are used in the pseudo strain functions in Equations 3.7 and 3.11), and the fatigue test starts with a stress amplitude within the linear viscoelastic range. In this case, $\delta_{NF} = \delta_{VE}$ and the stress-pseudo strain response will be represented by the line "I" because Equations 3.8 and 3.11 are in phase. If the applied stress increases but remains within the linear viscoelastic range, then the stress-pseudo strain relationship will be represented by the line labeled "II" in Figure 3.3. However, an increase in stress can cause one of the following responses: (i) damage of the linear viscoelastic material, (ii) nonlinear viscoelastic response of the intact (undamaged) material, or (iii) combined nonlinear viscoelastic response of the intact material and damage.

A decrease in the modulus and an increase in the phase angle relative to the linear viscoelastic properties also occur due to the nonlinear behavior of the intact material. However, as pointed out by Si et al. (*22*), the nonlinear viscoelastic properties (phase angle and modulus) and the nonlinear hysteresis loop remain unchanged as further loading is applied. This behavior is represented in Figure 3.3 by the curve labeled "III" that does not shift to position "IV" with further loading as long as damage is not initiated. Damage is identified by a decrease in the modulus and an increase in the phase angle relative to the nonlinear viscoelastic properties. The values of these

properties as well as the area of the hysteresis loop continue to change as loading cycles are applied.

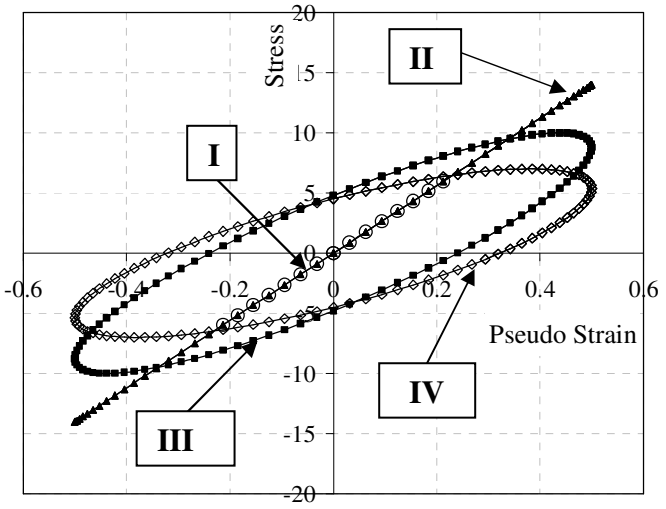

FIGURE 3.3 Illustrations of the Different Possible Responses of Stress-Pseudo Strain Relationships for Different Regions: (I) Linear Viscoelastic, Low Stress Amplitudes; (II) Linear Viscoelastic, Higher Stress Amplitudes Compared to (I); (III) Nonlinear Viscoelastic Response; and (IV) Damage Response.

It is also possible that the response combines both nonlinear viscoelastic behavior and damage. The energy associated with the nonlinear viscoelastic behavior can be separated from damage by properly selecting strain and stress amplitudes used in the fatigue test. These amplitudes can be selected such that no damage is observed (no change in the stress-pseudo strain relation) for a number of load cycles. Following this, loading can proceed in order to determine the energy associated with damage. Once the nonlinear viscoelastic properties are determined, they can be used as G^*_{VE} and δ_{VE} in Equations 3.7 and 3.11 in order to calculate the pseudo strain that accounts for the undamaged nonlinear state at the high strain and stress used in the fatigue test. In this case, Curve "III", in Figure 3.3 will become a line indicating that there is no damage at this state of stress.

Fatigue damage in HMA is manifested as an increase in the apparent phase angle, and a decrease in the pseudo stiffness. The term "apparent" is used here to indicate that this phase angle accounts for the effect of damage and it is not the same as the phase angle associated with viscoelastic deformation. In controlled-strain loading, the decrease in stiffness is associated with a decrease in the applied stress and a decrease in the area of the hysteresis loop, while the increase in the apparent phase angle causes an increase in the hysteresis loop. As such, the two manifestations of damage (increase in phase angle and decrease in stiffness) have opposing effects on the hysteresis loop area but with the net results being a decrease in the area. In controlled-stress loading, changes in both the apparent phase angle and stiffness cause an increase in the hysteresis loop area. Hence, the effect of damage on the hysteresis loop area depends on the mode of loading, and consequently, the loop areas calculated from the two modes of loading are not comparable.

A new approach is proposed here by which to calculate the DE. This approach divides the DPSE in three components. The first component accounts for damage that causes an increase in the apparent phase angle and an increase in the hysteresis loop with respect to a reference modulus that represents the intact undamaged material. For controlled-strain loading, the hysteresis loop area in the stress-pseudo strain domain can be represented by the following expression:

$$DPSE = \pi \tau_{0NF} \gamma_0^R \sin(\delta_{NF} - \delta_{VE}) \tag{3.12}$$

The above equation can also be written as follows:

$$DPSE = \pi \tau_{0NF} \frac{\tau_{0VE}}{G_R} \sin(\delta_{NF} - \delta_{VE}) = \pi \tau_{0NF} \frac{G_{VE}^* \gamma_{0F}}{G_R} \sin(\delta_{NF} - \delta_{VE}) \tag{3.13}$$

The reference modulus G_R can be selected to be equal to the undamaged modulus G^*_{VE}. This selection has the advantage of making the amplitude of the pseudo strain equal to the amplitude of the actual strain. The DPSE becomes equal to:

$$DPSE = \pi\tau_{0NF}\gamma_{0F}\sin(\delta_{NF} - \delta_{VE}) = \pi G^*_{NF}\gamma^2_{0F}\sin(\delta_{NF} - \delta_{VE}) \quad (3.14)$$

As discussed earlier, as the level of material damage increases, the modulus G^*_{NF} decreases while the apparent phase angle δ_{NF} increases, and the net result is a decrease in the DPSE. The effect of these two factors can be separated by dividing the DPSE by the ratio of the damage stiffness to the undamaged stiffness $\left(\frac{G^*_{NF}}{G^*_{VE}}\right)$ as follows:

$$W_{R1} = \pi G^*_{VE}\gamma^2_{0F}\sin(\delta_{NF} - \delta_{VE}) \quad (3.15)$$

The above expression gives the dissipated energy due to an increase in the apparent phase angle at a given reference undamaged modulus. It can also be viewed as the change in the viscoelastic energy $G^*_{VE}\gamma^2_{0F}$ due to damage that is quantified by the change in the phase angle from δ_{VE} to δ_{NF}.

The second component of the DE is due to permanent deformation caused by the loading and unloading within each cycle. The hysteresis loop area divided by $\left(\frac{G^*_{NF}}{G^*_{VE}}\right)$ is always larger than the area calculated using Equation 3.15. The difference between the actual hysteresis loop and the idealized loop (Figure 3.4) is attributed to permanent deformation in the mixture and is denoted as W_{R2}. During the first quarter of a loading cycle, damage is induced due to the increase in stress magnitude. Upon unloading in the second quarter of the cycle, some permanent strain remains in the specimen, which is manifested by a variable apparent phase angle within the cycle.

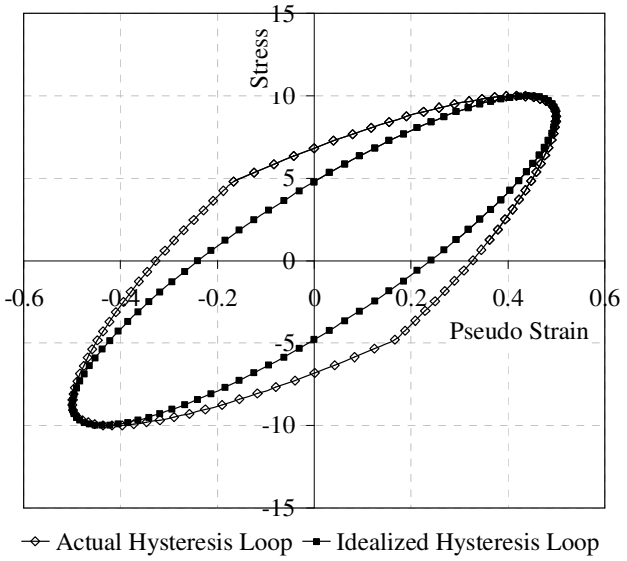

FIGURE 3.4 Illustrations of the Idealized Hysteresis Loop and Actual Hysteresis Loop.

The third component of the DE (W_{R3}) is associated with the difference between the pseudo stiffness of the undamaged material and the pseudo stiffness after damage. The DE associated with the reduction in the pseudo stiffness is calculated as follows:

$$W_{R3} = \frac{1}{2}\gamma_{0F}^{R}\left(\tau_{0VE} - \tau_{0NF}\right) = \frac{1}{2}\frac{\tau_{0VE}}{G_R}(\tau_{0VE} - \tau_{0N}) \tag{3.16}$$

and for $G_R = G_{VE}^{*}$, W_{R3} becomes:

$$W_{R3} = \frac{1}{2}\frac{G_{VE}^{*}\gamma_{OF}}{G_{VE}^{*}}\left(G_{VE}^{*}\gamma_{OF} - G_{NF}^{*}\gamma_{OF}\right) = \frac{1}{2}\gamma_{OF}^{2}\left(G_{VE}^{*} - G_{NF}^{*}\right) \tag{3.17}$$

The same analysis presented above can be applied in the controlled-stress case, and the DPSE can be written as in Equation 3.18:

$$DPSE = \pi\tau_{0F}\gamma_{0NF}\sin(\delta_{NF} - \delta_{VE}) = \pi\frac{\tau_{0F}^2}{G_{NF}^*}\sin(\delta_N - \delta_{VE}) \quad (3.18)$$

The above equation is multiplied by $\left(\frac{G_{NF}^*}{G_{VE}^*}\right)$ in order to calculate the DE in the hysteresis loop at the reference undamaged pseudo stiffness. The expression for W_{R1} becomes:

$$W_{R1} = \pi\frac{\tau_{OF}^2}{G_{VE}^*}\sin(\delta_{NF} - \delta_{VE}) \quad (3.19)$$

The above expression has the same significance as in controlled-strain loading as it represents the effect of damage, which changes the phase angle from δ_{VE} to δ_{NF} on the viscoelastic energy $\frac{\tau_{OF}^2}{G_{VE}^*}$. The expression for W_{R3} is:

$$W_{R3} = \frac{1}{2}\tau_{0F}(\gamma_{0NF}^R - \gamma_{0VE}^R) = \frac{1}{2}\tau_{0F}\left(\frac{G_{VE}^*\tau_0}{G_{NF}^*G_R} - \frac{G_{VE}^*\tau_0}{G_{VE}^*G_R}\right) \quad (3.20)$$

and for $G_R = G_{VE}^*$, W_{R3} becomes:

$$W_{R3} = \frac{1}{2}\tau_{0F}^2\left(\frac{1}{G_{NF}^*} - \frac{1}{G_{VE}^*}\right) \quad (3.21)$$

Fracture-Based Analysis Approach for Asphalt Mixtures

The fracture model adopted in this study is based on Paris' law written in terms of the *J*-integral of the DPSE for viscoelastic materials (*10*):

$$\frac{d\bar{r}}{dN} = A[J_R]^n \tag{3.22}$$

where, $\bar{r}$ is the average crack radius in the specimen, A and n are material constants, and J_R is the J-integral, which is the pseudo strain energy release rate per unit of crack area evaluated within a region represented by the dashed curve in Figure 3.5. J_R is defined in Equation 3.23.

$$J_R = \frac{\frac{\partial W_R}{\partial N}}{\frac{\partial (c.s.a)}{\partial N}} \tag{3.23}$$

where, W_R is the DPSE ($W_{R1}+W_{R2}+W_{R3}$), and $c.s.a$ is the crack surface area, which is equal to $2\pi\bar{r}^2$ for a circular crack with radius equal to $\bar{r}$.

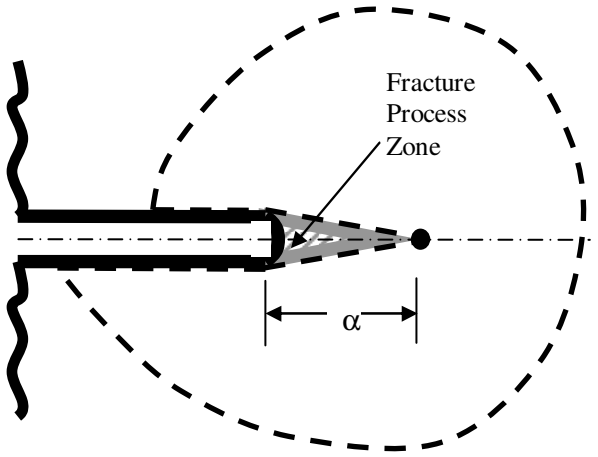

FIGURE 3.5 Schematic of the Crack Radius and Fracture Process Zone.

Integration of Equation 3.22 yields the following expression for the crack size as a function of loading cycles.

$$\bar{r}(N) = \left(\frac{2n+1}{n+1}\right)^{\frac{n+1}{2n+1}} \left(\frac{A}{(4\pi M)^n}\right)^{\frac{1}{2n+1}} \left(\int_{N=0}^{N} \left(\frac{\partial W_R}{\partial N}\right)^{\frac{n}{n+1}} dN\right)^{\frac{n+1}{2n+1}} \tag{3.24}$$

where, M is the number of cracks in a specimen and n is a function of the exponent of time in the power law equation of relaxation modulus. As shown by Lytton et al. (*16*) and Masad et al. (*10*), A can be expressed as follows:

$$A = K\left[\frac{G_R}{G_1 \Delta G_f}\right]^n \tag{3.25}$$

where, K is a constant for each material that is inversely proportional to the square of the tensile strength of the asphalt mixtures. ΔG_f is the adhesive bond energy. It was determined based on the analysis of experimental measurements in this study that the relationship between W_R and number of cycles N can be described by either $W_R = a + b\ Ln(N)$ or $W_R = a + cN^b$. For the $W_R = a + b\ Ln(N)$ relationship, Equation 3.24 can be written as in Equation 3.26:

$$\begin{aligned} \bar{r}(N) &= K^{\frac{1}{2N+1}} (2n+1)^{\frac{n+1}{2n+1}} \left(\frac{A}{(4\pi M)^n}\right)^{\frac{n}{2n+1}} b^{\frac{n}{2n+1}} N_f{}^{\frac{1}{2n+1}} \\ \bar{r}(N) &= K^{\frac{1}{2n+1}} (2n+1)^{\frac{n+1}{2n+1}} \left(\frac{G_R}{4\pi M G_1 \Delta G_f}\right)^{\frac{n}{2n+1}} b^{\frac{n}{2n+1}} N_f{}^{\frac{1}{2n+1}} \end{aligned} \tag{3.26}$$

where, N_f is the number of loading cycles at failure.

The influence of M cracks can be replaced by an equivalent crack with radius equal to $\bar{r}$. It was found by Masad et al. (*10*) that the variability in the analysis of the crack radius can be reduced by normalizing with respect to tensile strength or the K parameter. Consequently, the fracture equation can be written as follows:

$$R(N) = \frac{\bar{r}(N)}{K^{\frac{1}{2n+1}}} = \left[(2n+1)^{n+1}\left(\frac{G_R b}{4\pi G_1 \Delta G_f}\right)^n N\right]^{\frac{1}{2n+1}} \tag{3.27}$$

Depending on the applied strain or stress amplitude, energy might be dissipated in the first loading cycle ($a \neq 0$ in W_R - N relationship), and the initial damage should be accounted for in the fracture equation. Therefore, the fracture equation is written as follows to account for initial damage:

$$\Delta R(N) = R(N) - R_1 = \left[(2n+1)^{n+1} \left(\frac{G_R b}{4\pi G_1 \Delta G_f} \right)^n N \right]^{\frac{1}{2n+1}} \tag{3.28}$$

where, R_1 represents the crack radius due to initial damage in the mixture. Following the above derivation but for the relationship $W_R = a + cN^b$ yields Equation 3.29 for the fracture radius:

$$\Delta R(N) = R(N) - R_1 = \left[\left(\frac{2n+1}{nb+1} \right)^{n+1} \left(\frac{G_R bc}{4\pi G_1 \Delta G_f} \right)^n N^{nb+1} \right]^{\frac{1}{2n+1}} \tag{3.29}$$

The viscoelastic properties of the intact material ahead of the crack affect the rate of crack propagation (Figure 3.5). Schapery (*55*) derived the relationship between the exponent n in Equation 3.22 and m, which is the exponent of time in the power law equation of the relaxation modulus ($G(t) = G_\infty + G_1 t^{-m}$). He found that if the surface energy of the material and the fracture process zone with length α ahead of the crack are constants, then $n = 1/m$. If the tensile strength of the material and surface energy are constants during fracture, then $n = 1 + 1/m$. The third case is when the crack opening displacement at the left end of the failure zone and α are constants. In this case, $n = 1/(m \times (1+C))$. C is the nonlinearity exponent for the continuum in the neighborhood of the crack tip. The analysis of the experimental measurements presented later in this chapter demonstrates that J_R is not constant during loading, and hence α is not constant. Therefore, the relationship $n = 1 + 1/m$ is adopted to represent the case of constant surface energy and constant tensile strength.

ANALYSIS AND RESULTS

The data analysis focuses on: (i) the ability of the DE (W_R) and fracture radius ($R(N)$) to describe the results from both controlled-strain and controlled-stress tests, (ii) the DE associated with permanent deformation (W_{R2}) and the influence of mode of loading on this energy, and (iii) the variability in a number of parameters used to characterize the fatigue resistance of HMA based on DMA testing. The average parameters used in Equation 3.28 are shown in Table 3.3.

TABLE 3.3 Average Model Parameters That Are Common for the Different Analysis Methods

Parameter	Mixture A	Mixture B	Mixture C
G_1 (Pa)	40,916,094	30,064,608	12,091,724
m	0.34	0.54	0.45
n	3.94	2.85	3.22
ΔG_f (Jole/m^2)	0.0916	0.0875	0.0813

Controlled-Strain versus Controlled-Stress Loading

The mixtures evaluated in this study exhibited very rapid changes in the measured properties within the first 20 cycles, and the change in material properties occurred at a much lower rate afterwards. Also, there was substantial variability (around 10 percent) in the measured properties within the first few cycles, and this variability decreased significantly (down to less than three percent) after about 20 loading cycles. If the response in the first 20 cycles was associated with actual damage, then change in material properties should have continued at an increasing rate with further loading especially in the controlled-stress test mode, which was not the case. As such, it is reasonable to assume that the response in the first 20 cycles is primarily due to material conditioning. Thus the measurements of material properties and DE was selected for this study to start at *N=20*, and the term first cycle used herein refers to *N=20*.

As discussed earlier, the controlled-stress test was conducted at stress amplitude equal to about 50 percent of the initial stress recorded for the same material tested in the controlled-strain mode. Three cases are considered in the data analysis in order to determine whether the changes in materials properties are due to nonlinearity of intact material, damage, or both. In case 1, it is assumed that all the energy is attributed to damage and the nonlinear behavior of the intact material is negligible. In this case, the viscoelastic properties used in Equations 3.7 and 3.11 are those determined from the linear viscoelastic test.

In the second analysis (Case 2), it is assumed that the energy in the first cycle in both modes of loading is all due to nonlinearity of the intact undamaged material, and this energy should be subtracted from the hysteresis loop area of all cycles when the damage energy is calculated. This case implies that R_1 in Equations 3.28 and 3.29 is zero for both modes of loading, and the viscoelastic properties used in Equations 3.7 and 3.11 are those determined from the first cycle of the fatigue test for each mode of loading. The controlled-strain test has a higher initial strain than the controlled-stress test, and the properties in the first cycle are different in these two tests. It is emphasized that using the viscoelastic properties from the first cycle of the fatigue test causes the area of the hysteresis loop to vanish in the first cycle (Curve "III" in Figure 3.3 becomes a line), which is equivalent to the nonlinearity correction term that was introduced by Si et al. (*22*).

The third analysis (Case 3) is an intermediate case between cases 1 and 2; the energy dissipation in the first cycle is attributed to both nonlinear behavior of the intact material and damage. In other words, the intact part of the asphalt mixture exhibits nonlinear behavior, and at the same time the stresses in the fatigue test are high enough to cause damage. The viscoelastic properties for this case should be between those used in cases 1 and 2. It was found that the difference in energy between cases 1 and 2 for the controlled-stress test is very small, and consequently, the initial damage in the controlled-stress test was small compared with the controlled-strain test. As such, the

viscoelastic properties in Equations 3.7 and 3.11 are selected to be those of the first cycle of the controlled-stress test (cases 2 and 3 are the same for the controlled-stress test).

The parameter $R(N_f)$ represents the crack radius in the material at the end of the fatigue test. This parameter should be the same for a given mixture irrespective of the testing mode. The data analysis provides the value of $\Delta R(N_f)=R(N_f)-R_1$, while R_1 is a function of the energy dissipated due to the initial damage in the mixture. The comparison between controlled-strain results and controlled-stress results in terms of $\Delta R(N_f)$ are shown in Figure 3.6. The results from case 3 are the closest to the equality line.

The difference in R_1, which is related to the initial DE, between controlled-strain and controlled-stress tests should be considered in order to compare the results based on $R(N_f)$ rather than $\Delta R(N_f)$. In case 1, the initial energy for the controlled-strain loading is much higher than that of the controlled-stress loading (an example result is in Figure 3.7). As such, the initial crack radius R_1 for controlled-strain is expected to be higher than that of the controlled-stress, which means that the data points in Figure 3.6 will shift to the right farther away from the equality line if $R(N_f)$ is plotted in this figure instead of $\Delta R(N_f)$.

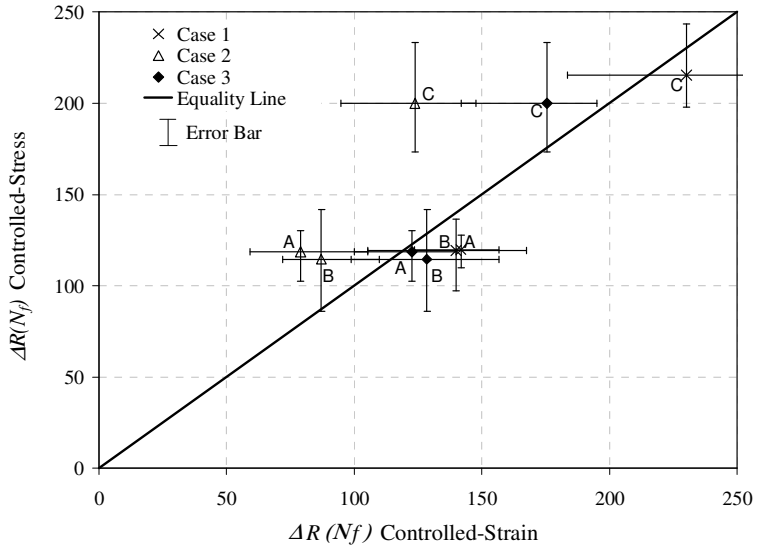

FIGURE 3.6 $\Delta R(N_f)$ for Cases 1, 2 and 3 Analyses.

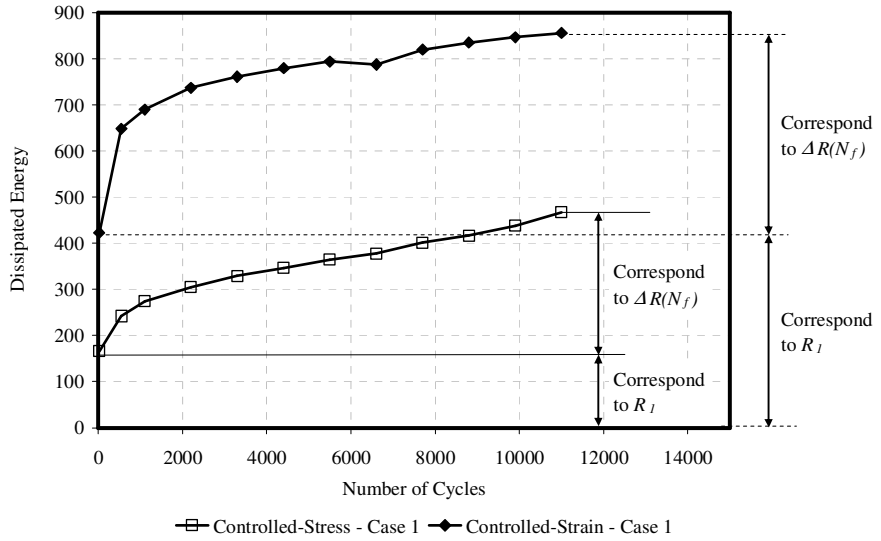

FIGURE 3.7 Examples of the Dissipated Energy (DE) in Controlled-Strain and Controlled-Stress Loading for Case 1 Analysis.

As discussed earlier, R_1 is equal to zero and the points for case 2 will be the same for $R(N_f)$ and $\Delta R(N_f)$ plots (all initial energy is assumed to be due to nonlinearity). The results from case 2 are away from the equality line indicating that assuming all the initial energy in both tests to be due to nonlinearity is not accurate and does not unify the results from the two modes of loading. This is supported by the finding that the material properties for the controlled-strain test changed from the beginning of the testing indicating that damage occurred from the first cycle in this test. In case 3, R_1 is taken to be zero for the controlled-stress test (no initial damage), but there is some damage in the controlled-strain test. In this case, the data points in Figure 3.6 will shift to the left (less than the shift in case 1) for $\Delta R(N_f)$, but the points will remain closer to the equality line than the other two cases. As such, the case 3 analysis seems to be able to unify the results from both modes of loading.

The relationship between W_{R1} to W_{R3} is plotted in Figure 3.8. The two modes of loading give the same ratio of these two components of energy dissipation for case 3 only. These results prove once again that proper proportioning of the nonlinear

viscoelastic energy and damage energy leads to unification of the results from the two modes of loading.

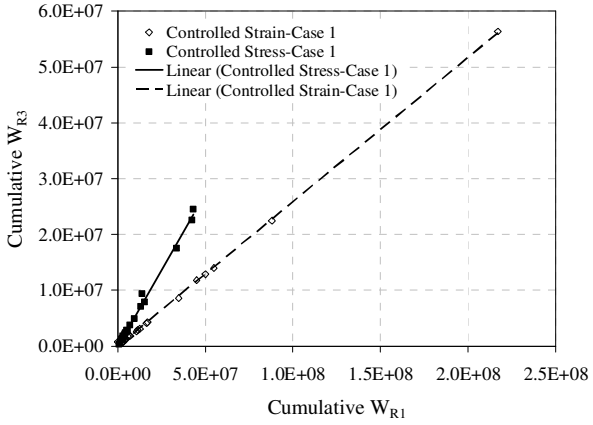

(a) Case 1

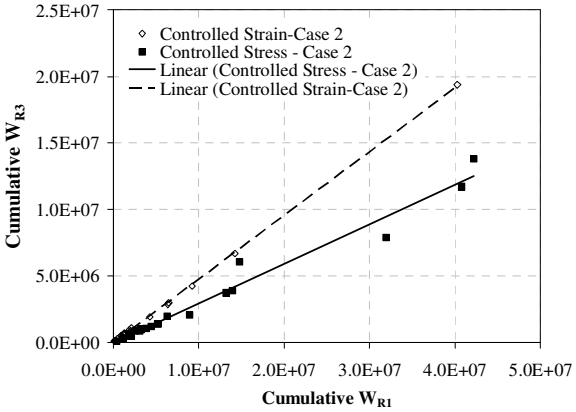

(b) Case 2

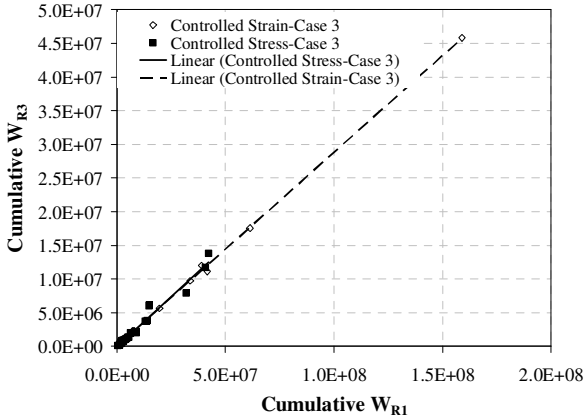

(c) Case 3

FIGURE 3.8 The Relationship between W_{R3} and W_{R1} for Cases 1, 2 and 3 Analyses.

Dissipated Energy (DE) Due to Permanent Deformation

As discussed earlier in this chapter, part of the area in the hysteresis loop is attributed to permanent deformation (W_{R2}). W_{R2} is determined by subtracting W_{R1} from the hysteresis loop area. The W_{R2} (%) with respect to the hysteresis loop area is shown in Figure 3.9. First, it is evident that this percentage is much smaller for the controlled-strain loading. This is attributed to the method used in the DMA device to control the strain and stress functions. In the controlled-strain loading, the DMA adjusts the strain function continuously in order to have a sinusoidal function with a constant phase angle throughout the cycle. However, this is not the case for the controlled-stress loading. Here the strain function does not have a constant phase angle at all points within the cycle due to the accumulation of permanent deformation in the loading phase of each cycle. Based on this discussion, the controlled-stress loading is better suited to capture W_{R2}. It is interesting to note that the percentage of the hysteresis loop determined to be permanent deformation, W_{R2}, is much less for mixture A, which is known to perform much better than either mixtures B or C. It should be emphasized that permanent deformation represented as W_{R2} is not due to plastic flow only, but also includes the effect of cracking as it contributes to permanent strain at a stress free state.

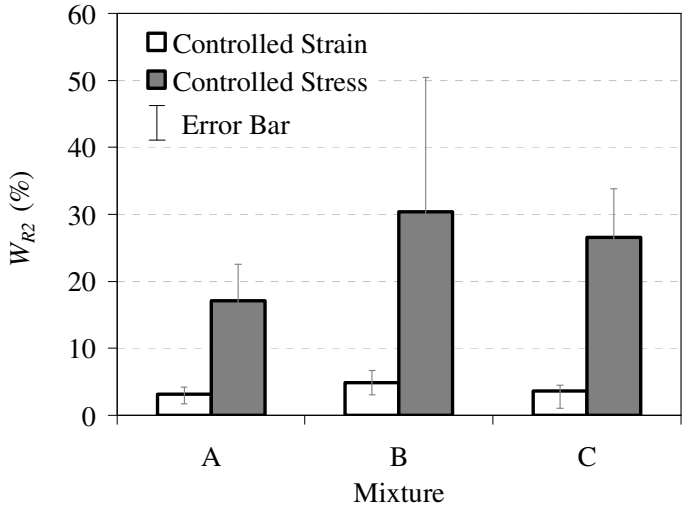

FIGURE 3.9 W_{R2} (%) in Controlled-Strain and Controlled-Stress Modes of Loading.

Selection of Fatigue Damage Parameters

A number of parameters have been proposed in the past to represent fatigue damage. The first parameter is the number of cycles to failure, which is defined in Figure 3.10 by the peak of the function $N \times G'/G$, where G' is the modulus at a certain number of cycles and G is the initial modulus. The second parameter is the cumulative DE at the failure point. The average, standard deviation and coefficient of variation for these two parameters are shown in Tables 3.4 and 3.5. The average values of these two parameters show that mixture A is superior to mixtures B and C, which are shown to perform comparably. However, the coefficients of variation of these two parameters are very high, which is an undesirable characteristic that might limit their ability to differentiate among the performances of asphalt mixtures.

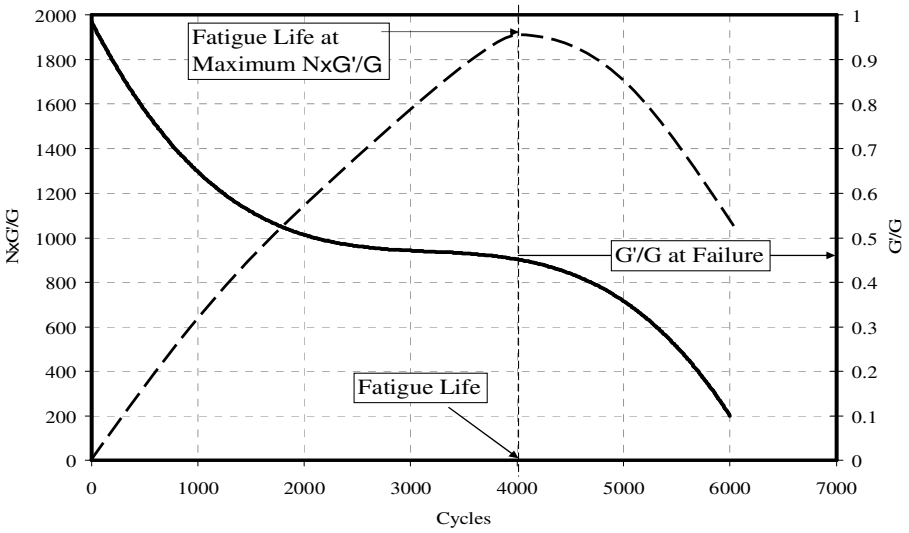

FIGURE 3.10 Schematic Definition of the Failure Point.

TABLE 3.4 Statistical Parameters of the Number of Cycles at Failure

Analysis Case	Mixture ID	Controlled-Strain			Controlled-Stress		
		Ave.	St. Dev.	CV (%)	Ave.	St. Dev.	CV (%)
1, 2, 3	A	69,000	51,413	74.51	139,600	62,870	45.04
	B	6,325	3,345	52.88	22,000	15,492	70.42
	C	7,750	4,047	52.21	20,875	11,731	56.19

TABLE 3.5 Statistical Parameters of the Cumulative Dissipated Energy (DE)

Analysis Case	Mixture ID	Controlled-Strain			Controlled-Stress		
		Ave.	St. Dev.	CV (%)	Ave.	St. Dev.	CV (%)
1	A	1.03×10^{8}	7.9×10^{7}	77.03	4.60×10^{7}	1.94×10^{7}	42.20
	B	5.93×10^{6}	2.06×10^{6}	34.70	5.59×10^{6}	3.89×10^{6}	69.63
	C	1.18×10^{7}	7.29×10^{6}	61.75	8.34×10^{6}	5.00×10^{6}	59.99
2	A	1.98×10^{7}	1.84×10^{7}	92.81	3.74×10^{7}	1.57×10^{7}	42.04
	B	1.44×10^{6}	8.52×10^{5}	59.00	3.91×10^{6}	3.06×10^{6}	78.41
	C	1.61×10^{6}	1.03×10^{6}	64.33	$6.56\text{E}\times10^{6}$	4.38×10^{6}	66.69
3	A	7.60×10^{7}	5.97×10^{7}	78.66	3.74×10^{7}	1.57×10^{7}	42.04
	B	4.99×10^{6}	3.05×10^{6}	61.19	3.91×10^{6}	3.06×10^{6}	78.41
	C	6.03×10^{6}	3.25×10^{6}	53.88	6.56×10^{6}	4.38×10^{6}	66.69

In this study, we propose two parameters that have reasonable coefficients of variation and at the same time demonstrate an improved ability to characterize fatigue

properties of mixtures. The first parameter is the projected crack radius $\Delta R(N_f)$ at a fixed number of cycles, which is chosen to be 50,000 in this study. The results are shown in Table 3.6. The coefficient of variation for this parameter ranges from about four percent to about 28 percent. Most of the coefficients of variation values are less than 15 percent. The second parameter is the ratio of $\Delta R(N_f)$ to $ln(N)$, which is summarized in Table 3.7. The choice of this parameter was motivated by the finding that the $\Delta R(N)$ to $ln(N)$ relationship is linear for the majority of the test specimens, and the parameter is approximately equal to the value of the slope of this relationship. The coefficient of variation of this parameter ranges between approximately four percent and 22 percent. Both of the two parameters indicate that mixture A performs best, mixture C performs poorest, and mixture B is intermediate. This finding is consistent with the field experience of these mixtures as reported by Zollinger (*9*).

TABLE 3.6 Statistical Parameters of $\Delta R(N_f)$ at *N=50,000* Cycles

Analysis Case	Mixture ID	Controlled-Strain			Controlled-Stress		
		Ave.	St. Dev.	CV (%)	Ave.	St. Dev.	CV (%)
1	A	139.95	12.75	9.11	108.57	8.64	7.95
	B	197.30	45.20	22.91	139.40	8.61	6.18
	C	301.08	28.48	9.46	246.59	9.14	3.71
2	A	78.37	8.14	10.38	96.81	20.14	20.80
	B	121.68	20.20	16.60	178.69	49.61	27.76
	C	161.83	18.25	11.28	283.25	37.41	13.21
3	A	122.34	9.91	8.10	96.85	20.15	20.80
	B	179.03	22.94	12.81	174.44	48.43	27.76
	C	229.97	15.07	6.55	276.26	36.48	13.21

TABLE 3.7 Statistical Parameters of the Ratio of $\Delta R(N_f)$ to $ln(N)$

Analysis Case	Mixture ID	Controlled-Strain			Controlled-Stress		
		Ave.	St. Dev.	CV (%)	Ave.	St. Dev.	CV (%)
1	A	12.98	1.12	8.63	10.25	0.80	7.76
	B	16.46	3.53	21.42	12.22	0.82	6.70
	C	26.15	2.58	9.85	21.97	0.87	3.96
2	A	7.29	0.78	10.66	10.16	1.17	11.48
	B	10.17	1.62	15.97	11.70	1.34	11.46
	C	14.06	1.64	11.65	20.36	1.19	5.85
3	A	11.36	0.78	6.90	10.16	1.17	11.48
	B	14.97	1.84	12.29	11.70	1.34	11.46
	C	19.97	1.32	6.63	20.36	1.19	5.85

IMPLICATIONS IN THE ANALYSIS OF ASPHALT MIXTURES AND PAVEMENTS

The analysis presented in this chapter focused on calculating the crack growth index ($R(N)$) based on DMA measurements of a FAM. However, the same method is applicable for analysis of fatigue resistance of asphalt mixtures subjected to dynamic loading. Similar to the testing program discussed in this chapter, asphalt mixture testing should include small strain or stress amplitude loading to determine the viscoelastic properties (G_1 and n in Equations 3.28 and 3.29), and fatigue dynamic loading in order to induce damage and calculate the parameter b in Equations 3.28 and 3.29.

The mixture crack growth index can also be used to analyze the fatigue resistance of asphalt pavements. However, this requires using a structural finite element (FE) model that incorporates a nonlinear viscoelastic representation of the asphalt layer. This model can then be used to calculate DPSE within the asphalt pavement layer as a function of loading cycles and applied stresses. Consequently, the parameters b and $R(N)$ in Equations 3.28 and 3.29 can be calculated as indicators of fatigue damage. Recent efforts have already focused on developing a structural FE model with a nonlinear viscoelastic representation of the asphalt layer (*46, 56*). Current research by some of the authors of this chapter focuses on using these structural FE models and the crack growth index in predicting fatigue damage in asphalt pavements.

CONCLUSIONS

Fatigue damage is one of the most frequently encountered distresses in flexible pavements. This study focuses on the development of a fracture-based approach for DMA of asphalt mixtures that is independent of the mode of loading used in testing. Although the experiments and analysis of this study were based on FAM, the approach can be applied to the dynamic analysis of full asphalt mixtures.

Three asphalt mixtures were subjected to DMA testing using: (i) low strain/stress amplitudes, and (ii) high strain/stress amplitudes. The low amplitude loading was used to determine the linear viscoelastic material properties, while the high amplitude loading is used to determine the nonlinear viscoelastic properties and DE associated with damage.

A new analysis approach was developed in this study that considers pseudo strain energy to consist of two parts: (i) the nonlinear response of the intact part of the mixture, and (ii) damage. Furthermore, the damage energy was shown mathematically to consist of: (i) a component that is associated with an increase in the apparent phase angle and increase in the hysteresis loop (W_{R1}), (ii) a component that accounts for permanent deformation (W_{R2}), and (iii) a component that accounts for the change in pseudo stiffness due to damage (W_{R3}). This new approach is able to unify the results of the controlled-strain and controlled-stress modes of loading when proper partitioning of the energy between nonlinearity and damage is achieved. The ratio of W_{R3} to W_{R1} was found to be the same when the results for both modes of loading are unified.

The value of W_{R2} is associated with permanent deformation, which accumulates during the loading portions of the cycles and ceases to disappear during the unloading portions. The result is a variable phase angle throughout the cycle. W_{R2} is calculated by subtracting the energy calculated by assuming a constant phase angle measured at the peaks of the strain and stress functions from the actual area of the stress-pseudo strain hysteresis loop.

The average and variation of a number of parameters that can be used to assess fatigue life in DMA were also examined in this study. The average values for the number of cycles to failure and the total DE ranked the mixtures in accordance with their field performance. However, the coefficient of variation for these two parameters was quite high (around 75 percent). Two new parameters are proposed to characterize fatigue damage and unify the results from the controlled-strain and controlled-stress modes of loading. These two parameters are the projected crack radius $\Delta R(Nf)$ at a fixed number of cycles and the ratio of $\Delta R(Nf)$ to $ln(N)$. These parameters had a reasonable coefficient of variation, which was substantially less than those of the other parameters.

CHAPTER IV

FATIGUE ANALYSIS OF ASPHALT MIXTURES INDEPENDENT OF MODE OF LOADING*

OVERVIEW

This chapter evaluates an analytical method that is independent of the mode of loading (controlled-strain or controlled-stress) to quantify the fatigue resistance of asphalt mixtures. The evaluation was based on fatigue tests conducted on the fine aggregate matrix (FAM) portion of an asphalt mixture using the dynamic mechanical analyzer (DMA). A number of tests were performed by applying oscillatory torque under controlled-strain and controlled-stress conditions at a frequency of 10 Hz and at a temperature of 25ºC. The data from these tests are analyzed using a facture model for viscoelastic materials to calculate a fatigue damage parameter, $R(N)$, that quantifies crack growth in the FAM. This damage parameter has a lower coefficient of variation when compared to conventional parameters such as load cycles to failure or cumulative dissipated energy (DE). In addition, this parameter provides comparable results for a given material independent of the mode of loading.

OBJECTIVE

The objective of this study is to evaluate whether the crack growth index yields similar results for the same material independent of the mode of loading, and strain and stress amplitudes.

---

*Presented at the 87th Annual Meeting of the Transportation Research Board, January 15, 2008, Washington, D.C., and accepted for publication in the 2008 series of the *Transportation Research Record*: *Journal of the Transportation Research Board* (forthcoming). Reprinted with permission of the Transportation Research Board.

To achieve this objective, specimens of the FAM portion of an asphalt mixture were subjected to a fatigue test using the DMA. The specimens were tested using controlled-strain and controlled-stress modes of loading with different strain and stress amplitudes. The crack growth index was determined and compared among the different tests. In addition, the variability in the crack growth index was compared to the variability in conventional indices that are used to characterize fatigue cracking (i.e., number of load cycles to failure and cumulative DE).

ENERGY METHOD TO CHARACTERIZE FATIGUE DAMAGE IN ASPHALT PAVEMENTS

Definition of Dissipated Energy (DE) Components

The rate at which damage accumulates in a fatigue test depends on mode of loading, i.e, controlled-strain or controlled-stress. For a controlled-strain test, the applied strain amplitude is constant and the response stress amplitude decreases as the specimen accumulates damage with each cycle. Whereas, for a controlled-stress test, the applied stress amplitude is constant and the response strain amplitude increases as the specimen accumulates damage. In either case, as the test progresses, fatigue damage in the sample is manifested as a decrease in the dynamic modulus and a simultaneous increase in the phase angle. However, for a controlled-strain test, the two manifestations of damage have the opposite effect on the area of the stress-strain hysteresis loop, i.e., a decrease in the dynamic modulus causes the area of the hysteresis loop to decrease, whereas, an increase in the phase angle causes the area of the hysteresis loop to increase. Typically, the net effect of these two changes is that the area of the hysteresis loop decreases with the progression in the number of load cycles. On the contrary, in a controlled-stress test, both manifestations of damage (decrease in the dynamic modulus and increase in phase angle) tend to increase the area of the hysteresis loop (Figure 4.1).

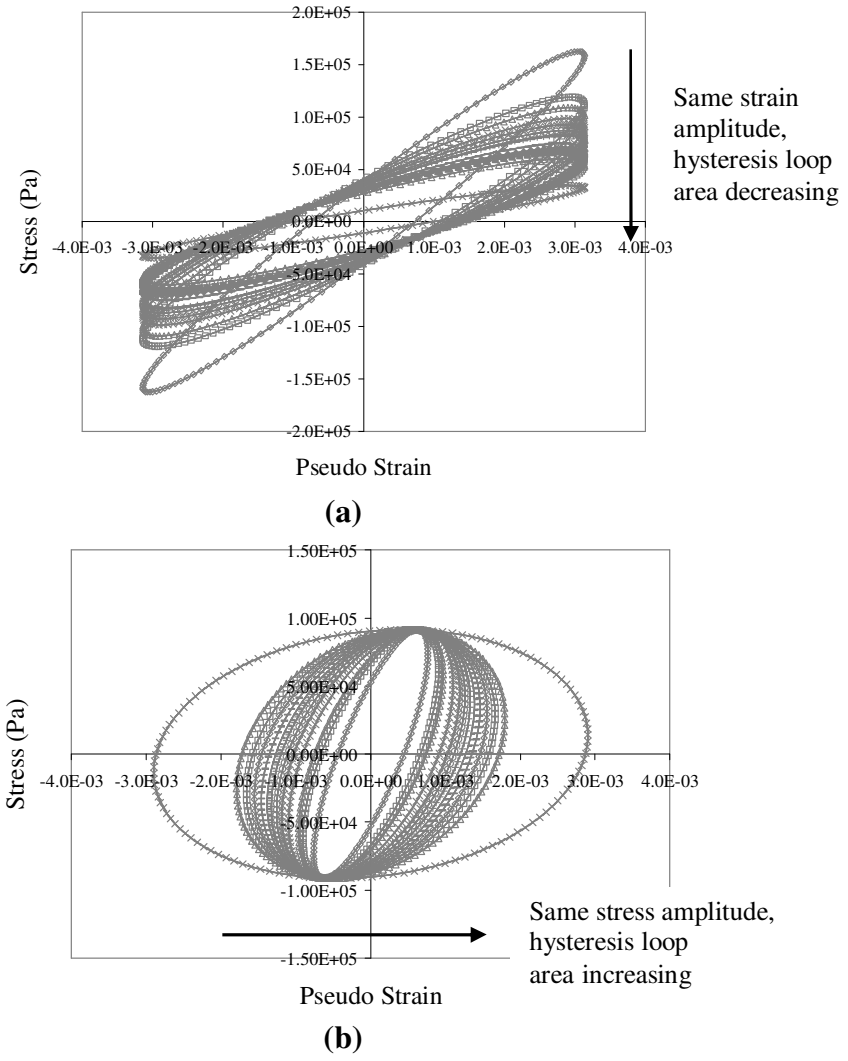

FIGURE 4.1 Hysteresis Loop Areas for: (a) Controlled-Strain, and (b) Controlled-Stress Modes of Loading.

The approach proposed by Masad et al. (*5*) and in Chapter III identified three different forms of the DPSE due to fatigue damage that are associated with: (i) change in the phase angle between consecutive cycles (W_{R1}), (ii) change in the phase angle within the same cycle (W_{R2}), and (iii) change in the dynamic modulus or mixture stiffness (W_{R3}). Table 4.1 enumerates the expressions used to calculate these three forms. In Table 4.1, G^* and δ are the dynamic modulus and phase angle, respectively. The terms γ_{OF} and τ_{OF} are the strain and the stress amplitudes, respectively. The subscript *NF*

represents properties at a specific load cycle. The subscript VE denotes viscoelastic properties. The VE properties (G^*_{VE} and δ_{VE}) are needed in order to calculate DPSE associated with damage by removing the viscoelastic energy from the total strain energy (area of stress versus strain hysteresis loop). The expressions in Table 4.1 mathematically illustrate the way the DPSE terms W_{R1} and W_{R3} incorporate the difference between material properties measured at a given load cycle and viscoelastic material properties. The approach to determine material viscoelastic properties is discussed later in this chapter.

TABLE 4.1 Components of Dissipated Pseudo Strain Energy (DPSE) for Both Modes of Loading

Parameter	Mode of Loading	
	Controlled-Strain	**Controlled-Stress**
W_{R1} *(energy dissipated due to change in phase angle between cycles)*	$\pi G^*_{VE}\gamma^2_{0F}\sin(\delta_{NF}-\delta_{VE})$	$\pi\frac{\tau^2_{oF}}{G^*_{VE}}\sin(\delta_{NF}-\delta_{VE})$
W_{R2} *(energy dissipated due to change in phase angle within each cycle)*	$\left(\text{Area of Stress vs Pseudo Strain Loop}/\frac{G^*_{NF}}{G^*_{VE}}\right)-W_{R1}$	$\left(\text{Area of Stress vs Pseudo Strain Loop}\times\frac{G^*_{NF}}{G^*_{VE}}\right)-W_{R1}$
W_{R3} *(energy dissipated due to change in stiffness)*	$\frac{1}{2}\gamma^2_{OF}(G^*_{VE}-G^*_{NF})$	$\frac{1}{2}\tau^2_{0F}(\frac{1}{G^*_{NF}}-\frac{1}{G^*_{VE}})$

W_{R2} accounts for the not uniform energy dissipation within the hysteresis loop. In a cyclic load test, the phase angle computed by an instrument is typically based on the time shift between the maximum values of strain and stress. However, the experimental measurements conducted in this study have shown that the instantaneous phase angle is not constant throughout a loading cycle. For example, the phase angle computed using the time shift between zero strain and zero stress is different from the phase angle

computed using the time shift between maximum (or minimum) strain and maximum (or minimum) stress.

For any given load cycle, a threshold of strain and stress amplitudes exists such that no damage (cracking and plastic deformation) occurs while the stress state of the material is within this threshold. The corollary to this is that damage evolution will occur only in the portion of the cycle where the stress state of the material exceeds the threshold value. As a result, energy dissipation corresponding to damage is not uniform throughout the cycle leading to a change in the phase angle. The nonlinear viscoelastic behavior is also responsible for part of the non-uniformity because it causes the phase angle to vary as a function of the instantaneous stress amplitude within a load cycle. Since VE properties, or more specifically δ_{VE}, is determined by using the highest permissible stress amplitude that does not impart damage to the material, the effect of non-linearity on the phase angle is inherently considered. However, the change in phase angle within the cycle due to not uniform damage evolution is not considered. This is quantified using W_{R2} as the difference between the hysteresis area based on measured data at every point and the theoretical hysteresis area (W_{R1}) based on phase angle measured from the peak strain or stress as illustrated in Figure 4.2.

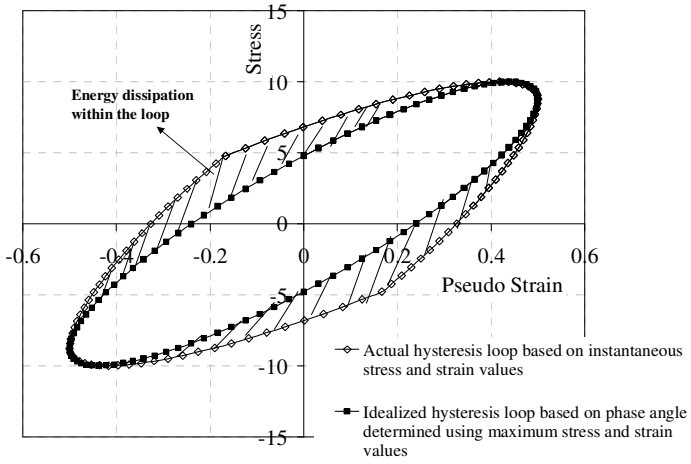

FIGURE 4.2 The Difference between the Actual and the Idealized Hysteresis Loops.

Crack Growth Model

The crack growth index is defined as in Equation 4.1, which is presented earlier in Chapter III (Equation 3.27).

$$R(N) = \frac{\bar{r}(N)}{K^{\frac{1}{2n+1}}} = \left[(2n+1)^{n+1} \left(\frac{G_R b}{4\pi G_1 \Delta G_f} \right)^n N \right]^{\frac{1}{2n+1}} \tag{4.1}$$

where, K is a constant for each material that is inversely proportional to the square of the tensile strength of the asphalt mixture, G_R is the reference modulus, b represents the rate of change of the DPSE ($W_R = W_{R1}+W_{R2}+W_{R3}$) with respect to load cycles (N) based on the relationship, $W_R = a + bLn(N)$. G_1 is obtained from the relaxation modulus-time relationship ($G(t) = \frac{\tau(t)}{\gamma_0} = G_\infty + G_1 t^{-m}$), ΔG_f is the adhesive bond energy, and n is related to the exponent m in the relaxation modulus-time relationship as follows (*27*):

$$n = 1 + \frac{1}{m} \tag{4.2}$$

MATERIALS AND TESTING PROCEDURE

The FAM used in this study was designed to represent a proper FAM proportion of the full mixture. The asphalt mixture was a dense graded mixture designed with a PG 64-22 binder. The FAM was designed using natural sand (72 percent) and limestone sand (28 percent) following the proportions used in the full mixture. The percentage of binder in the FAM was 7.3 percent by mass of the total mixture. The specimen preparation procedure as well as the test method used in this study follows that described in Chapter III. Aggregates and binder were mixed at the mixing temperature and aged in

the oven for two hours prior to compaction. This protocol simulates short term aging following the Superpave mixture design procedure (*57*).

Dynamic Mechanical Analysis (DMA)

The DMA is used in many fields, such as engineering, chemistry, and polymer physics. The DMA provides valuable information related to the rheological properties of a material by applying an oscillatory torque to the sample. DMA can also be used to provide information on the ability of viscoelastic materials to store and dissipate mechanical energy upon deformation (*58*).

Figure 4.3a shows DMA test specimens and Figure 4.3b illustrates the equipment (CVOR-200-050) from Bohlin Instruments (currently Malvern Instruments, Inc.) that was used in this study. Also shown in Figure 4.3b are supporting accessories including: (i) test station, (ii) controller system (to capture gap and normal force and also control the instrument speed), (iii) temperature control unit, (iv) data acquisition system, and (v) solids fixtures. The equipment is able to apply torque ranging from 0.1×10^{-6} N.m to 200×10^{-3} N.m, at frequencies ranging from 10^{-6} to 150 Hz, and temperatures from -150 to 550ºC.

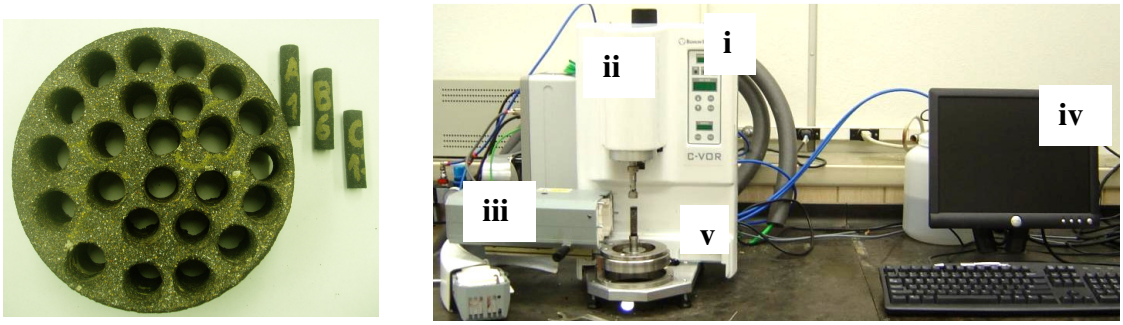

(a) **(b)**

FIGURE 4.3 (a) Superpave Gyratory Compactor (SGC) and Dynamic Mechanical Analyzer (DMA) Specimens, and (b) Dynamic Mechanical Analyzer (DMA) Equipment (Bohlin Instruments, CVOR-200-050).

A relaxation test was performed to determine the parameters, G_1 and m, that are required in Equations 4.3 and 4.4. Sinusoidal torsional tests were then carried out to determine δ_{VE}, G^*_{VE} and DE. All sinusoidal tests were conducted at a frequency of 10 Hz and a temperature of 25ºC. Data were collected every five cycles, and 128 points per cycle were recorded. These data collection parameters were based on preliminary testing mixtures with different stiffness values and were found to be the optimum values for capturing the details of loading cycles without exceeding the maximum number of cycles that the DMA can apply and number of points it can store. The equipment applies Fourier Transform (FT) to fit the raw data (displacement and torque) and compute strain, stress, and phase angle values. It is up to the user the selection of the number of cycles and the number of points per cycle to be used in the FT to output data.

There are limitations on the strain or stress amplitudes that should be used to determine the viscoelastic properties. Using a very small stress value is advantageous because no notable damage is done to the sample. However, due to nonlinear behavior of the material viscoelastic properties determined at small strain or stress amplitudes are not the same as those at high strain or stress amplitudes used in the typical fatigue testing. As a result, the calculated DPSE shown in Table 4.1 overestimates the magnitude of damage by incorporating the contribution due to nonlinear viscoelastic energy. On the other hand, the use of high strain or stress amplitudes from the first few cycles of a fatigue test as representative viscoelastic parameters would underestimate the magnitude of damage computed using DPSE. A reasonable approach, which is a compromise between these two extremes, is to determine the viscoelastic properties by applying cyclic loads at the highest possible strain or stress amplitudes beyond which damage becomes imminent. Damage is detected by changes in the mechanical properties of the material (G^* and δ).

Figure 4.4 shows the stress amplitude that was used to determine the viscoelastic properties. At this stress amplitude, fatigue lives were much longer, and the mechanical properties and hysteresis loop began to change after applying many cycles. Consequently, there was either no damage or minimal damage at the beginning of this

test and the measured properties can be considered to closely approximate viscoelastic properties.

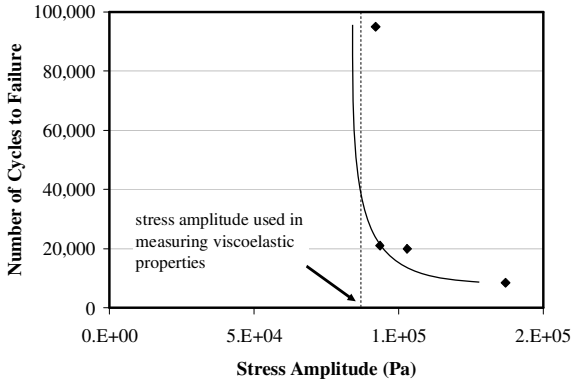

FIGURE 4.4 Number of Cycles to Failure versus Stress Amplitude.

High strain and stress amplitudes were used in the oscillatory tests to induce fatigue cracking. The controlled-strain cyclic fatigue test was performed at strain amplitudes of 0.1 percent and 0.2 percent (labeled as CStrain-0.1% and CStrain-0.2%, respectively). Controlled-stress fatigue testing was performed at eight different stress amplitudes based on the results from the controlled-strain test (0.1 percent and 0.2 percent) as follows:

- stress amplitude equal to the response stress measured in the initial cycles of the controlled-strain test (labeled as CStress-initial),
- stress amplitude equal to the response stress measured at 30 percent of fatigue life when tested under controlled-strain mode (labeled as CStress-30%),
- stress amplitude equal to the response stress measured at 50 percent of fatigue life when tested under controlled-strain mode (labeled as CStress-50%), and

- stress amplitude equal to the response stress measured at 70 percent of fatigue life when tested under controlled-strain mode (labeled as CStress-70%).

Table 4.2 enumerates the strain and stress amplitudes used in the different tests. At least three specimens were run for each kind of test.

TABLE 4.2 Strain and Stress Amplitudes Used in Dynamic Mechanical Analyzer (DMA) Tests

Test Label	Stress Amplitudes (Pa) Calculated Based on 0.1% Strain Amplitude	Stress Amplitudes (Pa) Calculated Based on 0.2% Strain Amplitude
CStress-initial	1.32×10^5	1.65×10^5
CStress-30%	1.04×10^5	1.11×10^5
CStress-50%	9.51×10^4	9.14×10^4
CStress-70%	9.41×10^4	9.08×10^4

RESULTS

Damage Analysis

R(N) values for controlled-strain and controlled-stress tests were calculated using Equation 4.3. The values for G_1, m and n values used in Equation 4.3 were 30×10^6 Pa, 0.54, and 2.85, respectively. Adhesive bond strength (ΔG_f) for the selected mixture was computed to be 0.0875 J/m^2 (*9*), based on surface energy measurements. The viscoelastic properties (G^*_{VE} and δ_{VE}) used to compute W_{R1} and W_{R3} were determined to be 1.65×10^8 Pa and 21.90º, respectively. As in Chapter III, G_R was selected to be equal to the undamaged VE modulus, which makes the maximum value of the pseudo strain equal to that of the applied strain.

In this study, fatigue life was determined to be the number of load cycles at which the value of $N\times G_N/G_1$ becomes maximum, where N is the number of cycles, G_N is

the value of G^* at load cycle N, and G_1 is the value of G^* at the first load cycle (*32*). An example of the change in dynamic modulus and $N \times G_N/G_1$ is shown in Figure 4.5a, while an example of the change in W_R as a function of loading cycles is shown in Figure 4.5b. Table 4.3 enumerates the statistics for b and R at the failure point N_f.

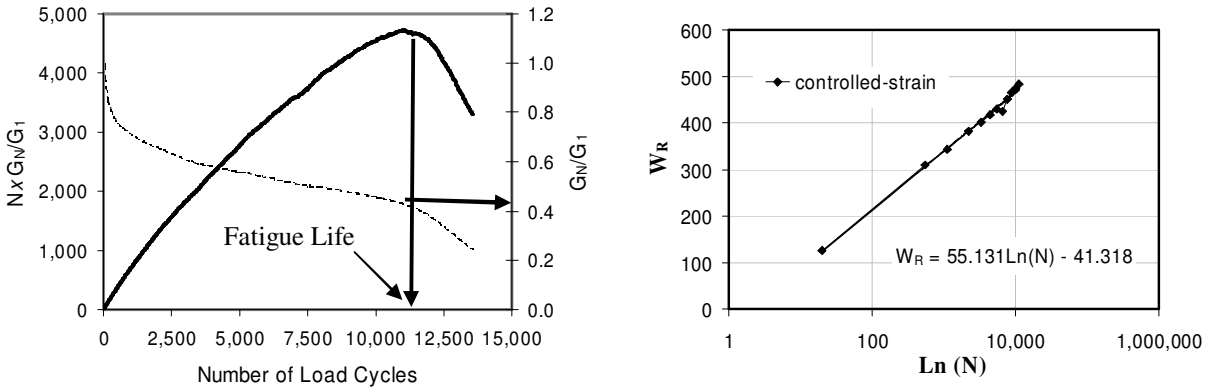

(a) (b)

FIGURE 4.5 (a) Fatigue Life Determination, and (b) W_R versus Number of Loading Cycles.

TABLE 4.3 Statistics for b and $R(N_f)$ Values

Test	b Value Statistics		$R(N_f)$ Statistics	
	Ave.	CV(%)	Ave.	CV(%)
CStrain-0.1%	24.58	11	89.38	10
CStress-initial	94.13	68	142.10	18
CStress -30%	43.06	47	126.26	28
CStress-50%	47.41	44	124.70	28
CStress -70%	30.30	37	125.41	42
CStrain -0.2%	69.82	31	112.25	13
CStress-initial*	182.29	23	215.42	6
CStress -30%	63.32	33	119.27	3
CStress -50%	42.36	24	117.58	17
CStress -70%	25.01	72	89.76	39
All tests	62.23	76	126.21	28
All tests, except *	48.89	47	116.30	15

The R values at N_f are plotted in Figure 4.6. In order to put the results in Figure 4.6 into perspective, a mixture with poor resistance to fatigue would have an $R(N_f)$ value higher than 200 (Chapter III). As such, in spite of the apparent differences in Figure 4.6, these results, with the exception of CStress-initial at 0.2 percent strain, are considered to be in the same range and would rank the performance of this mixture as fairly good in terms of resistance to fatigue cracking. One of the reasons for the high value for CStress-initial at 0.2 percent strain is the fact that the applied stress amplitude in this case (0.17 MPa) was significantly higher compared to the other cases (0.09 to 0.13 MPa). The high stress amplitude causes significant damage to the test specimen in the first few cycles of the test. In other words, the test specimen is already damaged before it achieves a steady state crack growth stage. As a result, in this particular case the parameter b does not represent the rate of steady state crack growth, as it does for other cases. The average $R(N_f)$ value for all tests is around 116.30 with a coefficient of variation (CV) close to 15 percent (Table 4.3).

Figure 4.7 illustrates the relationship between cumulative W_{R1} and cumulative W_{R3} values for both modes of loading. The good correlation ($R^2=0.96$) between these terms indicates that the ratio of energy dissipated due to changes in the viscous properties of the material (increase in phase angle) to the energy dissipated due to changes in stiffness (reduction in dynamic modulus) is in the same proportion irrespective of the mode of loading. In other words, the proposed analysis method partitions the energy into its components in the same manner for both modes of loading and all amplitudes.

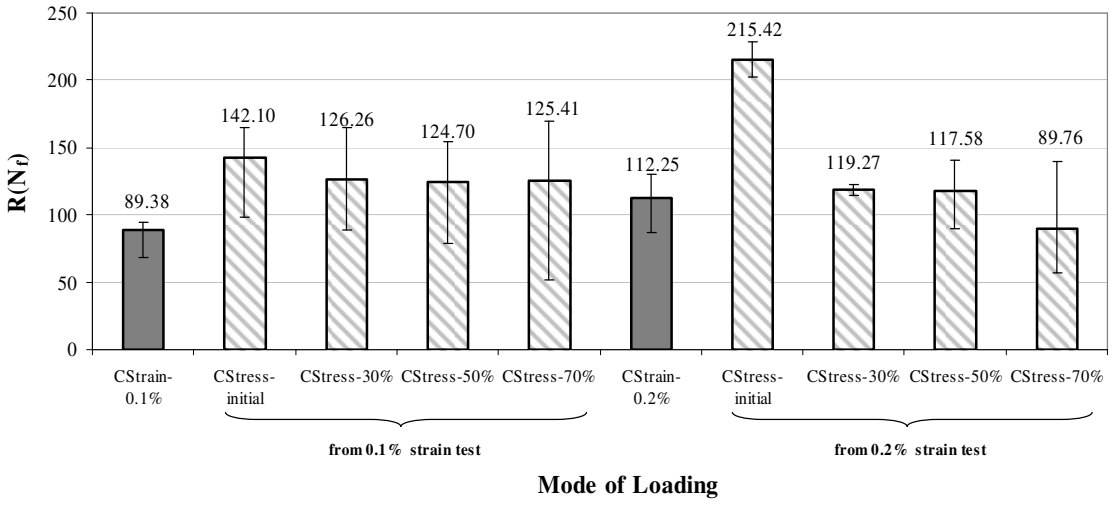

FIGURE 4.6 $R(N_f)$ Values for Controlled-Strain and Controlled-Stress Tests.

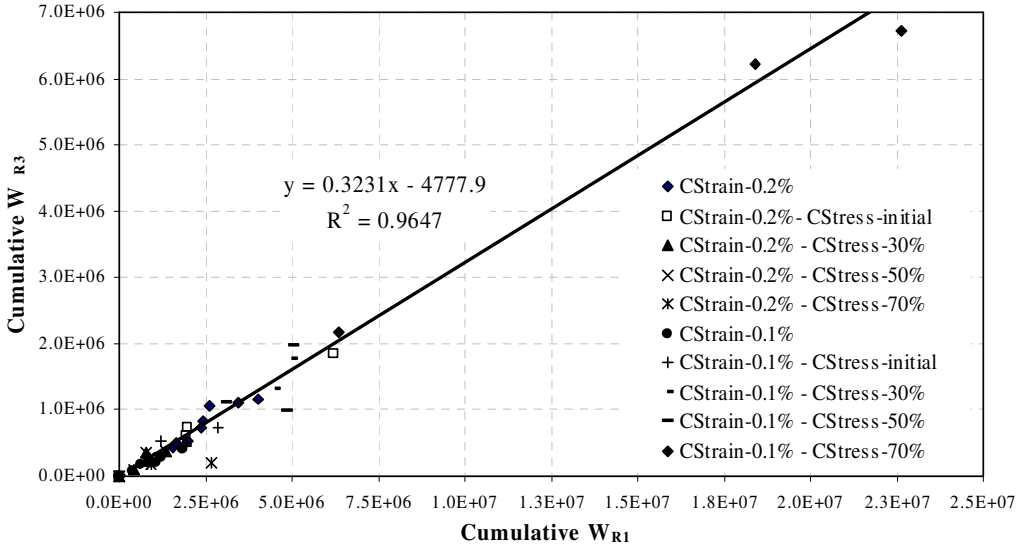

FIGURE 4.7 Cumulative W_{R1} and W_{R3} Values for All Controlled-Strain and Controlled-Stress Tests.

Figure 4.8 shows W_{R2} values expressed as a percentage of W_{R1}. It is clear that for a controlled-strain test, W_{R2} is only a small fraction of W_{R1}, whereas for a controlled-stress test W_{R2} is much more significant. This difference is, at least in part, due to the

way that the DMA applies strain or stress to the specimen. In the controlled-strain mode of loading, the DMA adjusts the strain continuously in order to achieve a sinusoidal function throughout the cycle. This adjustment tends to eliminate the not uniform change in phase angle throughout the cycle. However, this is not the case for the controlled-stress loading in which strain is allowed to change within the cycle resulting in not uniform damage without being adjusted by the DMA.

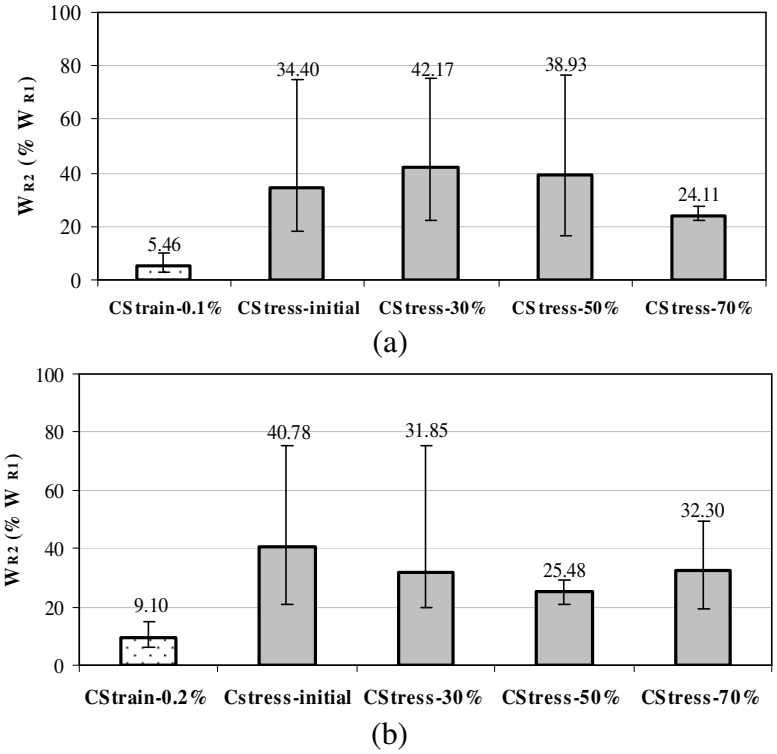

FIGURE 4.8 Energy Dissipation within the Loop (Percentage of W_{RI}) for: (a) CStrain-0.1% and Correspondent Controlled-Stress Tests, and (b) CStrain-0.2% and Correspondent Controlled-Stress Tests.

Table 4.4 presents the fatigue life and corresponding statistics. In general, lower strain or stress amplitude resulted in higher fatigue life. The CV for number of cycles to failure was at least 47 percent. However, the CV for the crack growth index determined

using the same test data was much lower generally ranging between three to 20 percent (Table 4.3).

Cumulative DPSE was computed as the area under the W_R versus number of load cycles curve, using equations as shown in Table 4.1. For 0.1 percent strain and corresponding controlled-stress tests, the controlled-strain tests had lower cumulative DPSE. For controlled-stress tests lower stress amplitudes resulted in higher cumulative DPSE. For 0.2 percent strain and corresponding controlled-stress tests no clear tendency was found. It is interesting to note that cumulative DPSE is limited in its ability to unify results from both modes of loading. High variability associated with this parameter limits its utility in identifying clear trends between strain or stress amplitudes and the fatigue cracking life. The average cumulative DPSE for all modes of loading was 7.3×10^6 J/m^3, but the CV was more than 100 percent (Table 4.4).

TABLE 4.4 Statistics for Fatigue Life and Cumulative Dissipated Pseudo Strain Energy (DPSE)

Test	Statistics for Fatigue Life		Statistics for Cumulative DPSE (J/m^3)	
	Ave.	CV (%)	Ave.	CV (%)
CStrain-0.1%	7,200	63	1.3×10^6	58
CStress-initial	6,620	81	2.7×10^6	52
CStress-30%	18,000	54	6.1×10^6	70
CStress-50%	20,250	70	7.2×10^6	49
CStress-70%	76,750	83	3.3×10^7	50
CStrain-0.2%	6,325	56	3.5×10^6	35
CStress-initial	8,100	84	5.8×10^6	64
CStress-30%	5,140	55	1.3×10^6	31
CStress-50%	22,000	75	7.4×10^6	63
CStress-70%	22,625	47	5.4×10^6	54
All tests	19,301	111	7.3×10^6	125

SUMMARY AND CONCLUSIONS

This chapter investigated the ability of the crack growth index to quantify fatigue cracking in an asphalt mixture independent of the mode of loading (controlled-strain and

controlled-stress). The FAM portion of an asphalt mixture was tested using the DMA by applying various strain and stress amplitudes. The crack growth index was developed based on the premises that the DE during the damage process is associated with three mechanisms: (i) change in the phase angle between consecutive cycles (W_{R1}), (ii) change in phase angle within the same cycle due to the nonlinear behavior of the mixture and not uniform damage within the cycle (W_{R2}), and (iii) change in the dynamic modulus or stiffness (W_{R3}).

Results from this study demonstrate that values of the crack growth index are similar whether they are derived from controlled-strain and controlled-stress modes of loading. As such, this parameter can be used to rank mixtures based on their fatigue cracking resistance irrespective of the mode of loading used in the test. The same analysis approach can be extended to determine fatigue resistance of full asphalt mixtures subjected to dynamic loading (*28*).

One of the current challenges in the characterization of fatigue resistance is that laboratory tests are conducted based on the anticipated strain or stress distribution in the pavement (i.e. controlled-strain test for thin asphalt concrete layers and controlled-stress test for thick asphalt concrete layers pavements). However, the purpose of the laboratory test should be to determine the model parameters for the relevant stress state, while the boundary conditions and pavement structure are accounted for in structural model. The crack growth index can be integrated in a structural model in order to account for the influence of pavement design and asphalt layer thickness on the strain and stress distribution and resistance to fatigue cracking.

CHAPTER V

QUANTITATIVE COMPARISON OF ENERGY METHODS TO CHARACTERIZE FATIGUE IN ASPHALT MATERIALS*

OVERVIEW

Different methods have been developed to assess fatigue cracking of asphalt mixtures based on dissipated energy (DE). Most of these methods have been motivated by the need to develop a unified fatigue criterion that is independent of the mode of loading. This chapter offers critical analyses of the energy methods based on their theoretical ability to: (a) unify the results from controlled-strain and controlled-stress modes of testing for the same material, and (b) accurately asses the fatigue cracking life of different materials. The efficacy of these methods is quantitatively compared using a common set of fatigue test data. The fatigue test data was obtained using the dynamic mechanical testing of three different mixtures that have been shown to exhibit different fatigue cracking resistance in the field.

INTRODUCTION AND BACKGROUND

Many laboratory test methods are available to characterize fatigue cracking of asphalt binders, mastics, and mixtures; collectively referred to as asphalt materials in this chapter. These methods vary in several attributes including: (i) sample geometry, (ii) loading configuration, (iii) state of stress within the sample, (iv) frequency of loading, and (v) form of cyclic load applied to the specimen.

---

*Reprinted from "Quantitative Comparison of Energy Methods to Characterize Fatigue in Asphalt Materials" by Amit Bhasin, Veronica T.F. Castelo Branco, Eyad Masad, and Dallas L. Little, *Journal of Materials in Civil Engineering* [2008]. In review (with permission from ASCE).

Tangella et al. (*6*) provide a comprehensive review of these different test methods. Examples of criteria that are used to determine the number of load cycles to fatigue failure from a laboratory test are: (i) specific percent reduction in stiffness relative to the initial stiffness (typically for a controlled-strain test), (ii) a 100 percent increase in the strain compared to the initial strain (for a controlled-stress test), (iii) specific value or upper limit for the phase angle, and (iv) complete failure of the specimen (typically for a controlled-stress test) (*7, 8, 10*). Consequently, for a given material the number of load cycles to failure determined from a fatigue test depends on the mode of loading (controlled-strain versus controlled-stress) as well as the criterion selected to define failure.

The aforementioned discussion highlights the need to develop a precise methodology and criterion to characterize the fatigue cracking life of asphalt materials. This need has prompted researchers to develop analytical methods that are based on the concept of dissipated energy (DE) in order to develop a fatigue damage criterion that is characteristic of the material and independent of the mode of loading. This is also the first step towards determining the inherent resistance of the material to fatigue cracking irrespective of the pavement structure (or boundary conditions) in which the mixture is used. An additional advantage of utilizing the concept of DE is that this approach has the potential to reduce the high variability in results commonly observed from laboratory fatigue tests (*59*).

The first part of this chapter presents the background and critical review of four different methodologies that are based on the concept of DE to characterize the fatigue cracking life of asphalt materials. These four approaches are based on: (i) the total DE, (ii) the change in DE, (iii) the cumulative dissipated pseudo strain energy (DPSE), and (iv) the rate of cumulative DPSE. The second part includes quantitative evaluation of the efficiency of each approach to: (i) reconcile the difference between controlled-strain and controlled-stress modes of loading, and (ii) accurately assess fatigue cracking life of asphalt materials. The quantitative evaluation was made by analyzing the same set of

fatigue test data for different materials tested under controlled-strain and controlled-stress modes of loading using each of the four different approaches.

Dissipated Energy (DE) Approaches

Approach 1: Total Dissipated Energy (DE)

One of the earliest attempts to characterize fatigue cracking in asphalt mixtures based on DE was by Van Dijk and co-workers (*12, 52, 60*). In some of their early works, they hypothesized that the total DE (W_{fat}) computed using Equations 5.1 and 5.2 for a fatigue test is constant irrespective of the mode of loading (controlled-strain versus controlled-stress).

$$W_{fat} = \sum_{i=1}^{n} W_i \tag{5.1}$$

The DE for any i^{th} interval of load cycles (W_i) is calculated using Equation 5.2.

$$W_i = \pi \times N_i \times \overline{\sigma_i} \times \overline{\varepsilon_i} \times \sin \overline{\varphi_i} \tag{5.2}$$

where, N_i is a fixed interval of load cycles, and $\overline{\sigma_i}$, $\overline{\varepsilon_i}$, and $\overline{\varphi_i}$ are mean values for stress amplitude, strain amplitude, and phase angle for that interval, respectively. Equation 5.2 is essentially the mathematical form for the total area enclosed by a stress-strain hysteresis loop multiplied by N_i number of load cycles for which the measured response can be approximated.

Van Dijk (*12*) utilized a semi-empirical relationship (Equation 5.3) to relate the number of cycles to failure for a controlled-stress test with the total DE. Van Dijk (*12*) also proposed that the results from the controlled-strain and controlled-stress tests would converge if the testing conditions were such that the value of Ψ from Equation 5.4 is one. However, by substituting the expression for ψ from Equation 5.4 into Equation 5.3,

one can infer that this is only possible when the only source of energy dissipation is due to viscoelasticity and not fatigue crack growth throughout the test.

$$N = \left[\frac{\pi \times S_{fat} \times \sin \varphi_0}{A \Psi} \right]^{\frac{1}{z-1}} \times \varepsilon_0^{\frac{2}{z-1}} \tag{5.3}$$

where, S_{fat} is the initial fatigue stiffness modulus, φ_0 is the initial phase angle value, A and z are mixture constants, ε_0 is the initial strain amplitude, and Ψ is given as:

$$\Psi = \frac{W_{initial}}{W_{fatigue}} \tag{5.4}$$

where, $W_{intital}$ represents the artificial total dissipated energy (based on initial values of stress, strain and phase angle) which may also be computed by replacing total number of load cycles N_i with N (total number of load cycles to fatigue), and $\overline{\sigma_i}$, $\overline{\varepsilon_i}$, and $\overline{\varphi_i}$ with σ_0, ε_0, and φ_0 (initial values for stress, strain and phase angle, respectively) in Equation 5.2, and $W_{fatigue}$ represents the total dissipated energy given by Equation 5.1. For controlled-stress tests: $\psi \leq 1$ and for controlled-strain tests: $\psi \geq 1$.

The simplicity of this approach and the semi-empirical formulation (Equation 5.3) prompted other researchers to pursue its incorporation in pavement design methods. Pronk and Hopman (*18*) compared results obtained by testing asphalt mixtures using a composite strain signal comprised of wave forms with different amplitudes to results obtained using a conventional sinusoidal wave form. They further improvised Equation 5.3 proposed by Van Dijk (*12*) to obtain the following form:

$$N_0 \left[a_3 . \varepsilon_0 \right]^{\frac{2}{1-z}} = \left[\frac{\psi . C . T_0}{\pi . S_0 . \sin(\varphi_0)} \right]^{\frac{1}{1-z}} . \frac{1}{T_0} = K_1 \tag{5.5}$$

where, N_0 is the fatigue life for a continuous sinusoidal strain-signal test, $a_3.\varepsilon_0$ is the amplitude of the applied strain-signal, z is a regression constant, ψ is obtained using

Equation 5.4, T_0 is the time period, S_0 is the initial stiffness, φ_0 is the initial phase angle, and K_1 is a constant. C is determined as:

$$C = W_{tot}.[N.T]^{-z} \tag{5.6}$$

where, W_{tot} is the total DE during the test, and $N.T$ is the total time. Equation 5.5 is similar in form to the Wöhler curve (*2*).

One of the hypotheses proposed by Van Dijk and co-workers (*12, 52, 60*) was that the total energy dissipated until failure for a given material must be the same irrespective of the mode of loading (controlled-strain or controlled-stress). Considering a controlled-strain test as a cyclic test with variable stress amplitude within each cycle, an important corollary to the proposed hypothesis is that the total energy dissipated until failure must also be constant for different strain or stress amplitudes for the same mode of loading.

Succinctly stated, the hypothesis proposed by Van Dijk and co-workers states that for a given material the total energy required for complete failure due to fatigue cracking is constant and independent of the loading history (type and magnitude of load and the number of cycles). Figure 5.1 supports this hypothesis (*52*). However, this figure was based on limited data for the same asphalt binder tested using controlled-strain and controlled-stress conditions.

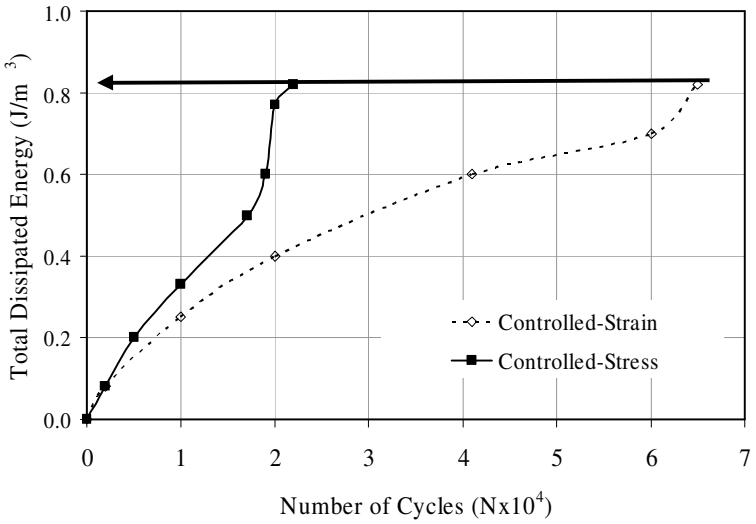

FIGURE 5.1 Total Dissipated Energy (DE) as a Function of Load Repetitions for Controlled-Strain and Controlled-Stress Tests (with permission from *52*, Vol. 1, Figure 1, page 355).

In subsequent work, Van Dijk and Visser (*60*), present fatigue test data for 13 different types of asphalt mixtures tested using a controlled-strain mode of loading at different strain amplitudes, frequencies, and temperatures. The following empirical relationship between cumulative DE to the number of load cycles to failure was reported:

$$W_{FAT} = AN_{FAT}^{z} \tag{5.7}$$

where, W_{FAT} is the total DE until failure due to fatigue cracking, N_{FAT} is the number of loading cycles to fatigue, and A and z are mixture constants. In fact, it can be easily shown that Equation 5.3 is derived by substituting Equations 5.1, 5.2 and 5.4 in the empirical form shown in Equation 5.7.

If the hypothesis that the total DE is independent of the mode of loading (W_{FAT}) was true, then the total DE should be a material parameter and independent of the number of load cycles to failure, i.e. the value of z in Equation 5.7 must be close to zero. Van Dijk and Visser (*60*) reported a value of z to be between 0.6 and 0.7 for the 13

mixtures. However, the reported value for each mixture was based on fatigue tests conducted at different frequencies and temperatures in addition to different strain and stress amplitudes. Therefore, the results reported by Van Dijk and Visser (*60*) cannot be used to prove or disprove the hypothesis that the sum of DE at failure is constant for different modes of loading for a given material. The validity of this hypothesis using an additional set of fatigue test data is examined in the later sections of this chapter.

Another important consideration in this approach is that the DE computed using Equation 5.2 is the cumulative energy dissipated due to: (i) viscoelastic damping, and (ii) incremental damage to the material due to plastic deformation or crack formation. In other words, the phase angle, φ, in Equation 5.2 is not the true viscoelastic phase angle but an apparent phase angle that quantifies the combined energy dissipation due to viscoelasticity, plastic deformation, and crack growth.

Approach 2: Change in Dissipated Energy (DE)

As discussed in the previous section, DE computed using Equations 5.1, 5.2, and 5.7 include energy dissipated due to viscoelasticity as well as energy dissipated due to incremental damage during cyclic loading. In order to overcome this limitation, Ghuzlan and Carpenter (*8*) proposed to quantify fatigue based on the relative change in DE between consecutive cycles rather than the total energy from each cycle.

They proposed that material failure is imminent when there is a significant increase in the magnitude of the DE between consecutive cycles (*61*). The change in DE is quantified using the ratio of dissipated energy change (RDEC) which is calculated as follows:

$$RDEC_a = \frac{\left|DE_a - DE_b\right|}{DE_a \times (b-a)} \tag{5.8}$$

where, DE_a and DE_b are the DE for the load cycles a and b (typically b-a = *100* depending on the sensitivity of the test equipment, how often the equipment acquires

data), respectively. The magnitude of DE_a and DE_b can either be computed graphically using several data points for each load cycle or mathematically using the strain amplitude, stress amplitude and phase angle for the particular cycle with Equation 5.2.

Ghuzlan and Carpenter (*8*) described the relationship between RDEC and the number of load cycles in three regions: (i) initial or region I: when there is a reorientation of the material due application of load; (ii) region II: when there is steady state fatigue crack growth, i.e. the incremental damage per cycle is constant; and (iii) failure or region III: when the rate of damage increases rapidly indicating failure. They referred to the value of RDEC during the steady state fatigue crack propagation zone (region II) as the plateau value (PV) and proposed that this value should be used as a failure criterion that was insensitive to the mode of loading.

Ghuzlan and Carpenter (*8*) demonstrate a strong correlation between the PV and the number of cycles to fatigue failure. The correlation was shown to be insensitive to the type of material or to the mode of loading (Figure 5.2). Ghuzlan and Carpenter (*8*), Shen and Carpenter (*14*), and Carpenter and Shen (*61*) used the following model to compare PV to the number of load cycles to failure:

$$PV = cN_f^d \tag{5.9}$$

where, c and d are regression constants, and N_f is the number of load cycles to failure determined using either the cycles required to reach 50 percent stiffness or the number of cycles at which there is a change from region II to region III.

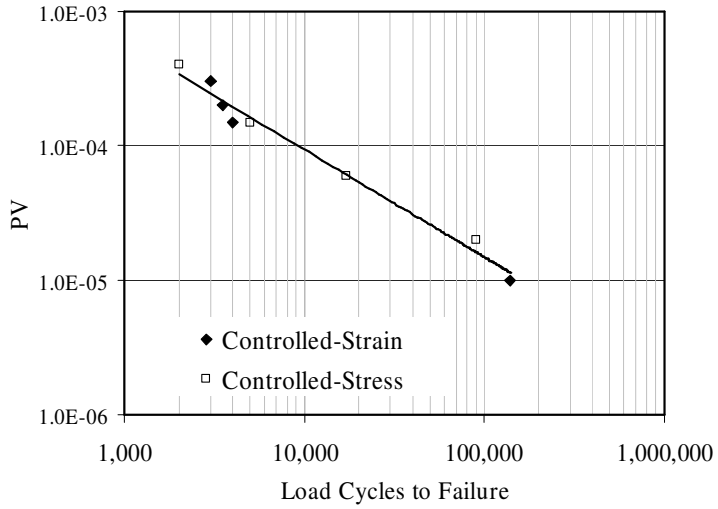

FIGURE 5.2 Correlation between Plateau Value (PV) and Number of Cycles to Fatigue Failure (with permission from *8*, *Transportation Research Record: Journal of the Transportation Board No. 1723*, Figure 9, page 148).

A pertinent question in this context is whether this approach can yield a parameter that is independent of the mode of loading. In this discussion we present an alternative analysis of the incremental energy approach in order to address this question.

The PV, which is also the RDEC value in the steady state crack growth region, can be rewritten based on the following three considerations:

- The DE for any load cycle *i*, is the sum of viscoelastic energy dissipation, E_i^{η}, and the energy dissipation due to damage or crack propagation, E_i^{ξ}.
- Viscoelastic energy dissipation does not change during cyclic loading, i.e.; E_i^{η} is constant and denoted by E^{η}.
- In any given load cycle, *i*, the energy dissipated due to damage is typically much smaller in magnitude as compared to the viscoelastic energy dissipation, i.e.; $E^{\eta} >> E_i^{\xi}$. This is a valid consideration for a fatigue load test where the applied strain or stress amplitude is typically much smaller than the fracture strength of the material and the material exhibits significant viscoelastic behavior at the test temperature and frequency.

Based on the above considerations, Equation 5.9 can be rewritten as:

$$PV = RDEC_a = \frac{DE_a - DE_b}{DE_a \times (b-a)} = \frac{E_a^{\xi} + E^{\eta} - E_b^{\xi} - E^{\eta}}{\left(E^{\eta} + E_a^{\xi}\right) \times (b-a)} \approx \frac{E_a^{\xi} - E_b^{\xi}}{(b-a)} \frac{1}{E^{\eta}} = \frac{\Delta E^{\xi}}{E^{\eta}} \tag{5.10}$$

where, ΔE^{ξ} is the energy dissipated per cycle due to damage. Substituting the form of PV from Equation 5.10 in 5.9 yields Equation 5.11 or Equation 5.12:

$$PV = \frac{\Delta E^{\xi}}{E^{\eta}} = cN_f^d \tag{5.11}$$

$$PV \times N_f = \frac{E_{Total}^{\xi}}{E^{\eta}} = cN_f^{d+1} \tag{5.12}$$

Equation 5.12 indicates that the total energy dissipated due to damage, E_{Total}^{ξ}, is a function of the viscoelastic energy dissipation and the number of load cycles to failure. At this point it is important to recognize the distinction between Equations 5.7 and 5.12. The former is based on the total energy dissipated at failure (sum of viscoelastic energy and damage) whereas the latter is based on the energy dissipated at failure due to incremental damage normalized by the energy dissipated due to viscoelastic damping.

In order for the parameter E_{Total}^{ξ}/E^{η} or $PV \times N_f$ to be independent of the mode of loading, the value of this parameter should be constant. In other words, the hypothesis is that although PV and N_f may change for different modes of loading, their product represents a material constant that is independent of the mode of loading and hence number of load cycles to failure. For this hypothesis to be valid, the value of the exponent *d* from Equation 5.12 must be -1. Interestingly, the value of the regression parameter *d* from Equation 5.9 reported by Ghuzlan and Carpenter (*8*) varies from -0.7 to -1.1. The deviation of this constant from the expected value of -1 may be due to several factors such as variability in measurements, differences in viscoelastic energy

dissipation at different stress amplitudes due to nonlinearity, and selection of failure criterion to determine *N*.

Another consideration for the use of this approach is the direction of change in RDEC or PV computed using Equation 5.10. The DE in any given cycle, DE_a is computed as the area within the hysteresis loop using the strain amplitude (ε_0), stress amplitude (σ_a), and phase angle (φ_α), as:

$$DE_a = \pi \sigma_a \varepsilon_0 \sin(\varphi_a) = \pi E_a^* \varepsilon_0^2 \sin(\varphi_a) \tag{5.13}$$

For a controlled-strain test (constant ε_0) the dynamic modulus (E_a*) decreases and phase angle (φ_a) increases with increasing load cycles. Therefore, the DE computed using Equation 5.13 will either decrease or increase depending on the relative increase in sin(φ_a) compared to the decrease in E_a*. Although, typically for asphalt materials the decrease in E_a* is much more significant relative to the increase in sin(φ_a), theoretically the magnitude of the change in DE based on Equation 5.13 can either increase or decrease. Not withstanding this limitation, the absolute value of RDEC was used for the analysis of controlled-strain data in the section "quantitative comparison of energy methods" of this chapter.

Approach 3: Dissipated Pseudo Strain Energy (DPSE)

As discussed before, area enclosed by the stress-strain plot for a give load cycle or DE for a viscoelastic material corresponds to the cumulative energy dissipated due to viscoelasticity as well as damage caused to the material during the load cycle, if any. It has been shown that by transforming strain to an equivalent pseudo strain, it is possible to eliminate the viscoelastic contribution to the DE (*27*). Therefore, area in the stress-pseudo strain hysteresis loop or DPSE corresponds exclusively to the energy dissipation due to damage.

Kim et al. (*29*) and Daniel and Kim (*62*) use pseudo strain in lieu to actual strain to model the evolution of damage using a continuum approach in asphalt mixtures. Kim et al. (*13*) employed this concept to evaluate the fatigue cracking life of sand asphalt mixtures, also referred to as fine aggregate matrix (FAM) using the dynamic mechanical analyzer (DMA). In a controlled-strain mode of loading, the applied strain (γ) and the measured stress (τ) responses are obtained from the following two equations:

$$\gamma = \gamma_0 \sin(\omega t) \tag{5.14}$$

$$\tau = \tau_0 \sin(\omega t + \phi) \tag{5.15}$$

where, γ_0 and τ_0 are the strain and stress amplitudes, respectively, ω is the angular frequency, t is the time, and ϕ denotes the phase angle between the applied strain and the stress response. The pseudo strain (γ_t^R) is obtained by dividing stress by a reference modulus G_R. Mathematically, this is represented as follows:

$$\gamma_t^R = \frac{G^*}{G_R}\gamma_0 \sin(\omega t + \phi) \tag{5.16}$$

where, G^* is the dynamic modulus. In Equation 5.16, the phase angle ϕ is the true viscoelastic phase angle, which can be determined by conducting cyclic tests at low strain or stress amplitudes without causing damage to the test specimen.

The apparent phase angle determined experimentally from the response of a cyclic fatigue test, θ, is the sum of the true viscoelastic phase angle, ϕ, and the apparent increase in phase angle due to damage accumulated during the load cycle. Only the true viscoelastic phase angle, ϕ, is used in Equation 5.16 to compute pseudo strain. Thus, the energy dissipated in the stress-pseudo strain loop corresponds exclusively to the energy dissipation due to damage. Figure 5.3 illustrates this concept graphically.

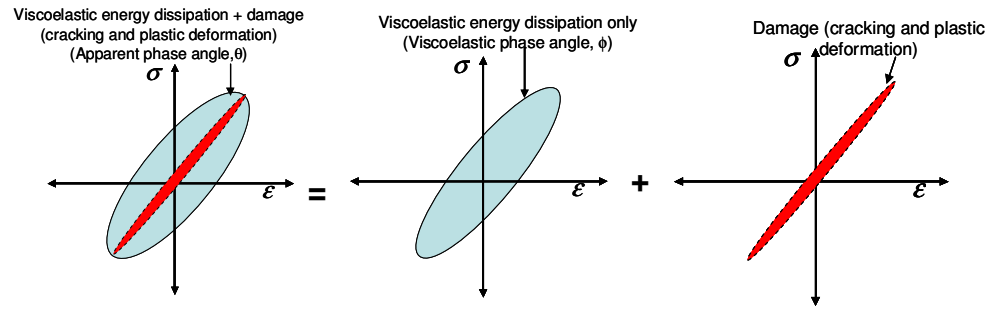

FIGURE 5.3 Illustration of the Hysteresis Loop Area for Different Viscoelastic Properties Selection.

Kim et al. (*13*) use a low strain amplitude (ensuring that no damage is caused to the specimen) to measure the true viscoelastic phase angle, ϕ. However, using the viscoelastic phase angle determined at low strain amplitudes to correct for viscoelastic energy dissipation at high strain amplitudes during a fatigue test introduces a bias due to nonlinearity in the viscoelastic properties of the material. Consequently, this approach underestimates the viscoelastic energy dissipated at high strain amplitudes and overestimates damage in the material.

Si et al. (*22*) estimate the true viscoelastic phase angle using data from the initial cycles of a high strain amplitude test (fatigue test) instead of measuring it from a low strain amplitude test. The premise for this approach is that the phase angle and concomitant DE from the first few cycles of a high strain amplitude cyclic test comprises mostly of viscoelastic dissipation and the contribution due to damage is minimal. This approach overestimates the true viscoelastic phase angle by neglecting any damage that may occur during the first few load cycles. Consequently, the damage in subsequent load cycles is slightly underestimated.

In Chapter III it was demonstrated that by careful selection of the strain or stress amplitude a reasonable estimate for the true nonlinear viscoelastic phase angle can be obtained. They also simplified Equation 5.16 by setting $G^* = G^R$. This is permissible since G^R is a reference modulus for an equivalent elastic case and is constrained by only having same dimensions as the modulus (*27*). Therefore, the stress-pseudo strain

hysteresis area that corresponds to the energy dissipated exclusively due to damage is mathematically calculated as:

$$DPSE_N = \pi G_N^* \gamma_0^2 \sin(\theta_N - \phi) \tag{5.17}$$

$DPSE_N$, G_N^*, and θ_N are the DPSE, apparent dynamic shear modulus, and apparent phase angle measured at cycle N and other terms are as described above. The equivalent of Equation 5.17 for a controlled-stress case is:

$$DPSE_N = \pi \frac{\tau_0^2}{G_N^*} \sin(\theta_N - \phi) \tag{5.18}$$

During a cyclic fatigue load test (controlled-strain or controlled-stress), the value of dynamic modulus (G^*) decreases and the value of phase angle (θ) increases with the progression in applied load cycles. Therefore in the case of a controlled-stress test, the magnitude of DE from Equation 5.18 increases with each consecutive cycle. However, in the case of a controlled-strain test, the magnitude of DE from Equation 5.17 can either increases or decreases with each consecutive cycle depending on the relative change in the phase angle (θ) and dynamic modulus (G^*). This is similar to the discussion following Equation 5.13 for the incremental energy approach.

In order to resolve this discrepancy, the study reported in Chapter III proposed to separate the DPSE due to the change in phase angle and dynamic modulus. For a controlled-strain test, these two forms of DPSE are:

$$W_{R1N} = \pi G_1^* \gamma_0^2 \sin(\theta_N - \phi) \tag{5.19}$$

$$W_{R3N} = \frac{1}{2}\gamma_0 \tau_1 - \frac{1}{2}\gamma_0 \tau_N = \frac{1}{2}\gamma_0^2 \left(G_1^* - G_N^* \right) \tag{5.20}$$

W_{R1N} and W_{R3N} are the total DE at cycle N due to the change in phase angle and dynamic modulus, respectively. G_1^* is the dynamic shear modulus for the first cycle of the high strain amplitude cyclic load test. Chapter III also reports a third form of DE: W_{R2}. This form of energy dissipation is significant when the θ_N value in Equation 5.19 is computed based on the time shift between the peak strain and peak stress. However, the contribution of W_{R2} is accounted for in computing W_{R1} if θ_N is computed based on the average time shift of the entire stress-strain wave form. The latter approach is used in the remainder of this chapter for simplicity in comparing results based on different approaches.

The corresponding equations for a controlled-stress test can be determined in a similar manner as:

$$W_{R1N} = \pi \frac{\tau_0^2}{G_1^*} \sin(\theta_N - \phi) \tag{5.21}$$

$$W_{R3N} = \frac{1}{2}\gamma_N \tau_0 - \frac{1}{2}\gamma_1 \tau_0 = \frac{1}{2}\tau_0^2 \left(\frac{1}{G_N^*} - \frac{1}{G_1^*} \right) \tag{5.22}$$

Approach 4: Rate of Dissipated Pseudo Strain Energy (DPSE)

In this approach fatigue crack resistance is quantified based on the rate of change in DPSE rather than the magnitude of DPSE as in the case of the former approach. Principles of fracture mechanics are used with the rate of change of DPSE along with other material properties to assess the fatigue cracking potential of asphalt materials (*5, 16*). Paris' law for crack growth is used to express the rate of growth of crack radius as a function of the *J*-integral, which by definition is the energy or work of fracture per unit area of crack surface.

The final form of the equation for crack growth index is shown as Equation 5.23. More details on this formulation can be found in the literature (*5, 9*).

$$R(N)=\left[(2n+1)^{n+1}\left(\frac{G_1^* b}{4\pi G_c \Delta G_f}\right)^n N\right]^{\frac{1}{2n+1}} \tag{5.23}$$

ΔG_f is the adhesive bond energy computed using the surface energy components of the asphalt binder and aggregates,

$$n = 1+\frac{1}{m} \tag{5.24}$$

m, G_E, and G_C are relaxation parameters obtained by fitting:

$$G(t) = G_E + G_C t^{-m} \tag{5.25}$$

b is obtained from the following relationship between W_R (total dissipated energy per cycle computed from the sum of dissipated energies from Equations 5.19 and 5.20 or 5.21 and 5.22) and N (number of load cycles):

$$W_R = a + b \times ln(N) \tag{5.26}$$

The theoretical premise for this methodology is the same as the DPSE approach with the exception that fatigue crack growth is characterized using a comprehensive crack growth index that is dependent on the rate of DPSE as well as other fundamental material properties. Considerations on the computation of DPSE discussed in previous section are also applicable to this approach. In addition, it must also be recognized that the crack growth index in Equation 5.23 is a function of:

- rate of DPSE, represented by the term b which is determined using Equation 5.26 with Equations 5.19 and 5.20 for controlled-strain mode of loading or 5.21 and 5.22 for controlled-stress mode of loading,

- material resistance to fracture, represented by the adhesive bond energy ΔG_f (constant for a material irrespective of the mode of loading),
- viscoelastic properties of the undamaged material, represented by the terms G_1^*, G_c, and n (constants for a material irrespective of the mode of loading), and
- number of load cycles N.

The crack growth index from Equation 5.23 can be computed at any arbitrary value for the number of load cycles N. However, the crack growth index from different modes of loading (for the same material) can be expected to be constant only when it is computed at N_f, where the subscript f represents the number of load cycles to failure for each case. This is easily verified by examining Equation 5.23 in which $b^n N$ is the only parameter that changes for different modes of loading or load amplitude (the others being material properties). It is also important to highlight the similarity and difference between the change in DE approach (approach 2) and this approach. The parameters $PV \times N_f$ from the former approach and $b^n N_f$ from the latter approach are both hypothesized to be constants for a material and independent of the mode of loading. However, although both PV and b represent the rate of energy dissipated due to damage, these are computed using different approaches as evident from Equations 5.8 and 5.26. Differences in results from both approaches are presented in the following sections.

QUANTITATIVE COMPARISON OF ENERGY METHODS

The approaches described in the first half of this chapter were developed and evaluated by their respective authors using different materials (binder, mastic, FAM, or whole asphalt mixture) and different modes of testing (cyclic loading on four point beam, direct shear, or torsion). However, the generic nature of energy methods allows these approaches to be extended to any class of asphalt materials such as FAM or full asphalt

mixtures. In this section, a common set of fatigue test data was used with each of the four energy methods and the results were compared.

Test Method and Materials

Fatigue tests using DMA were conducted on FAM (comprising of asphalt binder mixed with aggregates finer than 1.18 mm) portion of three different asphalt mixtures. The FAM test specimens were 50 mm in height and 12 mm in diameter. Test specimens were obtained by sawing and coring a 90 mm high and 150 mm diameter sample compacted using the Superpave gyratory compactor (SGC). Details on the mixture design procedure and preparation of test specimen can be found in Chapter III and in the literature (*9*).

The DMA applies a cyclic torsion on a cylindrical specimen of the FAM in either controlled-strain or controlled-stress mode. All tests were conducted at 25ºC at a frequency of 10 Hz. At least three replicates were tested for each case. Failure was identified as the number of load cycles corresponding to the maximum value of $N \times G^*_N / G^*_1$, where N is the number of load cycles, G^*_N is the dynamic modulus at N, and G^*_1 is the initial dynamic modulus (*13*). Since the strain/stress amplitudes selected are high enough to cause damage to the specimens, there is a stiffness reduction and a phase angle increase due to damage progression. Phase angle increases, approaches a peak and drops. Stiffness versus number of loading cycles curve presents three important points: (i) first inflection point, (ii) transition point, and (iii) second inflection point. The study done by Kim et al. (*63*) demonstrated (cross-plots and error analyses) that the transition point is the most reasonable estimate of failure. Qualitative performance of the three different types of mixtures was known based on field evaluations (*9*). Table 5.1 presents a description of the materials used, mode of cyclic load tests as well as the strain and stress amplitudes used in these tests. The same materials used in the field were also used for the lab experiments.

Mixture A is from section 2 constructed by TxDOT Atlanta District on IH-20 in Harrison County. This section was constructed following Superpave mixture design procedures in 2001. This section presented an overall good performance in respect to rutting, cracking and moisture damage (pavement condition rating – PCR dropped from 100 to 93 in five years). Mixture B was constructed in Ashland County, Ohio on SR 511 in 2000. This is a type 1 mixture. PCR for this section dropped from 95 to 89 in 4 years. Mixture C was constructed in Wayne County, Ohio on SR 226. This is a type 1 intermediate mixture. PCR for this section dropped from 97 to 60 in 6 years. Both, mixtures B and C, were considered poor performers. Mixture C was considered worst than mixture B. According to Zollinger (*9*), cracking was the most predominant distress for these mixtures (B and C).

TABLE 5.1 Composition of the Fine Asphalt Mixtures Used in This Study, Stress, Strain Amplitudes Used in the Tests, and Field Performance for These Mixtures

Mix ID	Location	Material	Percentage of Total Aggregate Weight	Binder PG / Source	Strain (%)		Stress ($\times 10^6$ Pa)		Relative Field Performance[a]
A	Texas IH 20, Atlanta, TX	Sandstone Screenings Granite Hydrated Lime	57 38 5	76-22 / Wright TX	0.20		0.10		Good (PCR = 93)
B	Ohio SR 511, Ashland, OH	Limestone Natural Sand	28 72	64-22 / Tri State OH	0.20	0.10	0.13	0.10	Fair to Poor (PCR = 89)
C	Ohio SR 226, Wayne County, OH	Limestone Natural Sand	50 50	64-28 / Marathon OH	0.20		0.10		Poor (PCR = 60)

[*]PCR (pavement condition rating) averages after five years of performance.

Approach 1: Total Dissipated Energy (DE)

Equations 5.1 and 5.2 were used to compute the total DE until failure for the three different materials tested under different modes of loading. Figure 5.4 compares the performance of the three different mixtures tested under controlled-strain and controlled-stress modes of loading. Figure 5.5 compares the performance of the same mixture tested under the two modes of loading as well as different strain or stress amplitude in each mode of loading.

A material with greater magnitude of total energy dissipated until failure has better resistance to fatigue cracking. From Figure 5.4, mixture A was a better performer than others, which was consistent with the field observation. However, contrary to field observations mixture C outperformed mixture B, although the difference was not significant. The results from Figure 5.5 illustrate that the total DE is sensitive to the mode of loading as well as to the amplitude of strain or stress for any given mode of loading.

The inconsistency in performance rating of different mixtures and lack of constancy in results from different modes of loading can be partially attributed to the fact that the total DE includes viscoelastic energy that is not due to incremental fatigue damage. Comparing fatigue cracking performance of different mixtures based on total DE can also be misleading. For example, a material with low viscoelastic energy dissipation may have a low magnitude of total DE until failure (falsely indicating poor performance) as compared to a material with significantly higher viscoelastic energy dissipation. These results reinforce the idea that fatigue cracking must be quantified based on energy dissipated due to damage after discounting for the recoverable viscoelastic energy.

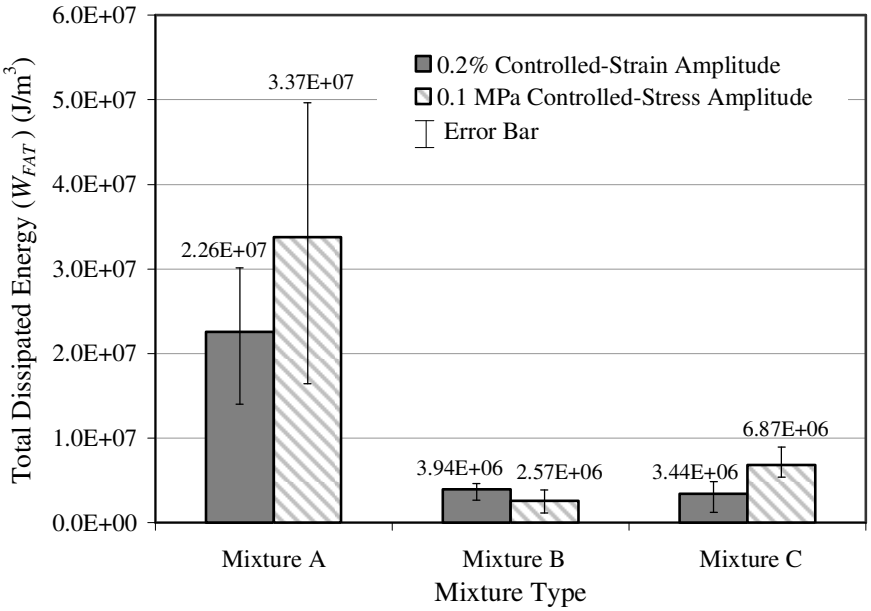

FIGURE 5.4 Comparison of Total Dissipated Energy (DE) for Three Mixtures Tested Using Different Modes of Loading.

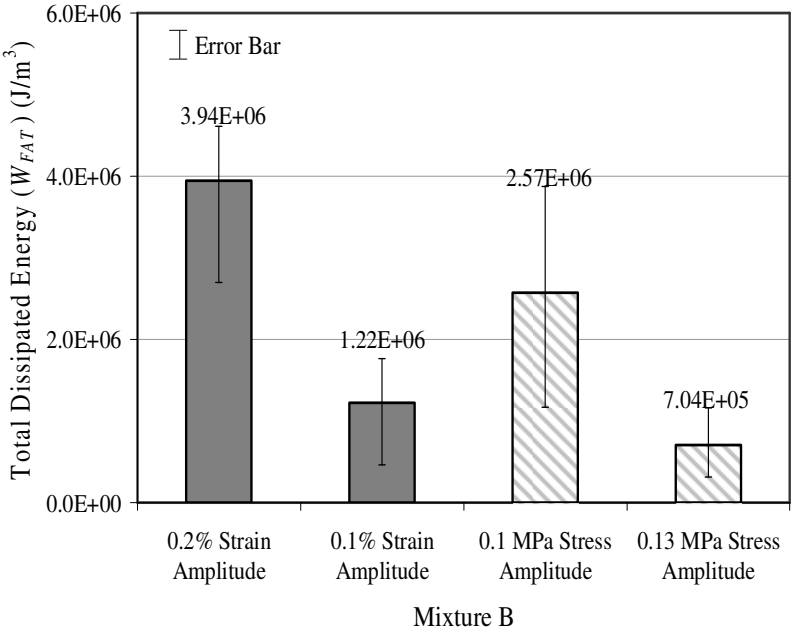

FIGURE 5.5 Comparison of Total Dissipated Energy (DE) for Mixture B Tested Using Different Strain and Stress Amplitudes.

Approach 2: Change in Dissipated Energy (DE)

A mixture with a lower value of plateau value (PV) indicates lower rate of damage accumulation and hence better resistance to fatigue cracking (Equation 5.10). From Figure 5.6, the rankings of the mixtures based on the PV from the controlled-stress tests are consistent with their observed field performance. The rankings from the controlled-strain test clearly indicate mixture A to be the best performer consistent with field observations, but were not significant to differentiate between mixtures B and C. This was mostly due to the variability in determining the PV from the test data.

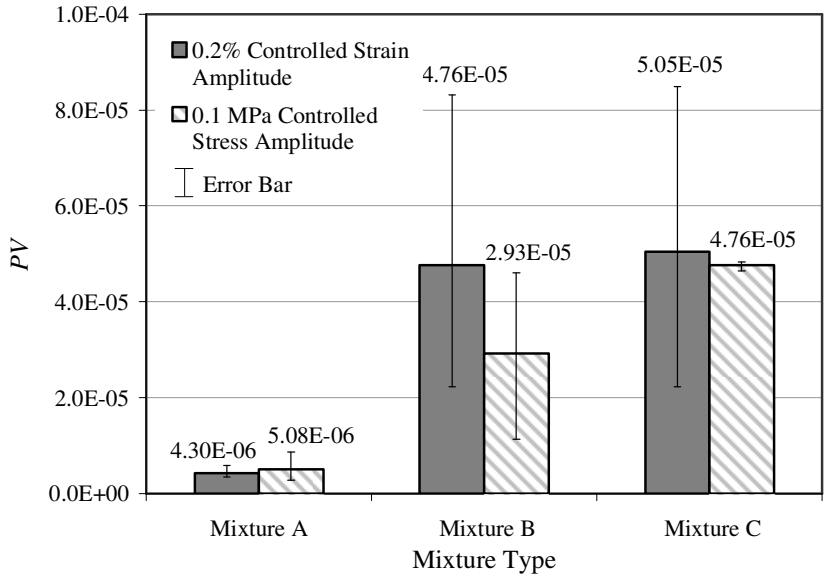

FIGURE 5.6 Application of Plateau Value (PV) to Compare Fatigue Damage Characteristics of Different Materials.

Based on the previous discussion and Equation 5.12, the possible parameter to characterize fatigue cracking independent of the mode of loading based on this approach is $PV \times N_f$. In other words, this parameter must be constant for a given mixture tested under different modes of loading. Figure 5.7 compares the $PV \times N_f$ values for mixture B

tested using different amplitudes of controlled-strain and controlled-stress modes of loading. Results from this figure indicate that the $PV \times N_f$ parameter is similar for different strain or stress amplitudes with the same mode of loading. However, this parameter was different when controlled-strain and controlled-stress modes of loading were compared. This may be partially attributed to the following theoretical limitation of this approach. The $PV \times N_f$ parameter represents the total energy due to damage which is approximated as a fraction of the viscoelastic energy dissipation (Equation 5.12). However, the viscoelastic energy dissipation may not be constant for a material under different modes of loading due to high levels of nonlinearity. It is likely that for full asphalt mixtures, like the ones used by Carpenter and co-workers, the effect of nonlinearity is not as pronounced as in the case of FAM used in this analysis.

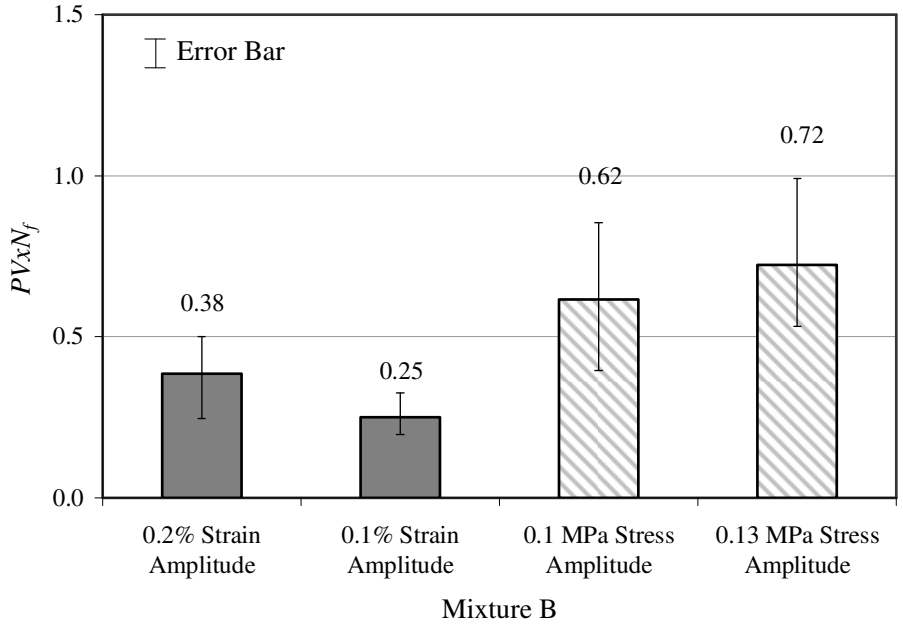

FIGURE 5.7 Comparison of $PV \times N_f$ for Mixture B Tested Using Different Strain and Stress Amplitudes.

Approach 3: Dissipated Pseudo Strain Energy (DPSE)

Figure 5.8 compares the total DPSE values for the three different mixtures tested using controlled-strain and controlled-stress modes of loading. The DPSE was computed as the area under the $W_{R1}+W_{R3}$ versus number of load cycles curve using Equations 5.19 through 5.22. Figure 5.9 compares the DPSE for mixture B tested using different strain and stress amplitudes. The true viscoelastic phase angle ϕ, in Equations 5.19 and 5.21 was determined as the phase angle from the highest strain or stress amplitude that did not yield any significant damage in the first few cycles.

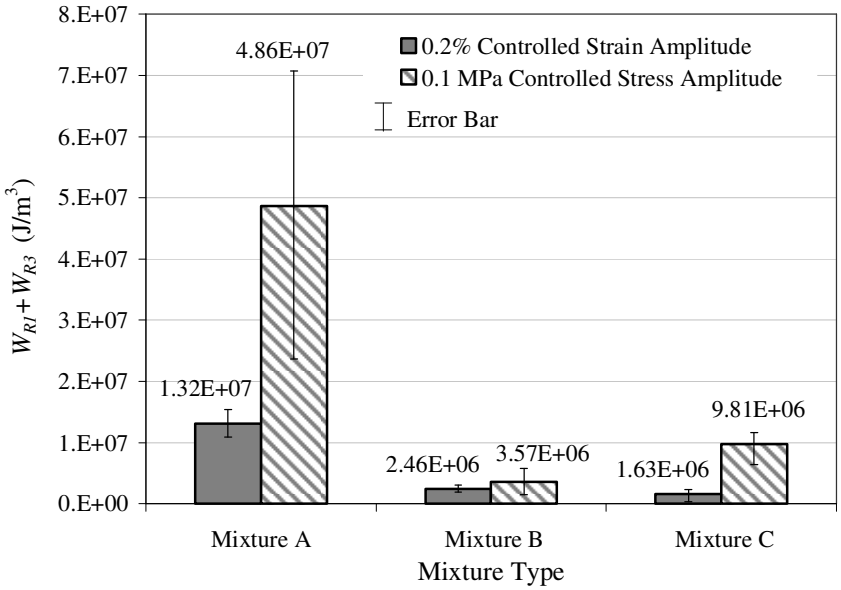

FIGURE 5.8 Application of Total Dissipated Pseudo Strain Energy (DPSE) to Compare Fatigue Damage Characteristics of Different Materials.

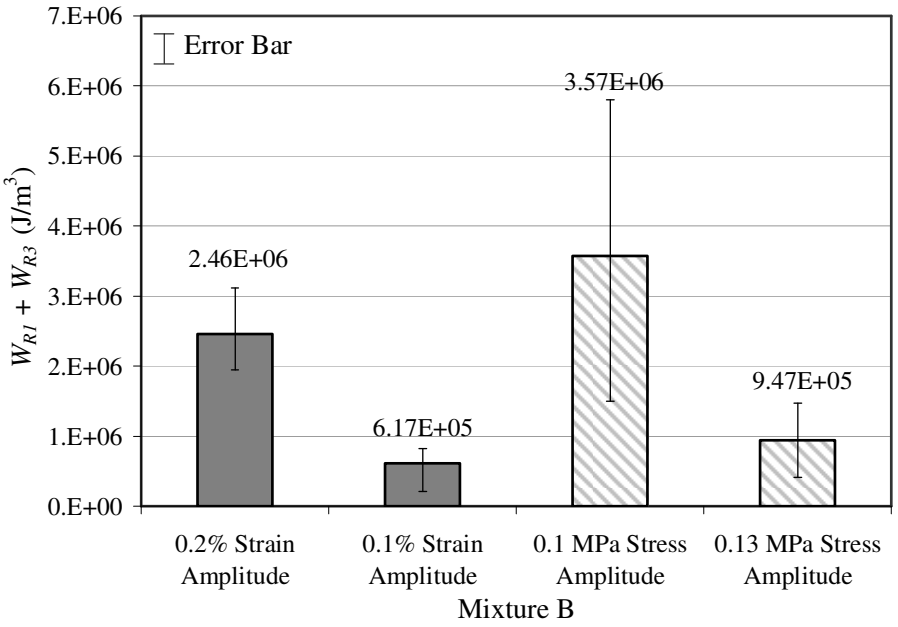

FIGURE 5.9 Application of Total Dissipated Pseudo Strain Energy (DPSE) to Compare Fatigue Damage Characteristics for Mixture B Tested Using Different Strain and Stress Amplitudes.

A material with greater magnitude of cumulative DPSE until failure has better resistance to fatigue cracking. From Figure 5.8, the ranking of three mixtures based on controlled-strain test was consistent with the field observation. Also, based on the controlled-stress test mixture A has the highest fatigue cracking resistance consistent with the field observation. However, the performance of mixtures B and C was not significantly different based on the results from the controlled-stress test. Results from Figure 5.9 illustrate that the DPSE is also sensitive to the mode and amplitude of loading.

Compared to the total DE approach (Figures 5.4 and 5.5), the use of DPSE showed some improvement in the ranking of the mixture performance. However, there was no improvement in the ability of this approach to deliver a parameter that is independent of the mode of loading. This was mostly due to the variability in the initial state of the test specimens (state of the material at the point where damage energy was first evaluated or calculated) and data collected. This will be evident from the following

approach that relies on the rate of DPSE rather than the absolute magnitude of the DPSE. It is important to recognize that the rate of DPSE does not depend on the initial state of the material, whereas the total DPSE can vary significantly for the same material if the initial state of the specimens is significantly different. As a result, it is possible to considerably reduce the variability in the test results with the use of rate of DPSE as demonstrated in the following section.

Approach 4: Rate of Dissipated Pseudo Strain Energy (DPSE)

The rate of DPSE, represented by parameter *b* was determined by fitting Equation 5.26 to the number of load cycles *N* and the total DE at any given cycle ($W_{R1} + W_{R3}$). The crack growth index was computed using Equation 5.23. In order to compare fatigue cracking characteristics of different mixtures, the crack growth index for these mixtures was computed and compared at the same value of *N* (50,000 cycles). Note that, since Equation 5.23 is based on the rate of energy dissipation, it is possible to compare the crack growth index of different mixtures at any arbitrary value of *N*. A smaller value of the crack growth index indicates better performance. Figure 5.10 compares the crack growth index for the three different mixtures. Results based on the crack growth index are consistent with field observations. This indicates that the crack growth index can be used to reliably differentiate between fatigue cracking characteristics of different materials.

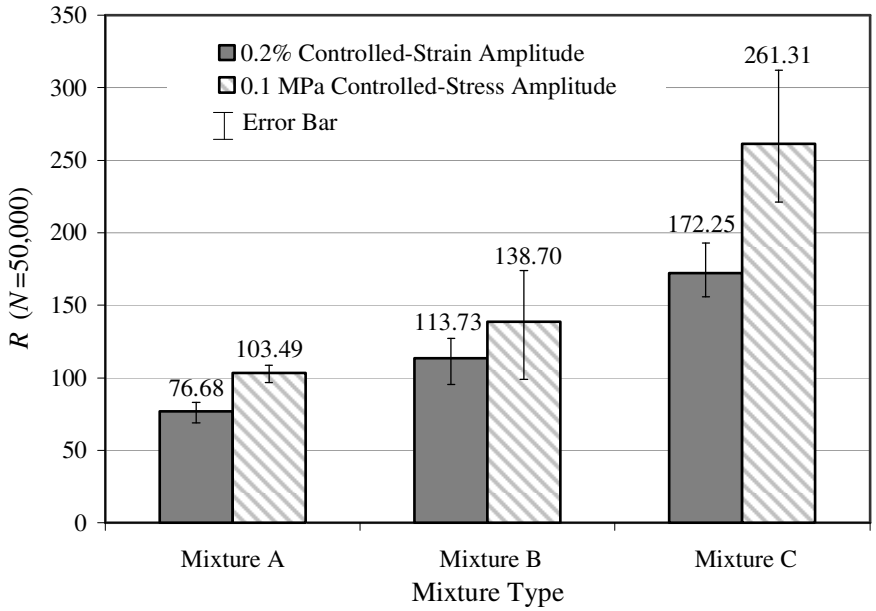

FIGURE 5.10 Comparison of Crack Growth Index at *N=50,000* Load Cycles for Three Mixtures.

In order to reconcile results from fatigue tests of the same material subjected to different modes of loading, the crack growth index for each case was computed at load cycles to failure for that specific case. This is because the crack growth index for the same material under different modes of loading can only be compared when the final state of the material is the same, i.e. complete failure. Figure 5.11 compares the crack growth index for mixture B tested using different strain and stress amplitudes and computed at the number of cycles at which the material fails ($N=N_f$). Figure 5.11 indicates that this parameter is reasonably independent of the mode of loading. The variability and departure from an expected constant crack growth index for the different modes of loading (Figure 5.11) is in part due to the inherent variability associated with the determination of the number of load cycles to failure (N_f).

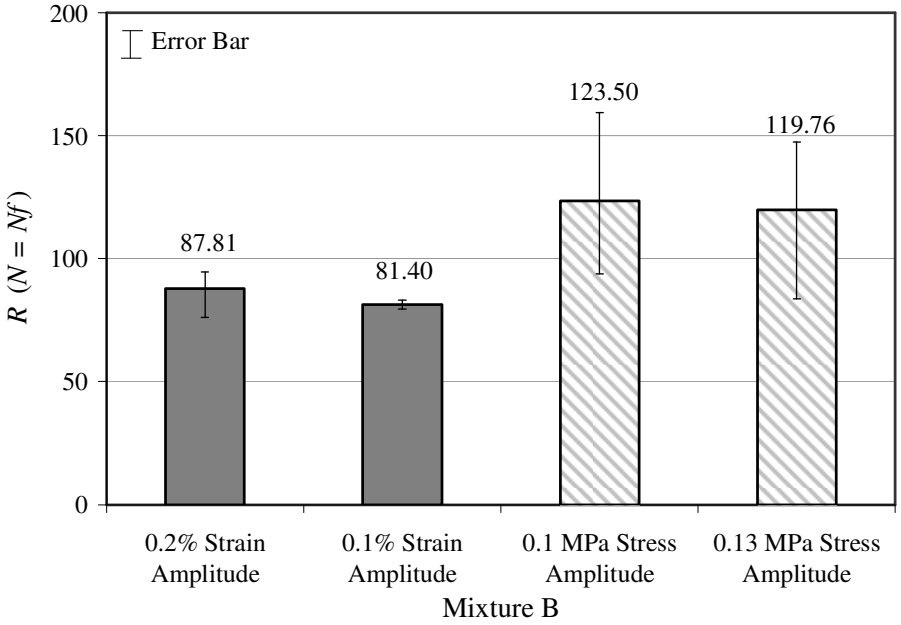

FIGURE 5.11 Comparison of Crack Growth Index at Number of Load Cycles to Failure for Mixture B Tested Using Different Strain and Stress Amplitudes.

CONCLUSIONS

Four different energy methods, which are candidates to characterize the fatigue damage resistance of asphalt materials, were analyzed in this chapter. The commonalities and differences among these methods were critically evaluated. A quantitative comparison of the results was made using the same set of fatigue test data with the four different approaches. The energy methods were evaluated using two important criteria: (i) the ability of the method to reconcile differences in controlled-strain test versus controlled-stress test, and (ii) the ability of the method to accurately asses the fatigue cracking life of different materials. The following are some of the important conclusions based on the evaluation of the energy methods:

- The total DE serves as a gross estimate of the energy dissipated in the fatigue damage process. Materials with substantially different damage characteristics can be characterized using this approach. However, this approach does not

separate the fraction of the DE due to damage from the fraction due to viscoelastic energy dissipation. As a result this parameter has low sensitivity to compare fatigue damage characteristics of different materials and does not unify the results based on different modes of loading.

- The PV provides a measure of the incremental energy dissipated due to damage in each cycle. This parameter was shown to be effective in differentiating the fatigue cracking resistance of different mixtures, albeit with high variability.
- The $PV \times N_f$ term was hypothesized to be independent of the mode of loading. There is limited support for this hypothesis based on results presented by Carpenter and co-workers as well as results from this study. This chapter demonstrates that this parameter represents total energy dissipated due to damage normalized by viscoelastic energy. As a result, authors conclude that this parameter may be considered as a measure of fatigue cracking that is independent of the mode of loading when non linearity in material response is not significant.
- The total DPSE provides a measure of energy dissipated due to damage at failure and may be used to differentiate the fatigue cracking resistance of different materials. However, results from this approach had high variability attributed in part to the initial damage state of the material. This effect was alleviated with the use of crack growth index that is based on the rate of DPSE instead of the total DPSE. This was mostly because the variability in the rate of crack growth (reduction in modulus) between replicates was very low as compared to variability in the number of load cycles to failure.
- The crack growth index, computed using the rate of DPSE, is an efficient parameter by which to separate the damage in the material from the viscoelastic effects and characterize the fatigue cracking life of FAM.

- The crack growth index computed at the load cycles to failure shows promise in its ability to serve as a parameter that is independent of the mode of loading.
- Results from this critical review indicate that there is a need to refine the methods to account for the nonlinear viscoelastic energy dissipation as well to account for plastic or permanent deformation in each cycle.

CHAPTER VI

SEPARATION OF NONLINEAR VISCOELASTIC RESPONSE FROM FATIGUE DAMAGE USING DYNAMIC MECHANICAL ANALYSIS (DMA)

OVERVIEW

An important aspect of characterizing fatigue damage is to differentiate between nonlinear viscoelastic response and incremental damage in the material. The challenge is that both nonlinearity and damage have similar effect on the mechanical response of the material, i.e. the measured dynamic modulus can decrease with an increase in the stress amplitude due to either nonlinearity or damage. This chapter presents an approach to determine the threshold or maximum value of stress (or strain) amplitude that yields nonlinear viscoelastic response without causing damage to the material during fatigue loading. Modified load (strain or stress) sweep tests were performed on six different types of fine aggregate matrix (FAM) mixtures using the dynamic mechanical analyzer (DMA). The strain (or stress) response of the material was monitored for a specified number of load cycles at different load amplitudes. At any given load amplitude, a constant strain (or stress) response (linear or nonlinear) with increasing number of load cycles indicates that there is no incremental damage to the test specimen. In the case when the applied stress (or strain) amplitude induces incremental damage, the response amplitude steadily changes with increasing number of load cycles. The aforementioned criterion was used in this chapter to identify the threshold value of load amplitude that differentiates between nonlinear viscoelastic response from damage. A rigorous statistical approach was also developed and used with the test results to identify this threshold value. Results from this study show that the threshold value depends on both the type of binder and aggregate used in the FAM. This approach can be used to quantitatively differentiate between the amount of energy that is dissipated due to

nonlinear viscoelasticity and damage during fatigue loading. The proposed methodology can also be potentially used with other materials such as full asphalt mixtures, and other modes of loading such as repeated tension or compression.

INTRODUCTION

The mechanical response of asphalt materials can be linear or nonlinear depending on the stress (or strain) amplitude, temperature, and rate of loading. The difference between linear and nonlinear behaviors is the fact that for the latter, the Boltzmann's superposition (the current strain can be determined by the superposition of the responses to the complete spectrum of stress increments) and the homogeneity (the ratio of strain response to any applied stress is independent of the stress amplitude) principles do not hold. The linear theory also assumes infinitesimal deformation (*50, 64*). There is extensive information in the literature on the linear viscoelastic analysis for polymers, binders, and asphalt materials (*43, 50, 65*). According to previous works, under low load amplitudes material's behavior can be approximated as linear, but under moderate to high load amplitudes, this approximation may not be valid (*26, 40, 41*).

The maximum stress (or strain) that can be applied without invoking nonlinear response depends on the type of material. Most analysis for dynamic tests on asphalt mixtures are based on the assumption that the material behaves linearly. Attempts to deal with nonlinear response are typically based on experimental characterization without modeling. There are several works in the literature that emphasize the need to characterize nonlinear viscoelastic behavior of materials. Shields et al. (*42*) investigated the nonlinear viscoelastic behavior of HMA using Schapery's theory (*25*). These authors demonstrated that, for strain values greater than 0.1%, the stress predicted using nonlinear viscoelastic theory was in agreement with measured values (relaxation test). Airey et al. (*43*) used the dynamic shear rheometer (DSR) and stress and strain sweep tests to investigate and define the linear viscoelastic range for different binders (base, modified, unaged, and short term aged). Bahia et al. (*23*), and Masad and Somadevan

(*24*) reported that average strain magnitudes within the asphalt binder were much higher than the bulk strain of the asphalt mixtures. Bahia et al. (*23*) demonstrated that the strains in the binder film can be from 10 to 100 times of the bulk strain in the total mixture. The high magnitudes were attributed to the difference in the stiffness of asphalt binder and aggregates. The study done by Kose et al. (*66*) indicated that the magnitude of localized strain in the asphalt mastic (binder plus mineral filler 40 μm in size or smaller) can be as high as 85 times the bulk strain of the HMA. They also reported that the average value for the mastic strain was approximately 4.3 times the HMA bulk strain.

One of the challenges in the characterization of fatigue damage is separating the mixture response due to fatigue crack growth from the response due to nonlinear viscoelastic response. The challenge is that both nonlinearity and damage have similar effect on the mechanical response of the material. For example, when a specimen is subjected to cyclic loads at high stress (or strain) amplitude, the measured dynamic modulus can be less than the expected value based on linear viscoelastic properties either due to nonlinear behavior of the material, or damage, or both. Similarly, the viscoelastic phase angle measured at high stress (or strain) amplitudes can be higher than the expected phase angle determined in the linear viscoelastic range either due to nonlinear behavior, or damage, or both (Figure 6.1).

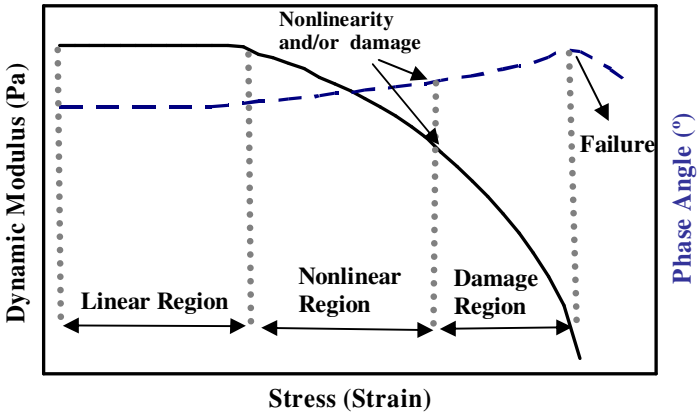

FIGURE 6.1 Dynamic Modulus and Phase Angle Behavior for Different Stress (Strain) Amplitudes.

OBJECTIVE

The objective of this study is to develop an experimental and analytical procedure that will be able to separate the dissipated energy due to nonlinear viscoelasticity from the energy dissipated due to fatigue damage. To achieve this objective six different types of FAM specimens were subjected to a modified form of stress (or strain) sweep tests using the DMA. The results from this study will provide an approach to determine the limiting value of stress (or strain) amplitude from a cyclic load test that marks the end of the nonlinear viscoelastic response for a given material. A stress (or strain) amplitude that exceeds this threshold value will introduce incremental damage to the material. The viscoelastic properties at the threshold amplitude can be used to: (i) quantitatively and accurately differentiate between the energy that is dissipated due to nonlinear viscoelastic response versus the energy that is dissipated due to incremental damage, and (ii) improve the fatigue damage characterization.

MATERIALS AND TEST PROCEDURE

Materials

Six different types of FAM (representing six different full asphalt mixtures) were used in the present study. Each mixture was a combination of one aggregate (RL, or RD) and one binder (AAD, AAB, or AAF). Aggregates and binders were obtained from the Strategic Highway Research Program (SHRP) materials reference library. RL is a gulf coast gravel (Fordyce Inc., Sullivan City, TX), and RD is a limestone (Genstar Stone Prod., White Marsh, MD) with low absorption (*67*). Robl et al. (*67*) also present other aggregate's properties: mineralogical composition, pH, particle sizes, shape, texture, etc. Binders' characteristics are in Table 6.1. More information about functional group analysis, elemental analysis, thin film oven test results, and viscoelastic properties for these binders can be found in Jones (*68*).

TABLE 6.1 SHRP Materials Reference Library Binders' Characterization (*68*)

Binder	Crude Oil Source	SHRP PG Grade	Component Analysis (%)				
			Asphaltenes (n-heptane)	Asphaltenes (iso-octane)	Polar aromatics	Napthene aromatics	Saturates
AAD	Ca Coast	58-28	20.5	3.4	41.3	25.1	8.6
AAB	WY Sour	58-22	17.3	2.0	38.3	33.4	8.6
AAF	W Tx Sour	64-10	13.3	3.1	38.3	37.7	9.6

Each of the six types of FAM followed the same aggregate gradation (Figure 6.2a). Figure 6.2a also illustrates the aggregate gradation for the full asphalt mixture that was used to derive the aggregate gradation for the FAM. The difference between the procedure used during this study to prepare DMA samples from the one in previous chapters is that the fine aggregates' proportions (aggregates smaller than 1.18 mm, including filler) were similar to their proportions in the HMA. The amount of binder used to prepare FAM samples was also the same used in the HMA obtained following

the Superpave mixture design (*57*). This simplification was assumed to be reasonable considering that the surface area is more affected by the percent of aggregate passing the smaller sieve sizes (*69*). The full asphalt mixture that used aggregates RL and RD required a percentage of binder equivalents to 4.35% and 3.35% by mass of the total HMA, respectively. These HMA mixtures had 22% of its aggregate passing on sieve No. 16. For the FAM design only aggregates passing on sieve No. 16 were considered resulting in a percentage of binder equivalents to 17.13% and 13.61% by mass of the total FAM for RL and RD mixtures, respectively.

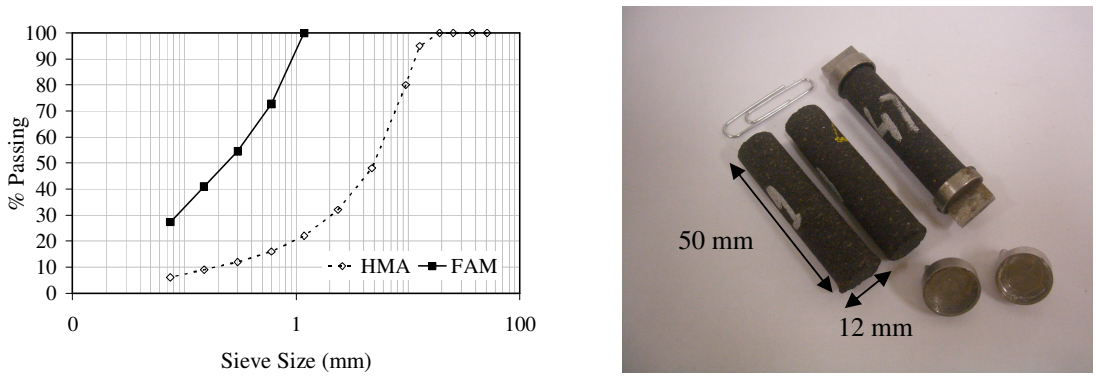

(a) (b)

FIGURE 6.2 (a) HMA and FAM Gradations, (b) DMA Samples.

Aggregate and binder were combined at mixing temperature for each mixture. Before compaction, the mixture was short term aged in the oven for 2 hours at mixing temperature, depending on asphalt type. The mixing temperature corresponds to a viscosity of 160±20 centipoises (*70*). DMA test specimens were prepared to achieve a target air void of approximately 4% (±1%) (Figure 6.2b). Around 10 DMA samples are obtained by coring a 100 mm diameter and 90 mm high specimen compacted using a Superpave gyratory compactor (SGC). To obtain the desired height (50 mm) for the DMA sample and also assure uniformity, the ends of the 100 mm SGC sample were

sawed off before coring. More details about the mixture preparation procedure can be found in Chapter IV and in Appendix A.

Test Procedure

The DMA used in this study is a commercial rheometer from TA Instruments® (AR 2000). A modified form of sinusoidal torsional stress (or strain) sweep tests were performed on the FAM specimens using DMA. The test applied a fixed frequency (10 Hz) with a variable value of shear stress (or strain). All tests were conducted at a temperature of 25ºC.

The parameters for the amplitude sweep test were developed by investigating optimal values for: (i) the range of stress (or strain) amplitudes to be utilized, (ii) the number of stress (or strain) amplitudes that would be swept in the selected range, and (iii) the number of loading cycles for which the same stress (or strain) amplitude would be applied. The last parameter (iii) is not typical for a sweep test and is important in order to be able to differentiate between nonlinear response from damage. The minimum load amplitude must be low enough to fall within the material's linear viscoelastic region (LVE). The maximum amplitude must be high enough to cause damage to the material. The number of load cycles at each load amplitude was optimized to avoid excessive load application. It was important to ensure that the number of load cycles at the same load amplitude were adequate to evaluate whether or not the response changed over time. Stress sweep tests were performed for a range of stress from 1.1×10^3 Pa to 1.1×10^5 Pa, for mixtures with binders AAD and AAB; and from 1.1×10^3 Pa to 2.0×10^5 Pa, for mixtures with binder AAF. Strain sweep tests were performed for a range of strain from 0.001% to 0.6%, for all mixtures. Twenty five loads were swept at equal intervals within the selected range, and 200 cycles were applied at each amplitude.

DATA ANALYSIS AND RESULTS

The response at each load amplitude was recorded. As the load amplitude is gradually increased (Figure 6.3a and 6.3c) the following sequence or three stages of response can be expected: (i) the response amplitude is linear with respect to applied load at low amplitudes, (ii) the response amplitude is nonlinear with respect to the applied load at intermediate amplitudes, and (iii) the response amplitude reflects incremental damage in the specimen at high load amplitudes. In stages (i) and (ii), i.e., when the response amplitude is linear or nonlinear, the response amplitude should not change with increasing number of load applications at the same load amplitude. On the other hand, for a given load amplitude, a change (increase or decrease) in the response amplitude with increasing number of load applications is indicative of accumulation of incremental or fatigue damage (Figure 6.3b and 6.3d). Therefore, by monitoring the change in the response amplitude over the applied 200 cycles at each load amplitude it is possible to identify the threshold load amplitude that differentiates between stages (ii) and (iii), i.e., separates the nonlinear viscoelastic response from the damage response. Quantitatively, this change, increase in response strain amplitude or decrease in response stress amplitude, can be identified by determining whether or not the slope of the response amplitude is significantly different from zero for the 200 cycles at each load amplitude. The statistical analysis used to identify this threshold value is further described in the following section.

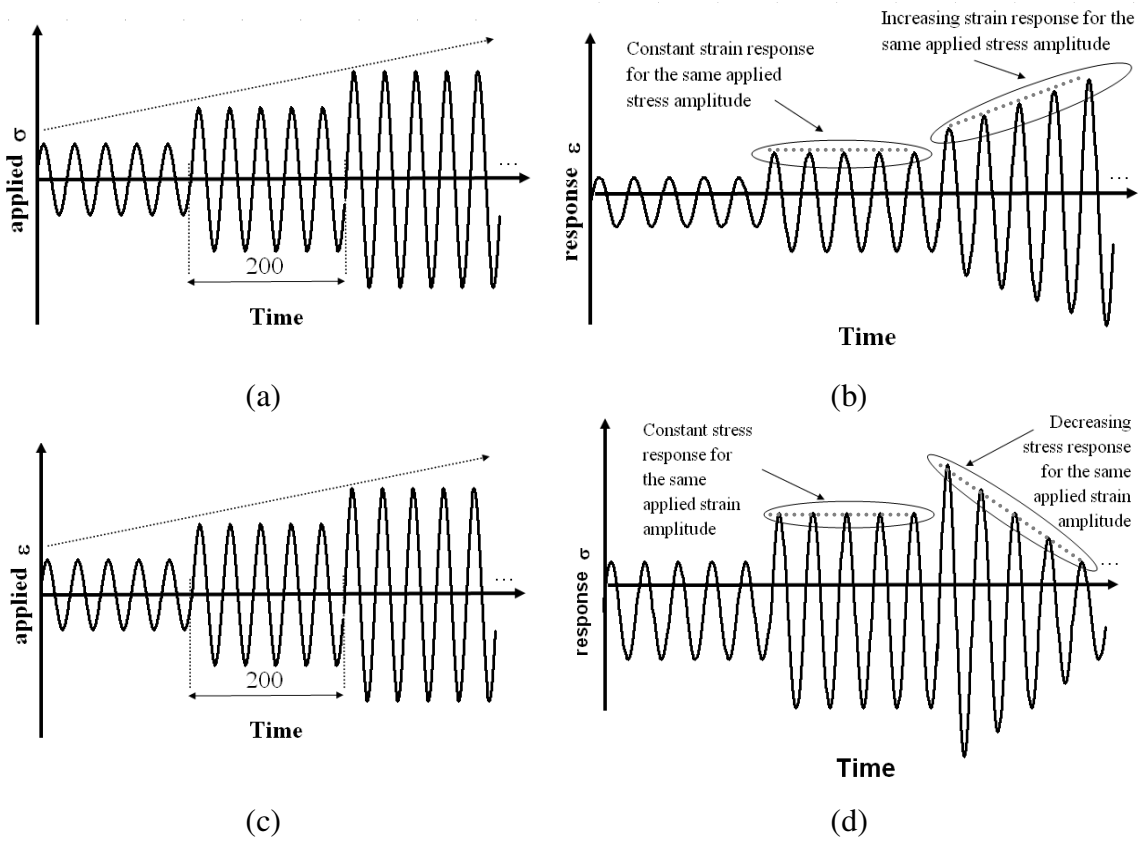

FIGURE 6.3 (a) Applied Stress, (b) Strain Responses, (c) Applied Strain, and (d) Stress Responses.

Statistical Analysis

An algorithm was developed to analyze the data from the sweep tests and determine the threshold amplitude value beyond which damage is imminent. Considering that y is the slope of the response amplitude over 200 load cycles and x is the load amplitude at which the slope is determined, the following analysis can be conducted. The algorithm fits the data with a horizontal line ($y=\alpha_0$) connected to a point x_0 to a linear function ($y = \beta_0 + \beta_1 x$) (for strain sweep tests), or a quadratic function ($y=\beta_0+\beta_1 x+\beta_2 x^2$) (for stress sweep tests). The parameter x_0 is called change point and can be interpreted as the point where the derivative is different from zero. The algorithm uses a least squares criterion subject to the constraint that the two pieces of the function intersect at x_0. Also,

for the quadratic case, the derivative at x_0 is constrained to be zero, this way the function is smooth at the change point. Let $x_{(i)}$ denote the ordered x values and $y^*_{(i)}$ denote the response corresponding to $x_{(i)}$. Then the function to be minimized for the linear case is:

$$min\left(\sum_{i:x(i)<x_0} (y^*_{(i)} - \alpha_0)^2 + \sum_{i:x(i)\geq x_0} \left(y^*_{(i)} - \left(\beta_0 + \beta_1 x_{(i)} \right) \right)^2 \right) \tag{6.1}$$

considering that $y=\beta_0+\beta_1 x$ passes through (x_0, α) with respect to α_0, β_0, β_1, and x_0.

For the quadratic case, the function to be minimized is:

$$min\left(\sum_{i:x(i)<x_0} (y^*_{(i)} - \alpha_0)^2 + \sum_{i:x(i)\geq x_0} \left(y^*_{(i)} - \left(\beta_0 + \beta_1 x_{(i)} + \beta_2 x^2_{(i)} \right) \right)^2 \right) \tag{6.2}$$

considering that $y=\beta_0+\beta_1 x+\beta_2 x^2$ passes through (x_0, α) and $\beta_1+2\beta_2 x=0$ at (x_0, α) with respect to α_0, β_0, β_1, β_2 and x_0.

The minimization is achieved by first selecting a grid of points covering the range of the x data that corresponds to potential values of x_0. Then for each potential value of x_0 along the grid, the minimization of α_0, β_0, β_1 (and β_2 for the quadratic case) is carried out using Excel's Solver. The choice of parameters, denoted by α_0, β_0, β_1, β_2 and x_0 in the output, that minimizes the objective function above, is selected as the least squares estimates.

Results

The amplitude responses (slopes of strain or stress response versus time plots) were monitored for the six different types of FAM used in this study. The slope of the amplitude response versus the number of load cycles was determined by plotting the strain (or stress) amplitude for each one of the 200 load applications and fitting a linear trend line. Once the slopes were determined, the statistic algorithm was applied and the stress (or strain) amplitude correspondent to the threshold (x_0) between the nonlinear and the damage regions was found. The results are in Tables 6.2 and 6.3 and in Figures 6.4 and 6.5.

TABLE 6.2 Statistic Parameters for Six FAM Used in This Study, Stress Sweep Tests

Parameter	Mixture*					
	RLAAD	RLAAB	RLAAF	RDAAD	RDAAB	RDAAF
x_0 (kPa)	92	87	56	87	33	131
α_0	0	0	0	0	0	0
β_0	0.05	0.01	3.39×10^{-5}	0.01	1.73×10^{-5}	0.00
β_1	-3.49×10^{-7}	-4.01×10^{-8}	-4.07×10^{-10}	-4.01×10^{-8}	-3.50×10^{-10}	-2.21×10^{-9}
β_2	1.90×10^{-12}	2.30×10^{-13}	3.66×10^{-15}	2.30×10^{-13}	5.33×10^{-15}	8.56×10^{-15}

* For mixture identification, the first two letters represent the aggregate and the latter three letters the type of binder.

TABLE 6.3 Statistic Parameters for Six FAM Used in This Study, Strain Sweep Tests

Parameter	Mixture					
	RLAAD	RLAAB	RLAAF	RDAAD	RDAAB	RDAAF
x_0 (%)	0.10	0.001	0.03	0.03	0.001	0.001
α_0	-3.19×10^{-7}	-1.53×10^{-6}	-3.39×10^{-6}	-3.80×10^{-7}	-3.16×10^{-6}	-2.62×10^{-6}
β_0	1.08×10^{-6}	-1.52×10^{-6}	-1.67×10^{-6}	3.18×10^{-8}	-3.15×10^{-6}	-2.56×10^{-6}
β_1	-0.001	-0.002	-0.007	-0.002	-0.001	-0.007

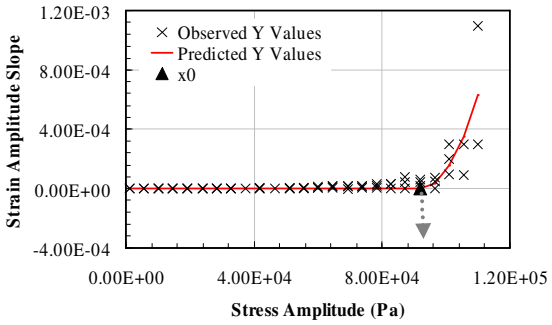

(a) RLAAD

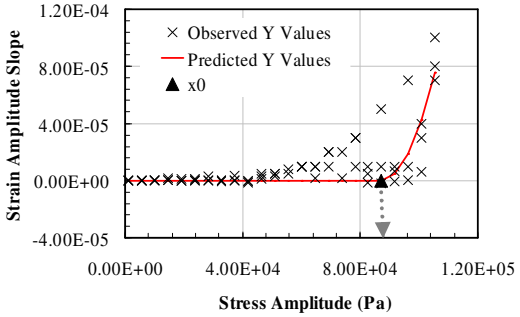

(b) RLAAB

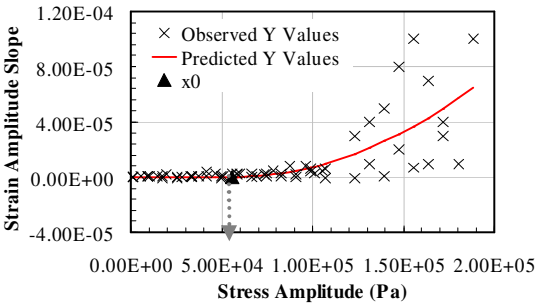

(c) RLAAF

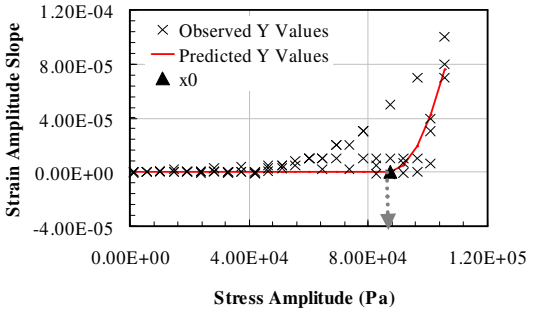

(d) RDAAD

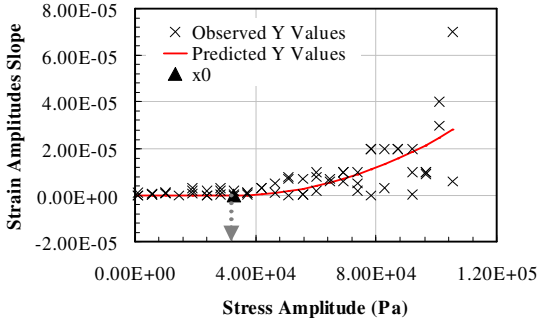

(e) RDAAB

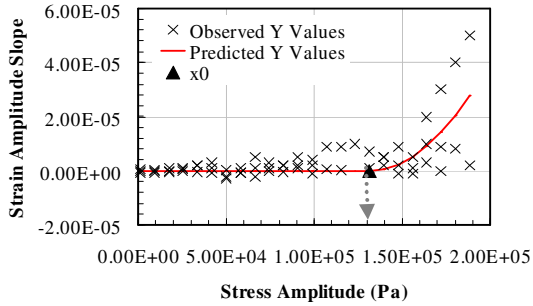

(f) RDAAF

FIGURE 6.4 Strain Amplitudes Slopes versus Stress Amplitude (Pa), Stress Sweep Tests.

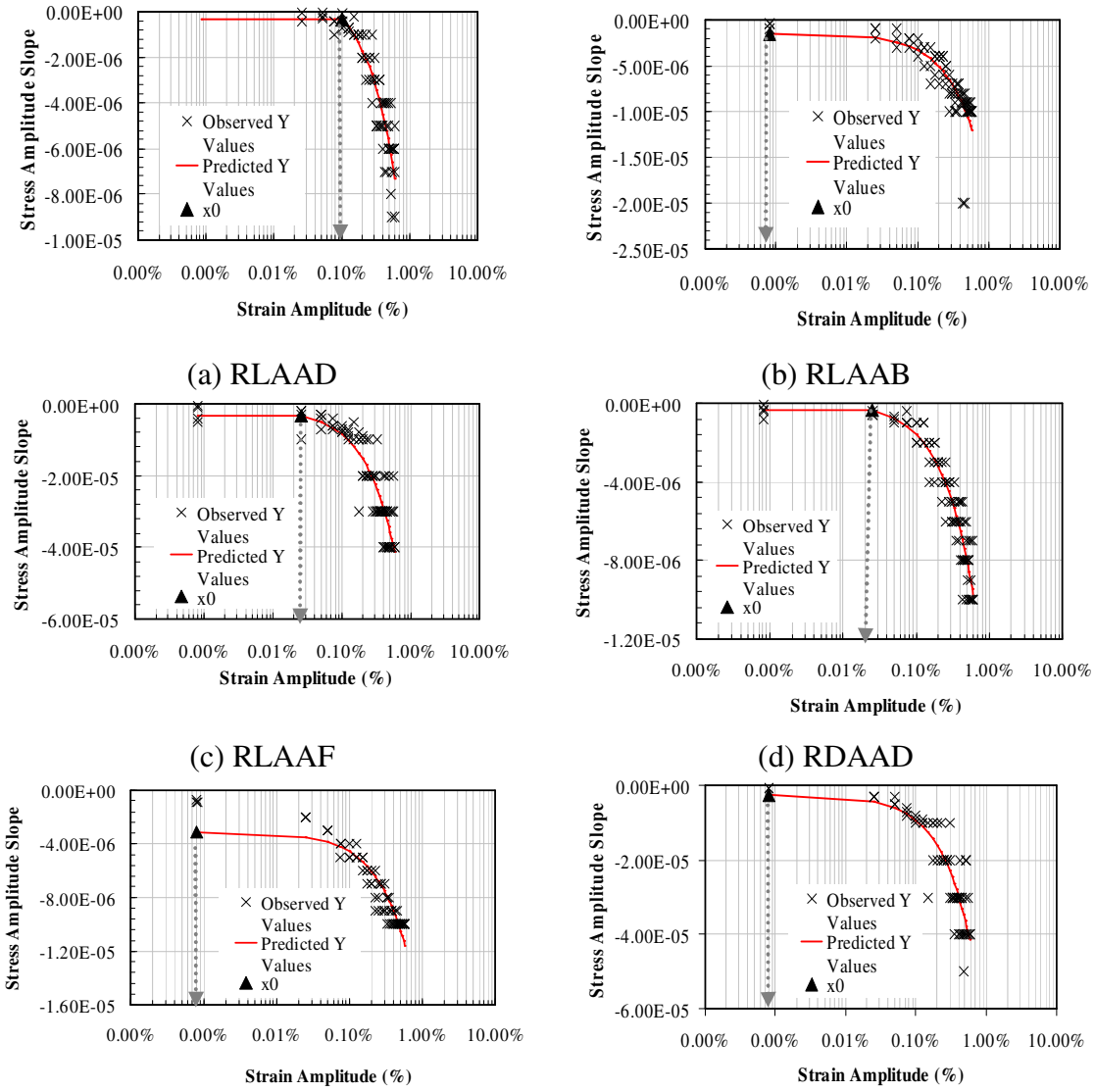

FIGURE 6.5 Stress Amplitudes Slopes versus Strain Amplitude (%), Strain Sweep Tests.

For the stress sweep tests, mixtures RLAAD, RLAAB, RDAAD, and RDAAB had similar behavior. Mixtures with binder AAD and AAB presented a higher value for the stress threshold when aggregate RL was used. An opposite trend was found for the mixtures with binder AAF. RLAAF mixture presented lower stress threshold in comparison with the RDAAF mixture.

For the strain sweep tests, the strain threshold values (x_o in Table 6.3) were very low for most of the mixtures analyzed (except for mixture RLAAD). These extremely low values were sometimes impossible to be used in the lab due to the equipment data acquisition limitations. For the sweep tests, the applied load amplitudes should be constant if the instrument is properly controlling those variables. In Figure 6.6a, stress amplitude slope versus applied stress amplitude was plotted for mixture RLAAB. In Figure 6.6b, strain amplitude slope versus applied strain amplitude was plotted for mixture RLAAB. It is noticed that the instrument was able to control the applied stress amplitude (Figure 6.6a), but the same did not happen for the applied strain amplitude (Figure 6.6b). It is believed that this difference was responsible for the very low x_o values found for strain sweep tests (Table 6.3). This was caused by the fact that the rheometer used during this study (AR 2000, from TA Instruments) is in reality a controlled-stress instrument (*71*). Controlled-stress instruments operate with feed-back loops making them act as controlled-strain rheometers. According to Menard (*58*) at low strains (within the material linear viscoelastic region) both rheometers, controlled-strain and controlled-stress, give the same results. On the other hand, for high strains (inside the material nonlinear viscoelastic region) the differences can be significant.

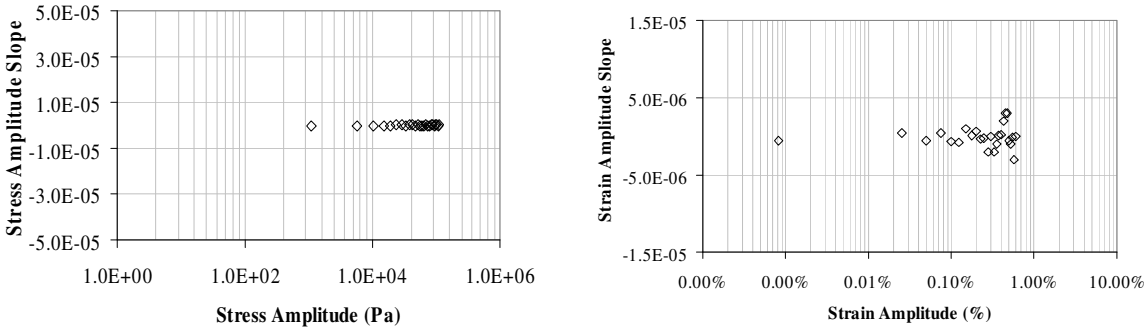

(a) (b)

FIGURE 6.6 Amplitude Slope versus Applied Amplitude for: (a) Stress Sweep Test (Mixture RLAAB), and (b) Strain Sweep Test (Mixture RLAAB).

In order to obtain the real values for the strain threshold that separates the nonlinear viscoelastic from the damage response, the following approach was developed. Considering that the nonlinear viscoelastic properties (dynamic modulus - G^*_{VE} and phase angle - δ_{VE}) should be the same independent of the mode of loading (stress sweep or strain sweep), G^* versus stress amplitude plots were generated for the stress sweep tests (Figure 6.7a). Knowing the stress threshold (x_o in Table 6.2), G^*_{VE} can be obtained for each mixture. Plotting G^* versus strain amplitude (for the strain sweep tests), the strain threshold can be backcalculated (Figure 6.7b). An example for this back calculation procedure for mixture RLAAB (one sample) is plotted in Figure 6.7. For the six mixtures analyzed during this study, strain threshold values were back calculated for each sample. At least three samples were used for each test and the average values are in Table 6.4.

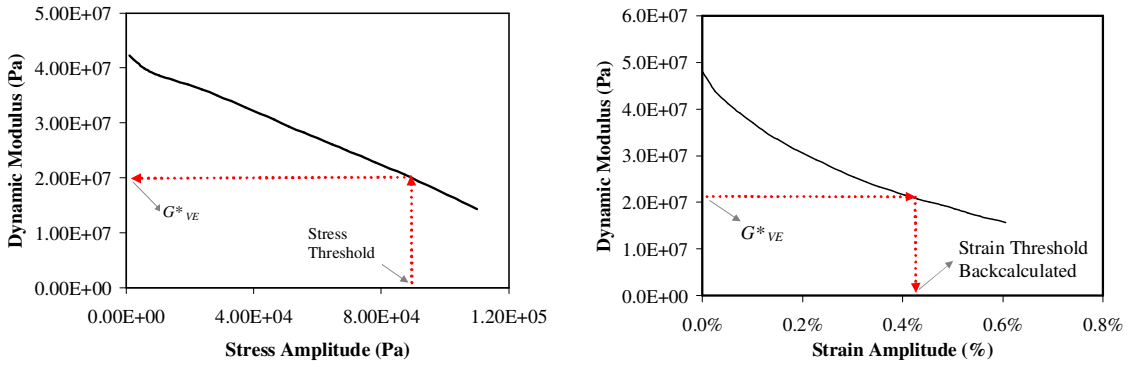

(a) Stress Sweep Test (b) Strain Sweep Test

FIGURE 6.7 Approach to Back Calculate Strain Threshold Using Stress Sweep Test Data: (a) G^*_{VE} Determination from Stress Sweep Test; and (b) Strain Threshold Back Calculated from Strain Sweep Test.

TABLE 6.4 Strain Thresholds Back Calculated from Stress Sweep Tests Results

Parameter	Mixture					
	RLAAD	RLAAB	RLAAF	RDAAD	RDAAB	RDAAF
x_0 (%)*	0.58	0.39	0.18	0.46	0.09	0.06

* Backcalculated values

For the strain sweep tests, all mixtures had similar behavior. Mixtures with aggregate RL presented higher value for the strain threshold back calculated from stress sweep tests (Table 6.4).

SUMMARY AND CONCLUSIONS

An experimental and analytical procedure to identify the load amplitude at which nonlinear viscoelasticity ends and damage initiates was presented. This procedure was applied to six different types of FAM using the DMA. A statistical algorithm was developed to analyze the results and calculate the threshold load amplitude in a cyclic load test. This threshold marks the end of the nonlinear viscoelastic region beyond which fatigue or incremental damage is imminent. Accurate determination of this threshold is important in order to improve the accuracy of fatigue damage characterization based on the dissipated energy concepts. This is because the threshold load amplitude and viscoelastic properties at the threshold allow the user to accurately differentiate between viscoelastic energy dissipation and energy dissipation due to fatigue damage. Results from this study demonstrate that the threshold value depends on both the type of binder and aggregate used in the FAM.

Strain sweep tests results were not considered in identifying the threshold magnitude because the rheometer used during this study is a controlled-stress device. Although these instruments operate using a feed-back loop, it was not capable of maintaining the application of a constant strain amplitude. Strain thresholds were back calculated from stress sweep tests. The proposed methodology can also be used with

other materials such as full asphalt mixtures as well as with tests conducted in other modes of loading such as repeated tension or compression. The results of this chapter are used in the following chapter to calculate parameters that quantify the nonlinear viscoelastic and damage parameters of FAM.

CHAPTER VII

NONLINEAR VISCOELASTIC AND DAMAGE CHARACTERIZATION OF FINE ASPHALT MIXTURES USING DYNAMIC MECHANICAL ANALYSIS (DMA)

OVERVIEW

This chapter presents two related approaches for the characterization of the nonlinear viscoelastic behavior and damage of asphalt mixtures. The first approach relies on identifying the various mechanisms of energy dissipation during fatigue cracking that are manifested in: (i) nonlinear viscoelastic deformation, (ii) fracture, and (iii) permanent deformation. Energy indices will be used to quantify each of these energy dissipation mechanisms and to quantify fatigue cracking irrespective of the mode of loading. The outcome of this approach is a fatigue damage parameter that provides comparable results for a given material, even when tested under different modes of loading, and has lower coefficients of variation when compared to a conventional parameter (number of load cycles to failure). The second approach relies on using a constitutive model that can describe both the nonlinear viscoelastic response and fatigue damage in one formulation. This analysis method yields the nonlinear viscoelastic parameters and damage parameters that are functions of stress (or strain) amplitudes. This second approach has the added advantage that the constitutive relationship can be extended to the general three-dimensional formulation and implemented in a numerical framework to describe the response of asphalt mixtures under various boundary conditions. The efficacy of these analysis methods is demonstrated by conducting oscillatory dynamic mechanical analysis (DMA) under controlled-stress and controlled-strain modes of loading and different load amplitudes for six different types of fine aggregate matrix. Results from this study show that both methods proposed are able to unify the ranking of different

mixtures from both modes of loading as long as the applied stresses are within the same range.

INTRODUCTION

Asphalt mixtures can exhibit linear or nonlinear behavior depending on a combination of factors, including: (i) stress (or strain) amplitudes, (ii) temperature, and (iii) rate of loading. Characterization of nonlinear behavior is important because materials that behave similarly in the linear region can present very different behavior in the nonlinear region, and nonlinear viscoelastic behavior needs to be considered and separated from damage.

Some work has been done attempting to characterize asphalt mixtures nonlinear viscoelastic behavior. Fitzgerald and Jalal (*72*) extended the Lebesgue-norm constitutive equation for nonlinear viscoelastic materials to characterize sand-asphalt mixtures. These authors performed relaxation tests at different strain amplitudes including: constant strain rate, interrupted-ramp strain rate (including rest periods), and reverse-ramp strain rate (raising the stress to an arbitrary amplitude using a constant strain rate and then decreasing the stress using the same but negative strain rate). Experimental and theoretical results presented good agreement with the nonlinear viscoelastic theory but deviated when linear theory was used. The study done by Bahia et al. (*23*) demonstrated the importance of considering the nonlinear viscoelastic behavior of asphalt mixtures when characterizing the fatigue performance of asphalt binders. These authors conducted parallel plate oscillation tests. They evaluated different materials' compositions (neat and modified asphalt binders), strain amplitudes, temperature, aging, healing effects and heating rates. One of the most important conclusions from this research is the fact that the strain dependence and fatigue are sensitive to the factors previously mentioned and also by the interaction between these factors. Pollaco et al. (*73*) used the nonlinear generalized Lodge's rubber-like liquid model to obtain shear viscosity and relaxation modulus for neat asphalts and polymer modified asphalts. These authors checked the

ability of this specific model by predicting experimental results for different temperatures and shear rates. Also, the correlation between the material molecular level structure and its viscoelastic properties were investigated.

Schapery's approach has been used successfully to predict nonlinear viscoelastic behavior for different materials: metals, polymers, composites, and wood (*38, 39, 40, 41, 74-80*). The same approach has been used to characterize nonlinear viscoelastic behavior of asphalt materials. Shields et al. (*42*) investigated the nonlinear viscoelastic behavior of HMA using Schapery's theory. These authors demonstrated that, for strain values greater than 0.1%, the stress predicted using nonlinear viscoelastic theory was in agreement with measured values using relaxation test. Dai et al. (*81*) presented a 2D micromechanical model for the linear and damage-coupled viscoelastic behavior of mastic and asphalt mixtures using the finite element (FE) method. These authors used Schapery's nonlinear viscoelastic model to develop an approach for the analysis of rate-independent and rate-dependent damage behavior. Experimental and model results were compared resulting in 11.7% difference attributed to model assumptions (rigid aggregates with infinity stiffness and elliptical shape). Masad et al. (*26*) used Schapery's approach and dynamic shear rheometer (DSR) binder test results to analyze binder nonlinear viscoelastic response under different conditions: stress amplitude, temperature, frequency, and aging. These authors implemented Schapery's model in FE and used it to predict binder creep response. They concluded that binder long term response can be found using short term experiments under different stress amplitudes and that aged binder response can be obtained using parameters from the non aged binder analysis with shift factors.

OBJECTIVES AND TASKS

The main objective of the current study is to present two approaches to characterize asphalt materials' nonlinear viscoelastic behavior and damage. The following tasks support this objective:

- Conduct DMA tests using different modes of loading (controlled-strain and controlled-stress) and different strain (stress) amplitudes on specimens representing six different FAM;
- For the first approach:
    - Obtain viscoelastic properties (dynamic modulus and phase angle) in order to separate the energy dissipated due to damage from the viscoelastic energy;
    - Use a fatigue damage parameter (crack growth index) to quantify crack growth in the FAM;
    - Evaluate the results variability.
- For the second approach:
    - Use Schapery's theory to determine nonlinear viscoelastic stress dependent ($\Delta g_1 \Delta g_2$) and strain dependent ($\Delta h_1 \Delta h_2$) parameters;
    - Monitor the change in material response with repeated loading at a given stress or strain amplitude and obtain two damage parameters: (i) V (damage parameter for controlled-stress analysis), and (ii) W (damage parameter for controlled-strain analysis);
- Investigate the efficacy of both approaches in respect to providing results that are able to rank different mixtures independent of the mode of loading used.

CRACK GROWTH INDEX APPROACH

Chapters III e IV of this dissertation evaluated the fatigue cracking characteristics (quantified as crack growth index) for several different types of FAM using principles of fracture mechanics. In these chapters, the energy in the first cycle of the fatigue test was partitioned between viscoelastic energy and damage energy. However, the viscoelastic energy dissipated at the threshold stress amplitude (beyond which damage is imminent) should be used to partition energy dissipated due to damage from the viscoelastic energy. The method developed in Chapter VI can be used to improve fatigue damage

characterization by selecting the threshold load amplitude that separates nonlinear viscoelastic response from damage. To illustrate this application, the fatigue parameter (crack growth index) determined in Chapters III and IV was calculated by making use of the threshold values determined in Chapter VI.

The crack growth index ($R(N)$) is shown in Equation 7.1.

$$R(N) = \frac{\bar{r}(N)}{K^{\frac{1}{2n+1}}} = \left[(2n+1)^{n+1} \left(\frac{E_R b}{4\pi E_1 \Delta G_f} \right)^n N \right]^{\frac{1}{2n+1}} \tag{7.1}$$

N is the number of load cycles, K is a constant for each material that is inversely proportional to the square of the tensile strength of the asphalt mixture, E_R is the reference modulus. E_R selection for this study will be discussed later. b represents the rate of change of the DPSE with respect to load cycles ($DPSE = a + bLn(N)$). E_1 is obtained from the relaxation modulus-time relationship ($E(t) = \frac{\tau(t)}{\gamma_0} = E_\infty + E_1 t^{-m}$), ΔG_f is the adhesive bond energy, and n is related to the exponent m in the relaxation modulus-time relationship ($n = 1 + \frac{1}{m}$) (*27*).

NONLINEAR VISCOELASTIC AND DAMAGE APPROACH

Schapery (*25*) developed a model to represent the nonlinear viscoelastic behavior for different materials. According to this model, the strain response (ε) for a given stress (σ) history can be represented using Equation 7.2:

$$\varepsilon(t) = g_0 D_0 \sigma + g_1 \int_0^t \hat{D}(t-\tau) \frac{\partial g_2 \sigma}{\partial \tau} d\tau \tag{7.2}$$

where, ε and σ are the uniaxial strain and stress, respectively. D_0 is the linear elastic creep compliance component. $\hat{D}$ is the linear transient creep compliance component which is dependent on time and temperature. t is the present time, while τ is the time

elapsed since load application. g_0, g_1 and g_2 are stress dependent nonlinear viscoelastic parameters. g_0 introduces nonlinear contributions in the elastic response due to stress amplitude, g_1 introduces nonlinear contributions in the complete transient response, and g_2 introduces nonlinear contributions due to the rate of applied load. The model reduces to the Boltzmann superposition integral for linear response (g_0, g_1, and g_2 are equal to one).

To account for oscillatory contributions, the function described in Equation 7.2 is expressed as in Equation 7.3:

$$\Delta\varepsilon(t) = D_0 \Delta g_0(\Delta\sigma) + (\Delta g_1) \int_0^t \hat{D}(t-\tau) \frac{\partial}{\partial\tau}(\Delta g_2)(\Delta\sigma) \partial\tau \tag{7.3}$$

Changing variables for the term inside the integral operator and performing some mathematical manipulations (see Appendix C), Equation 7.3 can be rewritten as:

$$\Delta\varepsilon(t) = D_0 \Delta g_0(\Delta\sigma) + (\Delta g_1)(\Delta g_2)(\Delta\sigma)(\hat{D}' + i\hat{D}'') \tag{7.4}$$

where, $\hat{D}'$ and $\hat{D}''$ are represented by Equations 7.5 and 7.6, respectively. LVE in the subscript stands for the linear viscoelastic properties.

$$\left|D^*\right|_{LVE} \cos\delta_{LVE} = D_0 + \hat{D}^*_{LVE} \cos\hat{\delta}_{LVE} = D_0 + \hat{D}' \tag{7.5}$$

$$\left|D^*\right|_{LVE} \sin\delta_{LVE} = \hat{D}^*_{LVE} \sin\hat{\delta}_{LVE} = \hat{D}'' \tag{7.6}$$

Creep compliance can be represented by real (stored) and imaginary (dissipated) parts ($D^* = \frac{\Delta\varepsilon}{\Delta\sigma} = \frac{\varepsilon_0}{\sigma_0} cos\,\delta + i\frac{\varepsilon_0}{\sigma_0} sin\,\delta$).

The same analysis can be conducted for the controlled-strain case to yield the equations in Table 7.1. Δg_i are controlled-stress nonlinear viscoelastic parameters and Δh_i are controlled-strain nonlinear viscoelastic parameters. σ_0, ε_0 and δ are stress

amplitude, strain amplitude, and phase angle at the applied load, respectively. E_∞ and D_0 are the parameters of the power law equation of the relaxation modulus ($E(t) = E_\infty + E_1 t^{-m}$) and creep compliance ($D(t) = D_0 + D_1 t^n$), respectively. Further information on the derivations of these equations is available in Golden et al. (*40, 41*) and in Appendix C.

As discussed earlier, the nonlinear parameters change with changing in load (strain or stress) amplitudes. However, their values should remain constant with repeated loading at a given load amplitude if no damage occurs. Damage causes change in response to repeated loading at a given load amplitude. In order to account for damage, two damage parameters are added to the equations: (i) *V* (damage parameter for controlled-stress analysis), and (ii) *W* (damage parameter for controlled-strain analysis). If no damage occurs (linear or nonlinear viscoelastic behaviors only), damage parameters (*V* and *W*) should be equal to one, and the first two equations in Table 7.1 will be equal to the last two. Table 7.2 presents a summary for the parameters (nonlinear and damage) depending on the region (linear, nonlinear, and damage).

TABLE 7.1 Equations for the Nonlinear Viscoelastic (NLVE) and Damage Parameters Characterization

Response	Mode of Loading	
	Controlled-Strain	Controlled-Stress
NLVE Response	$\frac{\sigma_0}{\varepsilon_0}\cos\delta = E_\infty(\Delta h_\infty) + (\Delta h_1)(\Delta h_2)\hat{E}'$	$\frac{\varepsilon_0}{\sigma_0}\cos\delta = D_0(\Delta g_0) + (\Delta g_1)(\Delta g_2)\hat{D}'$
	$\frac{\sigma_0}{\varepsilon_0}\sin\delta = (\Delta h_1)(\Delta h_2)\hat{E}''$	$\frac{\varepsilon_0}{\sigma_0}\sin\delta = (\Delta g_1)(\Delta g_2)\hat{D}''$
NLVE+Damage Response	$\frac{\sigma_0}{\varepsilon_0}\cos\delta = E_\infty(\Delta h_\infty) + (\Delta h_1)(\Delta h_2)(W)\hat{E}'$	$\frac{\varepsilon_0}{\sigma_0}\cos\delta = D_0(\Delta g_0) + (\Delta g_1)(\Delta g_2)(V)\hat{D}'$
	$\frac{\sigma_0}{\varepsilon_0}\sin\delta = (\Delta h_1)(\Delta h_2)(W)\hat{E}''$	$\frac{\varepsilon_0}{\sigma_0}\sin\delta = (\Delta g_1)(\Delta g_2)(V)\hat{D}''$

TABLE 7.2 Summary of Nonlinear Viscoelastic (NLVE) and Damage Parameters for Different Regions

Region	NLVE Parameter ($\Delta h_1 \Delta h_2$ or $\Delta g_1 \Delta g_2$)	Damage Parameter (W or V)
Linear	=1	=1
Nonlinear	≠1	=1
Damage	≠1	≠1

MATERIALS AND TEST PROCEDURES

Materials

The same materials and mixture design procedure used in Chapter VI were also used in the present study. Six FAM representing the fine portion of six full mixtures were investigated. Each FAM mixture is a combination of one aggregate (RL, or RD) and one binder (AAD, AAB, or AAF). All six FAM have the same aggregate gradation. Further information about these materials can be found in the literature (*67, 68*). Table 7.3 provides the composition of each FAM mixture.

TABLE 7.3 Compositions of FAM Used in This Study

Mixture*	Aggregate gradation sieve (percentage of total aggregate weight)	Aggregate type/Source	Binder PG/Source	Percentage of binder by mass of total FAM
RLAAD RLAAB RLAAF	#30 (27.27) #50 (18.18) #100 (13.64) #200 (13.64) <#200 (27.27)	Gulf Coast Gravel/Fordice Inc., Sullivan City, TX	58-28 / Ca Coast 58-22 / WY Sour 64-10 / W Tx Sour	17.13
RDAAD RDAAB RDAAF		Limestone/Genstar Stone Prod., White Marsh, MD	58-28 / Ca Coast 58-22 / WY Sour 64-10 / W Tx Sour	13.61

*For mixture identification, the first two letters represent the aggregate and the latter three letters the type of binder.

Test Procedures

Three types of DMA tests were performed: (i) relaxation modulus tests, (ii) amplitude sweep tests, and (iii) time sweep tests. All tests were conducted at a temperature of 25ºC.

Relaxation Modulus Test

Relaxation modulus tests at constant shear strain amplitude within the LVE region (0.001%) were performed for the FAM mixtures. The total time for the load step function was 600 seconds. The parameters E_∞, E_1, m, D_0, D_1, and n were obtained from this test. These parameters will be used for the first approach (Equation 7.1), and for the second approach (equations in Table 7.1).

Amplitude Sweep Test

Amplitude sweep tests were performed in order to differentiate the nonlinear viscoelastic from the damage response. The procedure developed in Chapter VI was used during this study to obtain strain and stress threshold amplitudes (Table 7.4). These amplitudes will be used to perform time sweep tests and obtain nonlinear viscoelastic properties.

TABLE 7.4 Threshold Amplitudes for Both Modes of Loading

Threshold amplitude	Mixture					
	RLAAD	RLAAB	RLAAF	RDAAD	RDAAB	RDAAF
Strain (%)	0.58	0.39	0.18	0.46	0.09	0.06
Stress (kPa)	92	87	56	87	33	131

Time Sweep Test

For the time sweep tests, specimens were subjected to a sinusoidal torsional loading at a frequency of 10 Hz at either constant strain amplitude (controlled-strain) or constant

stress amplitude (controlled-stress). These tests were conducted in two different stages: (i) using low strain or stress amplitudes to obtain material properties in the LVE range (0.001% strain for controlled-strain tests and 3.2×10^3 Pa for controlled-stress tests), and (ii) using high strain or stress amplitudes to determine the nonlinear viscoelastic material properties and to induce fatigue damage. For the high amplitude tests, controlled-stress and controlled-strain time sweep tests were performed using two amplitudes: (i) the threshold amplitudes determined using the procedure in Chapter VI and listed in Table 7.4, and (ii) a common amplitude for all mixtures (2.00×10^5 Pa and 0.6% for controlled-stress and controlled-strain tests, respectively). The second amplitude was selected as a common strain or stress amplitude because it is higher than all thresholds for the mixtures evaluated during this study. This amplitude did not cause significant damage to the specimen in the first few cycles of the test.

DATA ANALYSIS AND RESULTS

Crack Growth Index Approach

Relaxation modulus experimental data was predicted using a power law relationship ($E(t) = E_\infty + E_1 t^{-n}$) in order to determine the parameters, E_∞, E_1 and n. The nonlinear viscoelastic properties (VE), dynamic modulus (G^*_{VE}) and phase angle (δ_{VE}) obtained in the first cycle of the time sweep tests conducted at the threshold stress amplitude, for each mixture, were obtained. VE properties are needed in order to calculate DPSE associated with damage by removing the viscoelastic energy from the total strain energy. E_R was selected to be equal to the undamaged VE modulus (G^*_{VE}), which makes the maximum value of pseudo strain equal to that of the applied strain (*5*). Average model parameters are presented in Table 7.5. ΔG_f values were computed based on surface energy measurements (*53*). G^*_{LVE} and δ_{LVE} in Table 7.5 are the LVE properties.

TABLE 7.5 Average Model Parameters, Crack Growth Index Approach

Parameter	Mixture					
	RLAAD	RLAAB	RLAAF	RDAAD	RDAAB	RDAAF
G^*_{LVE} (Pa)	8.31×10^7	1.45×10^8	3.68×10^8	1.14×10^8	1.85×10^8	5.05×10^8
δ_{LVE} (º)	53.02	47.57	40.83	54.69	49.47	42.09
G^*_{VE} (Pa)	6.89×10^7	1.11×10^8	3.41×10^8	9.42×10^7	1.69×10^8	4.24×10^8
δ_{VE} (º)	55.92	51.23	39.88	57.80	52.35	41.99
ΔG_f (J/m^2)	0.083	0.158	0.126	0.066	0.102	0.090
m	0.75	0.42	0.46	0.58	0.37	0.48
E_1 (Pa)	1.41×10^7	9.00×10^6	1.00×10^7	2.00×10^6	1.00×10^7	7.00×10^6

Once the average model parameters were determined, controlled-stress time sweep fatigue tests were performed using a stress amplitude of 2.00×10^5 Pa, and controlled-strain time sweep fatigue tests were performed using a strain amplitude of 0.6%. $R(N=5{,}000)$ values for these controlled-stress and controlled-strain tests were calculated using Equation 7.1. Table 7.6 presents b, $R(N=5{,}000)$, fatigue life values, and corresponding statistics for the mixtures evaluated in this study. Fatigue life was determined in the same way as in Chapter IV. The coefficient of variation (CV) for fatigue life, in general, was much higher than the CV for the crack growth index (R at $N=5{,}000$) determined using the same test data. R values at $N=5{,}000$ for both modes of loading are plotted in Figures 7.1 and 7.2.

TABLE 7.6 Statistics for b, $R(N=5{,}000)$, and Fatigue Life Values

Mixture	Test	b		$R(N=5{,}000)$		Fatigue life	
		Ave.	CV(%)	Ave.	CV(%)	Ave.	CV(%)
RLAAD	CStress (2.00×10^5 Pa)	421.61	43	278.88	19	28,119	18
	CStrain (0.6%)	214.58	53	208.85	23	85,013	63
RLAAB	CStress (2.00×10^5 Pa)	217.84	13	219.90	6	90,526	59
	CStrain (0.6%)	225.02	8	223.23	3	36,128	18
RLAAF	CStress (2.00×10^5 Pa)	11.25	63	102.65	27	NFL	NFL
	CStrain (0.6%)	1,531.87	33	875.86	16	13,727	35
RDAAD	CStress (2.00×10^5 Pa)	340.44	13	710.07	6	60,118	11
	CStrain (0.6%)	172.14	12	532.53	5	88,650	22
RDAAB	CStress (2.00×10^5 Pa)	191.84	75	273.34	31	173,430	61
	CStrain (0.6%)	341.36	9	368.52	4	72,938	15
RDAAF	CStress (2.00×10^5 Pa)	9.34	22	145.41	10	NFL	NFL
	CStrain (0.6%)	1,459.60	22	1278.61	9	15,927	39

*NFL – samples do not failed after testing during eight hours

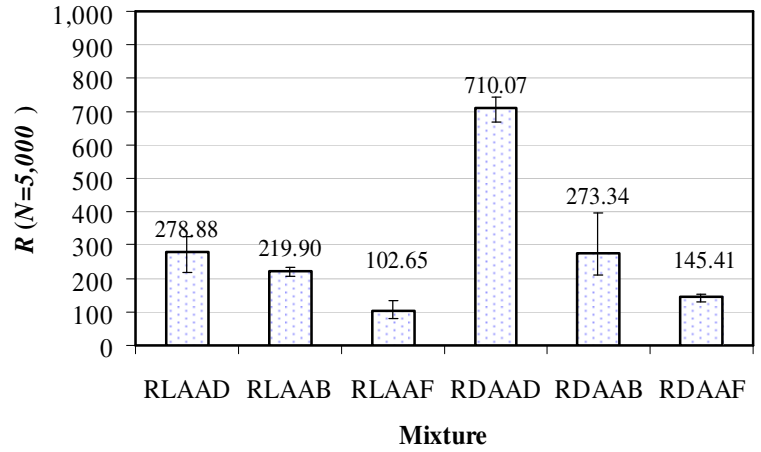

FIGURE 7.1 Crack Growth Index at *N=5,000*, Controlled-Stress Tests (2.00×10^5 Pa).

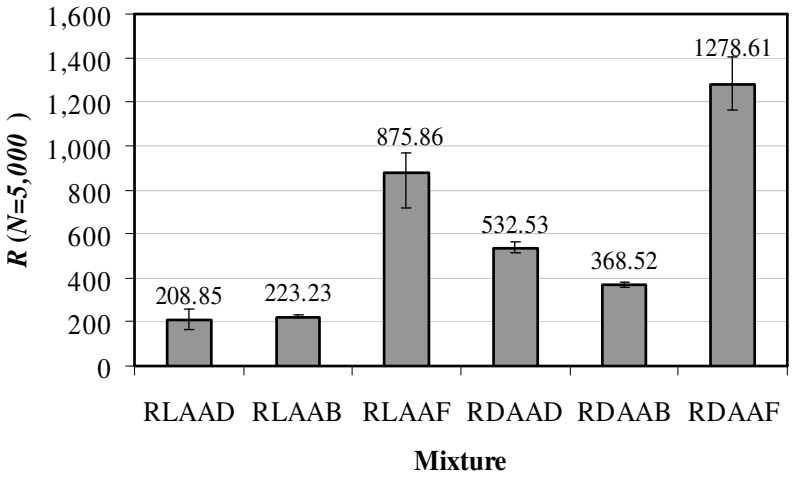

FIGURE 7.2 Crack Growth Index at *N=5,000*, Controlled-Strain Tests (0.6%).

The relation between crack growth index values at fatigue life, for both modes of loading, and the average stress amplitude is plotted in Figure 7.3. The apparent difference in the results in Figures 7.1 and 7.2 for these mixtures is due to the difference in the applied loads. The applied stresses during the controlled-strain for the two mixtures RLAAF and RDAAF turned out to be much higher that the stresses used in the

controlled-stress tests. Consequently, Figure 7.1 shows that crack growth index in these two mixtures for controlled-stress is lower than for controlled-strain. However, as the ratio between the average stress (average between initial and final stress amplitudes) in the controlled-strain test and the stress amplitudes used for controlled-stress tests approaches one, crack growth index values for both modes of loading are very close (Figure 7.3). As can be seen, once the average stress in controlled-strain is more than 60% the applied stress in controlled-stress, the crack growth index value in controlled-strain becomes higher. It is possible to find a relationship between the applied stress amplitude in controlled-stress and the range of stresses in the controlled-strain such that crack growth index values in both modes of loading are similar. As such, in spite of the apparent differences in Figures 7.1 and 7.2, the proposed method is able to unify both modes of loading (controlled-strain and controlled-stress), as long as the applied stresses are within the same range.

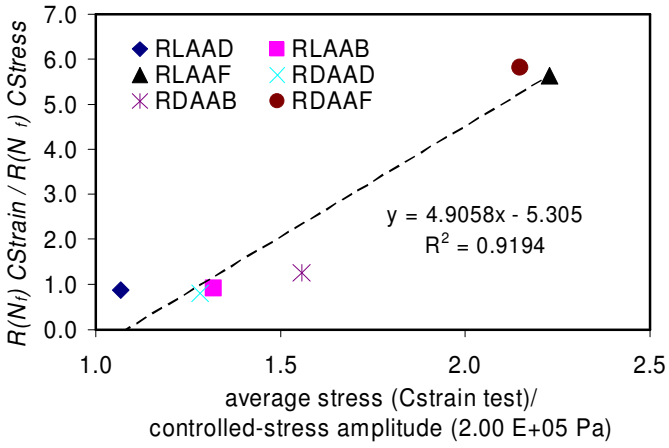

FIGURE 7.3 Relation between Crack Growth Index and Stress Amplitudes.

Nonlinear Viscoelastic and Damage Approach

Relaxation Modulus Test

Based on the work of Park and Kim (*82*), the relaxation modulus was converted to creep compliance ($D(t)$). Two interconversions were used: (i) power-law-based interrelationship ($E(t)D(t) = \frac{\sin n\pi}{n\pi}$), and (ii) quasi-elastic interrelationship ($E(t)D(t) \cong 1$). Both interconversions presented close results (Figure 7.4). Creep compliance was also predicted using a power law relationship ($D(t) = D_0 + D_1 t^m$). After completion of this experiment, E_∞, E_1, m, D_0, D_1, and n were obtained (Table 7.7). These parameters are required for the nonlinear viscoelastic and damage characterization (equations in Table 7.1).

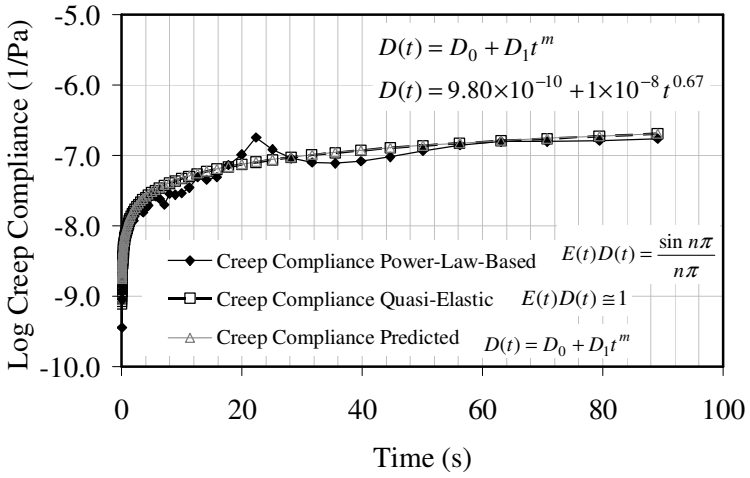

FIGURE 7.4 Creep Compliance Predictions.

Time Sweep Tests

Time sweep DMA tests were conducted using: (i) low load amplitude (LVE region), and (ii) high load amplitudes (NLVE and damage regions). Low stress (strain) amplitude

time sweep tests were used to determine LVE parameters: (i) $\hat{D}'$ and $\hat{D}''$ (controlled-stress analysis), and (ii) $\hat{E}'$ and $\hat{E}''$ (controlled-strain analysis) required for equations in Table 7.1. Results for these LVE parameters are in Table 7.7. High load amplitude time sweep tests were conducted using two amplitudes as follows:

- Amplitude correspondent to the limit between the nonlinear viscoelastic and the damage regions (Table 7.4). $\Delta g_1 \Delta g_2$ and $\Delta h_1 \Delta h_2$ parameters were calculated using equations in Table 7.1 for the first 10 cycles of these time sweep tests. Results for the six mixtures used during this study are in Table 7.7,
- Common amplitude: (i) 2.00×10^5 Pa, for controlled-stress tests, and (ii) 0.6%, for controlled-strain tests. For these tests, damage was also monitored using the equations in Table 7.1. $\Delta g_1 \Delta g_2$ and $\Delta h_1 \Delta h_2$ parameters were the same obtained from the time sweep tests conducted using the threshold amplitudes.

Since the values found for E_∞ and D_0 are much lower than $\hat{E}'$ and $\hat{D}'$, the terms with Δg_0 and Δh_∞ (Table 7.1) were much smaller than the remaining components, and they were dropped from the equations in Table 7.1.

TABLE 7.7 Average Model Parameters, Nonlinear Viscoelastic and Damage Approach

Parameter	Mixture					
	RLAAD	RLAAB	RLAAF	RDAAD	RDAAB	RDAAF
E_∞ (Pa)	2.00×10^4	5.00×10^2	5.00×10^2	5.00×10^2	5.00×10^2	5.00×10^2
E_1 (Pa)	1.41×10^7	9.00×10^6	1.00×10^7	2.00×10^6	1.00×10^7	7.00×10^6
n	0.75	0.42	0.46	0.58	0.37	0.48
D_0 (1/Pa)	4.68×10^{-10}	1.00×10^{-10}	1.00×10^{-10}	1.00×10^{-10}	1.00×10^{-10}	1.00×10^{-10}
D_1 (1/Pa)	2.32×10^{-8}	7.00×10^{-8}	7.00×10^{-8}	7.00×10^{-8}	7.00×10^{-8}	1.00×10^{-7}
m	0.55	0.42	0.46	0.38	0.38	0.48
$\hat{E}^*_{LVE}\cos\hat{\delta}_{LVE}$ (Pa)	3.91×10^7	7.68×10^7	2.08×10^8	4.52×10^7	9.86×10^7	2.70×10^8
$\hat{E}^*_{LVE}\sin\hat{\delta}_{LVE}$ (Pa)	5.14×10^7	8.17×10^7	1.77×10^8	6.36×10^7	1.14×10^8	2.48×10^8
$\hat{D}^*_{LVE}\cos\hat{\delta}_{LVE}$ (1/Pa)	1.26×10^{-8}	7.98×10^{-9}	9.80×10^{-9}	9.12×10^{-9}	5.76×10^{-9}	2.98×10^{-9}
$\hat{D}^*_{LVE}\sin\hat{\delta}_{LVE}$ (1/Pa)	1.84×10^{-8}	8.81×10^{-9}	9.71×10^{-9}	1.29×10^{-8}	6.27×10^{-9}	2.40×10^{-9}
$\Delta g_1 \Delta g_2$	1.04	1.10	1.01	1.15	1.04	1.10
$\Delta h_1 \Delta h_2$	0.50	0.41	0.52	0.43	0.76	0.82

Damage parameters (*V* and *W*) were calculated for different load amplitudes. *V* values were higher than one and increase with time, and *W* values were lower than one and decrease with time. Each damage parameter, *V* or *W*, includes two parts: (i) first part associated with damage in the stored component of the viscoelastic response, and (ii) second part associated with the damage in the dissipated component of the viscoelastic response. An example of the results for mixture RLAAD is presented in Figure 7.5.

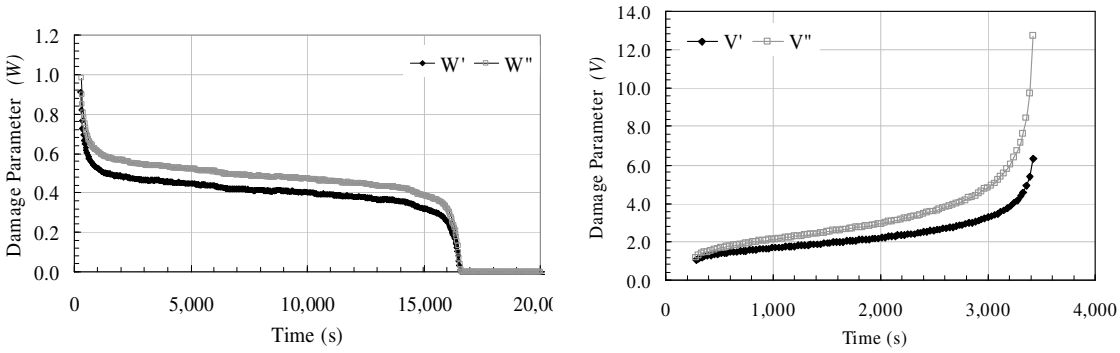

(a) Controlled-strain, 0.6% (b) Controlled-stress, 2.00×10^5 Pa

FIGURE 7.5 Damage Parameters for Different Modes of Loading, Mixture RLAAD.

V and *W* were calculated for a specific number of load cycles (*N=5,000*), for both modes of loading for all mixtures. Average values are in Figure 7.6. For controlled-strain tests, a higher *W* value indicates that the mixture accumulated less damage at that specific number of loading cycles. On the other hand, for controlled-stress tests, a lower *V* value indicates that the mixture accumulated less damage at that specific number of loading cycles. Similarly to what happened for the crack growth index approach, mixtures RLAAF and RDAAF presented different behaviors for the two modes of loading (Figure 7.6).

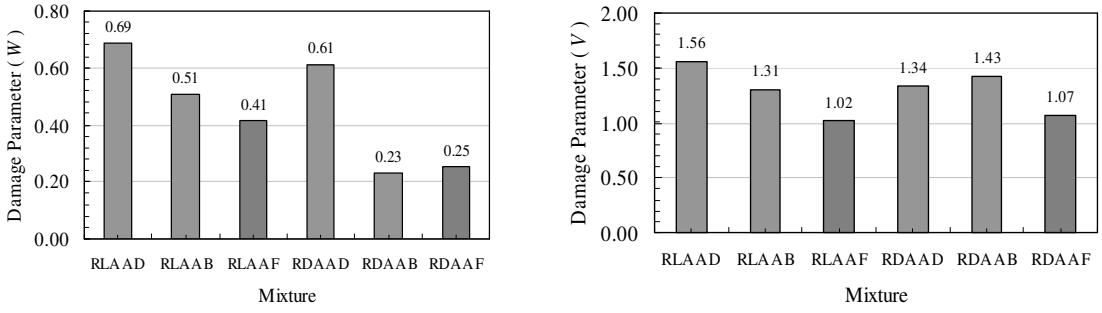

(a) Controlled-strain, 0.6% (b) Controlled-stress, 2.00×10^5 Pa

FIGURE 7.6 Damage Parameters for Different Modes of Loading at *N=5,000*.

The relation between damage parameters at fatigue life, for both modes of loading, and the average stress amplitude is plotted in Figure 7.7. In this figure, parameters *V-1* and *1-W* were selected to quantify damage because the higher deviation of *V* and *W* from 1 is, the higher is the damage caused in the material. The same explanation used for the first approach (crack growth index) applies here. It was found that all range of stresses applied during controlled-strain were higher than the stress amplitude used for controlled-stress tests. Consequently, Figure 7.6 shows that damage in these two mixtures (RLAAF and RDAAF) for controlled-stress is less than for controlled-strain. However, once the applied stress in controlled-stress is more than about half of the average stress in controlled-strain, the damage in controlled-stress becomes higher. This is caused by the fact that in the controlled-stress load, the material is subjected to the same stress amplitude irrespective of the damage that has accumulated in the material. On the other hand, in controlled-strain test, the applied stress decreases as more damage accumulates. Therefore, damage accumulates faster in controlled-stress than in controlled-strain. It is possible to find a relationship between the applied stress amplitude used for controlled-stress tests and the range of stresses in the controlled-strain such that damage in both modes of loading is similar.

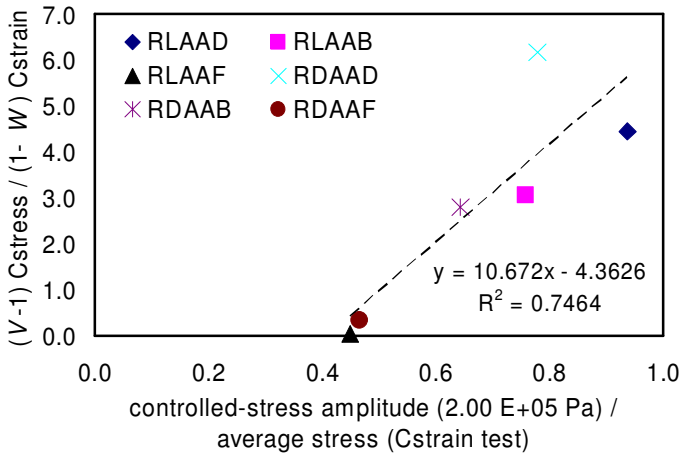

FIGURE 7.7 Relation between Damage Parameters and Stress Amplitudes.

SUMMARY AND CONCLUSIONS

This chapter presented two approaches for the analysis of nonlinear viscoelastic behavior and damage of fine aggregate matrix for different modes of loading and different strain or stress amplitudes. Six combinations of FAM representing six full asphalt mixtures were tested using the dynamic mechanical analyzer (DMA) under different modes of loading (controlled-strain and controlled-stress) and different stress (or strain) amplitudes. Results from this study demonstrated that: (i) for the first approach: crack growth index results can be used to rank mixtures based on their fatigue cracking resistance for different modes of loading. This parameter presented lower coefficient of variation when compared to fatigue life, (ii) for the second approach: nonlinear viscoelastic parameters ($\Delta g_1 \Delta g_2$ and $\Delta h_1 \Delta h_2$) as well as damage parameters (V and W) were obtained. The developed approach is able to describe both the nonlinear viscoelastic response and fatigue damage in one formulation. The proposed methods are able to explain results from both modes of loading (controlled-strain and controlled-stress) and to unify the ranking of mixtures from both modes of loading, as long as the applied stresses are within the same range.

CHAPTER VIII

CONCLUSIONS AND RECOMMENDATIONS

Fatigue cracking is one of the most common distresses encountered in asphalt pavements. Fatigue resistance characterization is usually based on approaches that are highly influenced by: (i) mode of loading (controlled-strain and controlled-stress), (ii) loading configuration and frequency, and (iii) specimen geometry. This study focused on the development of two related approaches to characterize fatigue damage in asphalt mixtures independent of the mode of loading. These approaches were used to analyze the results of dynamic mechanical analyzer (DMA) shear tests that were performed on fine aggregate matrixes (FAM). However, the analysis approaches can be applied for the characterization of fatigue resistance of full asphalt mixtures subjected to different stress states (repeated tension or shear).

CONCLUSIONS

- Experimental methods were developed for the use of the DMA to determine the nonlinear viscoelastic behavior and fatigue damage of asphalt mixtures. In the initial stages of this study, DMA specimens were prepared using a fixed gradation, filler and asphalt binder irrespective of the full mixture design. This procedure for preparing DMA specimens was used as part of the experiments reported in Chapters III, IV, and V of this study. Based on the experiences from these experiments, a new method was developed for preparing DMA specimens that consider the full mixture design as discussed in Chapters VI and VII. In this new procedure, fine aggregates' proportions (aggregate smaller than 1.18 mm and including filler) were similar to their proportions in the HMA. The asphalt content in the FAM was the same as in

the full mixture. This method is summarized in the protocol presented in Appendix A.

- A new approach for the analysis of DMA results was developed in this study. This approach considers pseudo strain energy to consist of two parts: (i) the nonlinear response of the intact part of the mixture, and (ii) damage. Damage energy was shown mathematically to consist of three components associated with: (i) change in apparent phase angle (W_{R1}), (ii) permanent deformation (W_{R2}), and (iii) change in pseudo stiffness (W_{R3}). The energy dissipated due to damage is used to derive an equation for calculating the crack growth index which quantifies the amount of fatigue damage in asphalt mixtures.
- In Chapter III, initial evaluation of the crack growth index using DMA experimental measurements was conducted. The results have shown that this index is able to unify the results of the controlled-strain and controlled-stress modes of loading when proper partitioning of the energy between nonlinearity and damage is achieved. The ratio between W_{R1} and W_{R3} was shown to be the same when results from both modes of loading were unified. W_{R2} results, associated with permanent deformation, were more significant when controlled-stress mode of loading was used. This conclusion was based on the fact that DMA for controlled-strain mode of loading adjusts the strain function continuously in order to have a sinusoidal function with a constant phase angle throughout the cycle. On the other hand, for controlled-stress mode of loading this did not happen.
- The average and variation of a number of parameters that can be used to assess fatigue life in DMA were also examined in this study. The average values for the number of cycles to failure and the total dissipated energy ranked the mixtures in accordance with their field performance. However, the coefficient of variation for these two parameters was quite high (around 75 percent). The coefficient of variation for the crack growth index was less than 20 percent.

- Chapter IV presented a more comprehensive evaluation of the crack growth index. The results confirmed that values of the crack growth index results are similar for the same material whether they are derived from controlled-strain and controlled-stress modes of loading, and using different strain (or stress) amplitudes.
- One of the current challenges in the characterization of fatigue resistance is that laboratory tests are conducted based on the anticipated strain or stress distribution in the pavement (i.e., controlled-strain test for thin asphalt concrete layers, and controlled-stress test for thick asphalt concrete layers pavements). The crack growth index should be integrated in a structural model in order to account for the influence of pavement design and asphalt layer thickness on the strain and stress distribution and resistance to fatigue cracking.
- In Chapter V, the results from the crack growth index were compared with the results of other energy methods available in the literature for characterizing asphalt mixture fatigue resistance. These methods were the total dissipated energy (DE), the plateau value (PV) calculated based on the change in the total dissipated energy, and the dissipated pseudo strain energy. The energy methods were evaluated using two important criteria: (i) the ability of the method to reconcile differences in controlled-strain test versus controlled-stress test, and (ii) the ability of the method to accurately asses the fatigue cracking life of different materials. The following are some of the important conclusions based on the evaluation of these energy methods:
    - The total DE serves as a gross estimate of the energy dissipated in the fatigue damage process. Materials with substantially different damage characteristics can be characterized using this approach. However, this approach does not separate the fraction of the DE due to damage from the fraction due to viscoelastic energy dissipation. As a result this parameter has low sensitivity to compare fatigue

damage characteristics of different materials and does not unify the results based on different modes of loading.

- The plateau value (PV) calculated based on the change in the total dissipated energy provides a measure of the incremental energy dissipated due to damage in each cycle. This parameter was shown to be effective in differentiating the fatigue cracking resistance of different mixtures, albeit with high variability.
- The $PV \times N_f$ term was hypothesized to be independent of the mode of loading. There is limited support for this hypothesis based on results presented in the literature as well as results from this study. This study demonstrates that this parameter represents total energy dissipated due to damage normalized by viscoelastic energy. As a result, it was concluded that this parameter may be considered as a measure of fatigue cracking that is independent of the mode of loading when non linearity in material response is not significant.
- The total dissipated pseudo strain energy (DPSE) provides a measure of energy dissipated due to damage at failure and may be used to differentiate the fatigue cracking resistance of different materials. However, results from this approach had high variability attributed in part to the initial damage state of the material (state of the material at the point where damage energy was first evaluated or calculated). This effect was alleviated with the use of crack growth index that is based on the rate of DPSE instead of the total DPSE.
- The crack growth index, computed using the rate of DPSE, is an efficient parameter by which to separate the damage in the material from the viscoelastic effects and characterize the fatigue cracking life of FAM.

  - The crack growth index computed at the load cycles to failure shows promise in its ability to serve as a parameter that is independent of the mode of loading.

- It became apparent in the analysis conducted in Chapters III, IV and V that it is critical to develop a method to define the stress (or strain) amplitudes at which damage initiates. These stress (or strain) amplitudes can be used to separate the energy associated with nonlinear viscoelastic response from damage. Chapter VI presented experimental and analytical procedures to separate the energy dissipated due to nonlinear viscoelasticity from the energy dissipated due to fatigue damage. A statistical algorithm was developed to analyze the results and calculate the threshold stress (or strain) amplitude in a cyclic load test that marks the end of the nonlinear viscoelastic region beyond which fatigue or incremental damage is imminent. This approach can be used for both modes of loading (controlled-strain or controlled-stress)
- In Chapter VII, the method developed in Chapter VI was used to separate the energy associated with nonlinear viscoelastic response and energy associated with fatigue damage. Consequently, the crack growth index and modified Schapery's nonlinear viscoelasticty theory were used to characterize nonlinear viscoelastic and damage behavior of FAM. The modified theory was able to describe both the nonlinear viscoelastic response and fatigue damage in one formulation. The proposed methods were able to explain results from both modes of loading (controlled-strain and controlled-stress), and to unify the ranking of mixtures from both modes of loading, as long as the applied stresses were within the same range.
- The crack growth index and the modified Schapery's theory are valuable methods to characterize the resistance of asphalt materials to fatigue cracking under cyclic loading. These methods unify the results of controlled-strain and controlled-stress modes of loading and presented lower coefficient of

variation when compared to conventional methods for the analysis of asphalt mixture fatigue cracking.

RECOMMENDATIONS

These are the recommendations based on the findings of this study:

- Use DMA experiments to evaluate the influence of frequency, temperature, moisture, volume of voids, aging, and healing on the material fatigue resistance using the analyses procedures proposed during this research;
- Investigate binder film thickness distribution for different aggregate sizes and binder proportions. Binder film thickness estimation is an important consideration for the design of FAM taking into account HMA characteristics;
- Verify the applicability of the methods developed in this study in the analysis of full asphalt mixtures tested using different modes of loading;
- Evaluate the influence of the initial condition of the test specimen on the results of both approaches: (i) crack growth index, and (ii) nonlinear viscoelastic and damage approach based on Schapery's theory;
- Evaluate the approach for separation between nonlinear viscoelastic and damage regions when: (i) strain sweep tests are conducted using a controlled-strain device, and (ii) rest periods are included in between different strain (or stress) amplitudes;
- Use the nonlinear viscoelastic and damage approach based on Schapery's theory to find nonlinear viscoelastic and damage parameters but considering that, due to the sinusoidal loading, the nonlinear parameters ($\Delta g_1 \Delta g_2$ and $\Delta h_1 \Delta h_2$), are not constant for the same loading cycle; and
- Determine the mode of loading (controlled-strain or controlled-stress) and load magnitude that should be used in the DMA test based on the asphalt pavement structure.

REFERENCES

1. Federal Highway Administration (FHWA) *Highway Statistics 2005*. U.S. Department of Transportation, Washington, D.C., Sections IV and V. http://www.fhwa.dot.gov/policy/ohim/hs04/index.htm. Accessed Nov. 6, 2006.
2. Bolotin, V.V. *Mechanics of Fatigue*. CRC Mechanical Engineering Series, Editor Frank A. Kulachi, University of Minnesota, Minneapolis, 1999.
3. Huang, Y.H. *Pavement Analysis and Design*. Prentice-Hall, Englewood Cliffs, NJ, 2004.
4. Walubita, L.F. *Comparison of Fatigue Analysis Approaches for Predicting Fatigue Lives of Hot-Mix Asphalt Concrete (HMAC) Mixtures*. Ph.D. dissertation, Texas A&M University, College Station, 2006.
5. Masad, E., V.T.F. Castelo Branco, D.N. Little, and R.L. Lytton. A Unified Method for the Analysis of Controlled-Strain and Controlled-Stress Fatigue Testing. *International Journal of Pavement Engineering* (In Press). ISSN: 1029-8436. Published in iFIRST, DOI: 10.1080/10298430701551219, 2007.
6. Tangella, R., S.C.S. Craus, J.A. Deacon, and C.L. Monismith. *Summary Report on Fatigue Response of Asphalt Mixtures*, Strategic Highway Research Program, National Research Council, Washington, D.C., 1990.
7. Reese, R. Properties of Aged Asphalt Binder Related to Asphalt Concrete Life. *Journal of the Association of Asphalt Paving Technologists,* Vol. 66, 1997, pp. 604-632.
8. Ghuzlan, K.A., and S.H. Carpenter. Energy-Derived, Damage-Based Failure Criterion for Fatigue Testing. In *Transportation Research Record: Journal of the Transportation Research Board. No. 1723,* TRB, National Research Council, Washington, D.C., 2000, pp. 141-149.

9. Zollinger, C.J. *Application of Surface Energy Measurements to Evaluate Moisture Susceptibility of Asphalt and Aggregates.* M.S. thesis, Texas A&M University, College Station, 2005.

10. Masad, E., V.T.F. Castelo Branco, D.N. Little, and R.L. Lytton. *An Improved Method for the Dynamic Mechanical Analysis of Fatigue Failure of Sand Asphalt Mixtures.* Publication FHWA-473630. FHWA, U.S. Department of Transportation, 2006.

11. Monismith, C.L., J.A. Epps, and F.N. Finn. Improved Asphalt Mix Design. *Journal of the Association of Asphalt Paving Technologists*, Vol. 54, 1985, pp. 347-406.

12. Van Dijk, W. Practical Fatigue Characterization of Bituminous Mixes. *Journal of the Association of the Asphalt Paving Technologists*, Vol. 44, 1975, pp. 38-74.

13. Kim, Y.R., D.N. Little, and R.L. Lytton. Fatigue and Healing Characterization of Asphalt Mixtures. *Journal of Materials in Civil Engineering*, Vol. 15, No. 1, 2003, pp. 75-83.

14. Shen, S., and S. Carpenter. Application of Dissipated Energy Concept in Fatigue Endurance Limit Testing. Presented at 84th Annual Meeting of the Transportation Research Board, Washington, D.C., 2005.

15. Lee, H.J, J.S. Daniel, and R.Y. Kim. Continuum Damage Mechanics-Based Fatigue Model of Asphalt Concrete. *Journal of Materials in Civil Engineering*, Vol. 12, No. 2, 2000, pp. 105-112.

16. Lytton, R.L., J. Uzan, E.G. Fernando, R. Roque, D. Hiltmen, and S. Stoffels. *Development and Validation of Performance Prediction Models and Specifications for Asphalt Binders and Paving Mixtures*. SHRP Report Nº A-357, Strategic Highway Research Program, National Research Council, Washington, D.C., 1993.

17. Seo, Y., Y.R. Kim, R.A. Schapery, M.W. Witczak, and R. Bonaquist. A Study of Crack-Tip Deformation and Crack Growth in Asphalt Concrete Using Fracture Mechanics. *Journal of the Association of Asphalt Paving Technologists*, Vol. 73, 2004, pp. 697-730.

18. Pronk, A.C., and P.C. Hopman. Energy Dissipation: The Leading Factor of Fatigue. Presented at Conference of the United States Strategic Highway Research Program: in Highway Research: Sharing the Benefits, 1990, pp. 255-267.

19. Tayebali, A.A., G.M. Rowe, and J.B. Sousa. Fatigue Response of Asphalt-Aggregate Mixtures. *Journal of the Association of Asphalt Paving Technologists*, Vol. 61, 1992, pp. 333-360.

20. Matthews, J.M., C.L. Monismith, and J. Craus. Investigation of Laboratory Fatigue Testing Procedures for Asphalt Aggregate Mixtures. *Journal of Transportation Engineering*, Vol. 119, 1993, pp. 634-654.

21. Bonnetti, K.S., K. Nam, and H.U. Bahia. Measuring and Defining Fatigue Behavior of Asphalt Binders. In *Transportation Research Record No. 1810, Journal of the Transportation Research Board*, TRB, National Research Council, 2002, pp. 33-43.

22. Si, Z., D.N. Little, and R.L. Lytton. Characterization of Microdamage and Healing of Asphalt Concrete Mixtures. *Journal of Materials in Civil Engineering*, Vol. 14, No. 2, 2002, pp. 461-470.

23. Bahia, H., H. Zhai, K. Bonnetti, and S. Kose Nonlinear Vicoelastic and Fatigue Properties of Asphalt Binders. *Journal of Association of Asphalt Paving Technologists*, Vol. 68, 1999, pp. 1-34.

24. Masad, E., and N. Somadevan. Microstructural Finite-Element Analysis of Influence of Localized Strain Distribution of Asphalt Mix Properties. *Journal of Engineering Mechanics*, 2002, Vol. 129 pp. 1105-1114.

25. Schapery, R.A. On the Characterization of Nonlinear Viscoelastic Materials. *Polymer Engineering and Science*, Vol. 9, No. 9, 1969, pp. 295-310.

26. Masad, E., C.H. Huang, G. Airey, and A. Muliana. Nonlinear Viscoelastic Analysis of Unaged and Aged Asphalt Binders. *Journal of Construction and Building Materials* (accepted for publication), 2008.

27. Schapery, R.A. Correspondence Principle and Generalized JIntegral for Large Deformation and Fracture Analysis of Viscoelastic Media. *International Journal of Fracture*, Vol. 25, 1984, pp. 194-223.

28. Arambula, E., E. Masad, and A. Epps Martin. Moisture Susceptibility of Asphalt Mixtures with Known Field Performance Using Dynamic Analysis and a Crack Growth Model. In *Transportation Research Record: Journal of the Transportation Research Board. No. 2001,* TRB, National Research Council, Washington, D.C., 2007, pp. 20-28.

29. Kim, Y.R., H.Y. Lee, and D.N. Little. Fatigue Characterization of Asphalt Concrete Using Viscoelasticity and Continuum Damage Theory. *Journal of the Association of Asphalt Paving Technologists*, Vol. 66, 1997, pp. 520-569.

30. Lee, H., and R.Y. Kim. Viscoelastic Constitutive Model for Asphalt Concrete under Cyclic Loading. *Journal of Engineering Mechanics,* Vol. 124, No. 11, 1998, pp. 32-40.

31. Benedetto, H. di, C. La Roche, H. Baaj, A. Pronk, and R. Lundström. Performance Testing and Evaluation of Bituminous Materials", *Materials and Structures*, Vol. 37, 2004, pp. 202-216.

32. Kim, Y.R., and D.N. Little. *Development of Specification-Type Tests to Assess Damage and Healing Properties of Bitumens and Mastics*. Publication FHWA-473630. FHWA, U.S., Department of Transport, VA, 2003.

33. Goodrich, J.L. Asphalt and Polymer Modified Asphalt Properties Related to the Performance of Asphalt Concrete Mixes. *Journal of the Association of Asphalt Paving Technologists,* Vol. 57, 1988, pp. 116-175.

34. Goodrich, J.L. Asphaltic Binder Rheology, and Asphalt Concrete Mix Properties. *Journal of the Association of Asphalt Paving Technologists,* Vol. 60, 1991, pp. 80-120.

35. Gubler, R, Y. Liu, D.A. Anderson, and M.N. Partl. Investigation of the System Filler and Asphalt Binders by Rheological Means. *Journal of the Association of Asphalt Paving Technologists*, Vol. 68, 1999, pp. 284-304.

36. Smith, B.J., and S.A.M. Hesp. Crack Pinning in Asphalt Mastic and Concrete. In *Transportation Research Record: Journal of the Transportation Research Board. No. 1728,* TRB, National Research Council, Washington, D.C., 2000, pp. 75-81.

37. Kim, Y.R., D.N. Little, and I. Song. Effect of Mineral Fillers on Fatigue Resistance and Fundamental Material Characteristics: Mechanistic Evaluation. In *Transportation Research Record: Journal of the Transportation Research Board. No. 1832,* TRB, National Research Council, Washington, D.C., 2003, pp. 1-8.

38. Strganac, T.W., A. Letton, D.F. Payne, and B.A. Biskup. Characterization of Nonlinear Viscoelastic Behavior Using a Dynamic Mechanical Approach. *AIAA Journal*. Vol. 33, No. 5, 1995, pp. 904-910.

39. Schapery, R.A. On the Thermodynamic Constitutive Theory and Its Application to Various Nonlinear Materials. Symposium on Thermoinelasticity. East Kilbride, Scotland, 1969, pp. 259-285.

40. Golden, H.J., T.W. Strganac, and R.A. Schapery. A Test and Analysis Protocol to Rapidly Characterize Nonlinear Viscoelastic Properties of Ballon Materials. *American Institute of Aeronautics (AIAA) Meeting*. Paper 96-0572, 1996.

41. Golden, H.J., T.W. Strganac, and R.A. Schapery. An Approach to Characterize Nonlinear Viscoelastic Material Behavior Using Dynamic Mechanical Tests and Analyses. *Journal of Applied Mechanics*, Vol. 66, 1999, pp. 872-878.

42. Shields, D.H., M. Zeng, and R. Kwok. Nonlinear Viscoelastic Behavior of Asphalt Concrete in Stress Relaxation. *Journal of Asphalt Paving Technologists*, Vol. 67, 1998, pp. 358-400.

43. Airey, G.D., B. Rahimzadeh, and A.C. Collop. Linear Viscoelastic Limits of Bituminous Binders. *Journal of the Association of Asphalt Paving Technologists,* Vol. 71, 2002, pp. 160-196.

44. Abbas, A.R., A.T. Papagiannakis, and E. Masad. Linear and Nonlinear Viscoelastic Analysis of the Microstructure of Asphalt Concretes. *Journal of Materials in Civil Engineering*, Vol. 16, No. 2, 2004, pp. 133-139.

45. Papagiannakis, A.T., A.R. Abbas, and E. Masad. A. Micromechanical Analysis of Viscoelastic Properties of Asphalt Concretes. In *Transportation Research Record: Journal of the Transportation Research Board. No. 1789,* TRB, National Research Council, Washington, D.C., 2002, pp. 113-120.

46. Huang, C., E. Masad, A. Muliana, and H. Bahia. Nonlinearly Viscoelastic Analysis of Asphalt Mixes Subjected to Shear Loading. *Journal of Mechanics of Time Dependent Materials*, Vol. 11, 2007, pp. 91-110.

47. Haj-Ali, R.M., and A. Muliana. Numerical Finite Element Formulation of the Schapery Non-Linear Viscoelastic Material Model. *Int. J. Numer. Methods Eng,* 59, 2004, pp. 25-45.

48. Gdoutos, E.E. *Fracture Mechanics: An Introduction*. 2nd edition. Springer, Norwell, MA, 2005.

49. Lytton, R.L. *Adhesive Fracture in Asphalt Concrete Mixtures*. Chapter in book edited by J. Youtcheff, In Press, 2004.

50. Kim, Y., and D.N. Little. Linear Viscoelastic Analysis of Asphalt Materials. *Journal of Materials in Civil Engineering*. Vol. 16, No. 2, 2004, pp. 122-132.

51. Abbas, A., E. Masad, T. Papagiannakis, and A. Shenoy. Modeling Asphalt Mastic Stiffness Using Discrete Element Analysis and Micromechanics-Based Models. *International Journal of Pavement Engineering*, Vol. 6, No. 2, 2005, pp. 137-146.

52. Van Dijk, W., H. Moreaud, A. Quedeville, and P. Uge. The Fatigue of Bitumen and Bituminous Mixes. *Proceedings of the Third International Conference on the Structural Design of Asphalt Pavements*, London, Vol. 1, 1972, pp. 354-366.

53. Bhasin, A., E. Masad, D.N. Little, and R.L. Lytton. Limits on Adhesive Bond Energy for Improved Resistance of Hot Mix Asphalt to Moisture Damage. In *Transportation Research Record: Journal of the Transportation Research Board. No. 1970,* TRB, National Research Council, Washington, D.C., 2006, pp. 3-13.

54. Paris, P.C., and F. Erdogan. A Critical Analysis of Crack Propagation Laws. *Journal of Basic Engineering*, Series D, Vol. 85, No. 3 1963, pp. 528-534.

55. Schapery, R.A. Nonlinear Fracture Analysis of Viscoelastic Composite Materials Based on a Generalized J Integral Theory, *Proceedings of the Japan – U.S. Conference on Composite Materials*, Tokyo, Japan, 1981, pp. 171-180.

56. Mun, S., M. Guddati, and Y.R. Kim. Fatigue Cracking Mechanisms in Asphalt Pavements with Viscoelastic Continuum Damage Finite-Element Program. In *Transportation Research Record: Journal of the Transportation Research Board. No. 1896,* TRB, National Research Council, Washington, D.C., 2004, pp. 96-106.

57. Asphalt Institute *Superpave Mix Design.* Superpave Series Nº 2 (SP-2). 3rd edition. Asphalt Institute, Lexington, KY, 2001.

58. Menard, K. P. *Dynamic Mechanical Analysis: a Practical Introduction.* CRC Press, Boca Raton, 1999.

59. Castelo Branco, V.T.F., E. Masad, A. Bhasin, and D.N. Little. Fatigue Analysis of Asphalt Mixtures Independent of Mode of Loading. *In Proc. 87th Annual Transportation Research Board Meeting*, Transportation Research Board of the National Academies, Washington, D.C. and accepted for publication In *Transportation Research Record: Journal of the Transportation Research Board,* TRB, National Research Council, Washington, D.C., 2008.

60. Van Dijk, W., and W. Visser. The Energy Approach to Fatigue for Pavement Design. *Journal of the Association of the Asphalt Paving Technologists*, Vol. 46, 1977, pp. 1-40.

61. Carpenter, S.H., and S. Shen. A Dissipated Energy Approach to Study HMA Healing in Fatigue. *In Proc. 85th Annual Transportation Research Board Meeting*, CD-ROM. Transportation Research Board of the National Academies, Washington, D.C., 2006.

62. Daniel, J., and Y.R. Kim. Development of a Simplified Fatigue Test and Analysis Procedure Using a Viscoelastic Continuum Damage Model. *Journal of the Association of Asphalt Paving Technologists*, 71, 2002, pp. 619-650.

63. Kim, Y., D.N. Little, and R.L. Lytton. Use of Dynamic Mechanical Analysis (DMA) to Evaluate the Fatigue and Healing Potential of Asphalt Binders in Sand Asphalt Mixtures. *Journal of the Association of Asphalt Paving Technologists*, 71, 2002, pp. 176-206.

64. Christensen, R.M. *Theory of Viscoelasticity*. 2nd edition. Diver Publications, Inc. Mineola, New York, 2003.

65. Oakley, J.G., A.J. Giacomin, and J.A. Yosick. Molecular Origins of Nonlinear Viscoelasticity. *Mikrochimica Acta*, 130, 1998, pp. 1-28.

66. Kose, S., M. Guler, H. Bahia, and E. Masad. Distribution of Strains within Hot-Mix Asphalt Binders Applying Imaging and Finite-Element Techniques. In *Transportation Research Record: Journal of the Transportation Research Board. No. 1728,* TRB, National Research Council, Washington, D.C., 2000, pp. 21-27.

67. Robl, T.L., D. Milburn, G. Thomas, J. Groppo, K. O'Hara, and A. Haak *The SHRP Materials Reference Library Aggregates: Chemical, Mineralogical, and Sorption Analyses*. SHRP-A/UIR-91-509, National Research Council, Washington, D.C., 1991

68. Jones, D.R. The *SHRP Materials Reference Library: Asphalt Cements: A Concise Data Compilation.* Strategic Highway Research Program (SHRP), SHRP-A-645, National Research Council, Washington, D.C., 1993.

69. Roberts, F.L., P.S. Kandhal, R.E. Brown, D. Lee, and T.W. Kennedy. *Hot Mix Asphalt Materials, Mixture Design, and Construction*. 2nd edition. NAPA Education Foundation, Lantham, MD, 1996.

70. Jung, D.H. *Low-Temperature Cracking Binder Validation*. Strategic Highway Research Program (SHRP), SHRP-A-399, National Research Council, Washington, D.C., 1994.

71. TA Instruments. *AR 2000 Rheometer, Operator's Manual.* Rheometrics Series. TA Instruments, New Castle, DE, 2006.

72. Fitzgerald, J.E., and V. Jalal. Nonlinear Characterization of Sand-Asphalt Concrete by Means of Permanent Memory Norms. *Proceedings of the 3rd SESA International Congress on Experimental Mechanics*. Los Angeles, CA, Vol. 3, 1973, pp. 406-412.

73. Polacco, G., J. Stastna, D. Biondi, and L. Zanzotto. Relation between Polymer Architecture and Nonlinear Viscoelastic Behavior of Modified Asphalts. *Current Opinion & Interface Science,* 11, 2006, pp. 230-245.

74. Lou, Y.C., and R.A. Schapery. Viscoelastic Characterization of a Nonlinear Fiber-Reinforced Plastic. *Journal of Composite Materials*, Vol. 5, 1971, pp. 208-234.

75. Rand, J.L., J.K. Henderson, and D.A. Grant. Nonlinear Behavior of Linear Low-Density Polyethylene. *Polymer Engineering and Science*, Vol. 36, No. 8, 1996, pp. 1058-1064.

76. Haj-Ali, R.M., and A. Muliana. A Micromechanical Constitutive Framework for the Nonlinear Viscoelastic Behavior of Pultruded Composite Materials. *International Journal of Solids and Structures*, Vol. 40, 2003, pp. 1037-1057.

77. Pooler, D.J., and L. Smith. Nonlinear Viscoelastic Response of a Wood-Plastic Composite Including Temperature Effects. *Journal of Thermoplastic Composite Materials*, Vol. 17, 2004, pp. 428-445.

78. Nordin, L., and J. Varna. Nonlinear Viscoelastic Behavior of Paper Fiber Composites. *Composites Science and Technology, Vol.* 65, 2005, pp. 1609-1625.

79. Marklund, E., J. Varna, and L. Wallstrom. Nonlinear Viscoelasticity and Viscoplasticity of Flax/Polypropylene Composites. *Journal of Engineering Materials and Technology,* Vol. 128, 2006, pp. 527-536.

80. Sridharan, S. Nonlinear Viscoelastic Analysis of Composites Using Competing Micromechanical Models. *Journal of Composite Materials*, Vol. 40, No. 3, 2006, pp. 257-282.

81. Dai, Q., M.H. Sadd, and Z. You. A Micromechanical Finite Element Model for Linear and Damage-Coupled Viscoelastic Behavior of Asphalt Mixture. *International Journal for Numerical and Analytical Methods in Geomechanics,* Vol. 30, 2006, pp. 1135-1158.

82. Park, S.W., and Y.R. Kim. Interconversion between Relaxation Modulus and Creep Compliance for Viscoelastic Solids. *Journal of Materials in Civil Engineering*, Vol. 11, No. 1, 1999, pp. 76-82.

APPENDIX A

STANDARD METHOD FOR PREPARING DYNAMIC MECHANICAL ANALYZER (DMA) SPECIMENS AND CONDUCTING TESTS

DISCLAIMER

This work was performed by a task force group at Texas Transportation Institute, Texas A&M University. The professionals in charge of this standard method are: Jonathan Howson, Kamilla L. Vasconcelos, Silvia Caro, and Veronica T.F. Castelo Branco.

1. SCOPE

This document presents the procedures for specimen preparation, mixture design, testing and data analysis of fine aggregate matrix (FAM) to be analyzed in the dynamic mechanical analyzer (DMA). The document also explains how the results obtained by these procedures can be used in a more complex fracture mechanics model that characterizes bituminous materials.

2. REFERENCE DOCUMENTS

AASHTO Standards:

- T 85, Specific Gravity and Absorption of Coarse Aggregates;
- T 312 – 04, Preparing and Determining the Density of the Hot Mix Asphalt (HMA) Specimens by Means of the Superpave Gyratory Compactor;
- T 166, Bulk Specific Gravity of Compacted Hot Mix Asphalt Using Saturated Surface-Dry Specimens;
- T 209, Theoretical Maximum Specific Gravity and Density of Bituminous Paving Mixtures;

- R 35, Superpave Volumetric Design for Hot Mix Asphalt (HMA);
- T 316, Viscosity Determination of Asphalt Binder Using Rotational Viscometer.

3. SIGNIFICANCE AND USE

This standard is used to characterize the rheological properties of FAM. The standard refers mainly to two different tests that can be performed using the DMA apparatus: (i) shear oscillation, and (ii) relaxation modulus. These tests provide relevant information regarding the behavior of the HMA fine matrix, which is composed by fine aggregates (particles passing sieve No.16, 1.18 mm) and asphalt binder.

The results from these procedures can be used to:

- Determine the fatigue life at different test conditions (i.e. temperature and/or frequency);
- Characterize the continuous damage of the sample in terms of the dissipated pseudo strain energy as a function of the number of cycles;
- Determine the relaxation modulus as a function of time, i.e. E_t;
- Use the data obtained from oscillation and relaxation tests into a model based on viscoelastic fracture mechanics principles to characterize fatigue damage phenomena, and;
- Evaluate moisture damage susceptibility using the same fracture mechanics model. This analysis provides important information about the moisture susceptibility of the FAM tested.

4. SUMMARY OF THE METHODS

DMA test provides fundamental information regarding the rheological properties of the fine matrix portion of asphalt mixtures.

The design methodology of DMA mixture attempts to obtain a representative sample of the FAM of a complete asphalt mixture (i.e., HMA). For this reason, a previously established HMA design is required for this process. The design procedure considers the granular material of the HMA mixture passing the sieve No. 16 (1.18 mm). The percent of asphalt is estimated by calculating the amount of binder that is expected to cover the total granular particles (coarse and fine aggregates). Just the amount of binder absorbed by the coarse aggregates (larger than 1.18 mm) is not used on the FAM design.

The first step in the preparation of the specimens consists in mixing and compacting, using the Superpave gyratory compactor (SGC), to obtain a 150 mm diameter cylindrical sample with an approximate height of 90 mm. This procedure is similar to the one used to prepare regular HMA mixtures specimens. The upper and lower parts of the cylinders are sawed in order to produce a new cylinder of 150 mm diameter by 50 mm height. This compacted sample is cored in small DMA cylindrical specimens of 12 mm in diameter by 50 mm in height. Each specimen is properly labeled and prepared for testing. Two methods of test-specimen preparation are herein considered: (i) when testing on dry condition; or (ii) when testing on specimens that have been subjected to a moisture conditioning process.

Two tests that are performed using the DMA apparatus are described in this document:

- shear oscillation test, and
- relaxation modulus test.

Oscillation tests are conducted in an average of six DMA specimens (depending on the coefficient of variation). The oscillation test is conducted in controlled-strain or controlled-stress modes using the oscillation procedure, and has two main parts: (i) two minutes of oscillation at low constant strain/stress amplitude, and (ii) fatigue test at higher constant strain/stress amplitude. Both tests are performed at a fixed frequency. The low and high strain/stress amplitudes should be determined from the results of a strain/stress sweep test according with the following criteria: the low strain/stress should

guarantee that the material's behavior is in the linear viscoelastic region (a value of 0.001 percent strain or 3.20×10^3 Pa are commonly used for controlled-strain and controlled-stress tests, respectively), and the high strain/stress amplitude should produce an initial damage behavior of the material (a value in the range of 0.1 to 0.2 percent or 9.08×10^4 Pa to 1.65×10^5 Pa are commonly used for controlled-strain and controlled-stress tests, respectively). Ideally, the high strain/stress amplitude should be on the threshold between the nonlinear viscoelastic region and the damage region. Other practical considerations in the selection of these values (e.g. total time of testing, time before failure, etc.) should also be taken into account. The oscillation test is normally conducted at room temperature, although the effect of temperature can be analyzed by repeating the procedures described above at different temperatures. For assessing the moisture damage susceptibility of the material it is necessary to use DMA specimens that have been subject to a moisture conditioning process (section 8).

The relaxation properties of the FAM can be obtained from a relaxation test. The test should be performed on at least three DMA specimens using a step load function at constant shear strain amplitude. The percent of shear strain should be the same selected in the first part of the oscillation procedure (i.e., low percent of strain). The raise strain time and the total time of the load step function should be determined according to the apparatus requirements and mixture characteristics. Typical values of 0.2 to 1 seconds for the raise strain time and 3 to 6 minutes to the load step function are recommended. For assessing the moisture damage susceptibility of the material it is necessary to repeat the previous procedure but using DMA specimens that have been subject to the moisture conditioning (section 9).

Several analyses regarding the characterization of FAM can be performed based on the data obtained from these tests as follows: (i) linear and nonlinear viscoelastic properties, (ii) fatigue life, (iii) crack growth potential, and (iv) moisture susceptibility (section 10).

5. APPARATUS

5.1. DMA – The machine must meet or surpass the following requirements:

- Torque range - 0.1×10^{-6} to 200×10^{-3} N.m
- Torque resolution - Minimum 10^{-9} N.m
- Range for measurable speed - 10^{-8} to 600 rad/sec
- Range for detectable speed - 10^{-8} to 600 rad/sec
- Angular position resolution - Minimum 0.05×10^{-6} rad
- Frequency range - 10^{-6} to 150 Hz
- Gap resolution - Minimum 1 micron
- Range for sample height - 1 to 50 mm
- Normal force measurement range - 0.1 to 2,000 g
- Environmental chamber: temperature range - -20 to 150°C
- Environmental chamber: temperature accuracy - ±1°C

In addition to the above requirements, the DMA must have attachments capable of handling 12 mm cylindrical samples. The software must provide the user with the following information based on the data acquired during the test:

- maximum and minimum strain per cycle;
- maximum and minimum stress per cycle;
- phase angle per cycle;
- maximum and minimum torque per cycle;
- maximum and minimum displacement per cycle;
- preferably a minimum of 128 data points per cycle for the torque, stress and strain with respect to time;
- time;
- temperature;
- frequency;
- normal force.

Figure A-1 presents two commercial rheometers that satisfied the previous requirements.

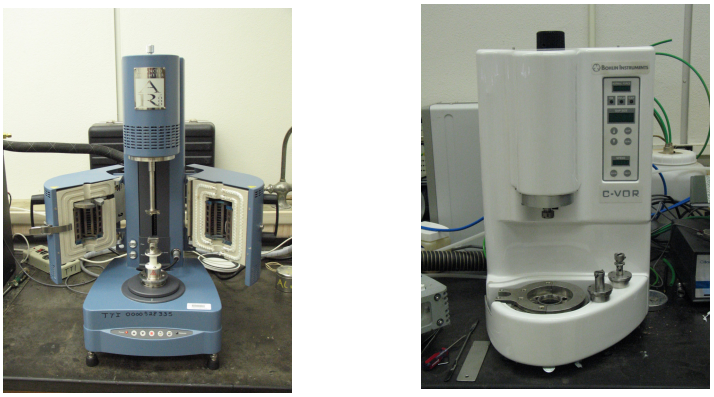

(a) AR 2000 TA® (b) CVOR-200 Bohlin®

FIGURE A-1 Dynamic Mechanical Analyzers (DMA).

5.2. Pressurized air supply – a compressed air supply that is capable of supplying clean, dry, oil free air at an approximate pressure of 30 psi (approximately 2 bars) at a flow rate of 50 liters. The dew point of the air supply should be -20°C or better.

5.3. Calipers – digital or analog calipers with an accuracy of ±0.005 in (0.01 mm).

5.4. Balance – standard balance meeting (AASHTO specification).

5.5. Glue – must be able to withstand force applied to sample by machine and must bond well to cylindrical sample and end caps.

5.6. End caps or holders – alloy. Used to secure sample to into DMA attachments for testing. Must be slightly larger than 12 mm in diameter and 2 mm deep.

5.7. Other apparatus required to perform the procedures described in this document include: oven, SGC, recipient to applied vacuum saturation.

6. HAZARDS

Observe standard safety precautions when preparing and testing HMA specimens.

7. MIXTURE DESIGN

The first part of this procedure describes the FAM design method used to fabricate DMA samples. FAM samples are compound by fine aggregates (smaller than 1.18 mm, including filler) and asphalt binder. The materials (fine aggregates and binder) are related to the reference HMA mixture.

7.1. Fine Aggregate Matrix (FAM) Design Method

7.1.1. Select the HMA that will be used as the reference for the FAM;

7.1.2. Obtain the following information for the HMA: (i) aggregate gradations, and (ii) percentage of binder. The series of sieves used should include sieves No. 16 (1.18 mm) and No. 30 (0.60 mm);

7.1.3. Identify the HMA aggregates that pass No. 16 sieve (1.18 mm). Develop the FAM gradation curve keeping the same proportions for each aggregate passing No. 16 (1.18mm) (Figure A-2);

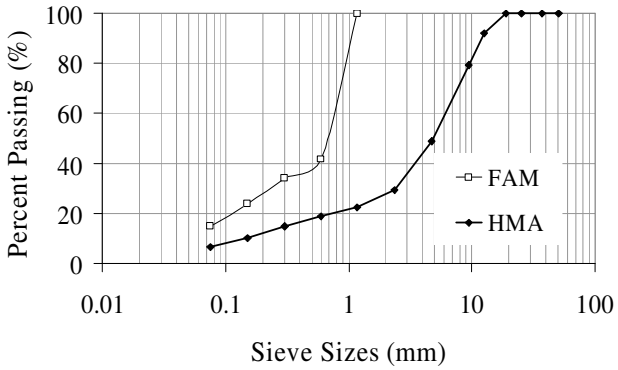

FIGURE A-2 Hot Mix Asphalt (HMA) and Fine Aggregate Matrix (FAM) Gradation Curves.

7.1.4. Establish the aggregates batch size (in grams) that will be used to compact the FAM sample according to the mold diameter and the desired sample height;

7.1.5. Calculate the weights of each size fraction of the aggregate required for one batch of the FAM. Use the gradation developed on step 7.1.3;

7.1.6. Calculate the amount of binder for the FAM using the aggregate batch size (step 7.1.4) and the percentage of binder used in the original HMA mixture.

$$Binder\,(g) = \left[aggregate\ \ batch\ \ size \times \left(\%\ binder\ HMA - \%\ binder\ absorbed\ by\ coarse\ aggregate\right)\right] \quad \text{(A-1)}$$

- The absorption of the coarse aggregate should be determined through the standard procedure AASHTO T85;
- Annex A-2 presents an example for this design method.

8. MIXTURE PREPARATION

The preparation of cylindrical specimens for using in DMA tests (i.e., DMA specimens) consists in four parts:

8.1. Preparation of a 150 mm (6 inches) compacted sample of fine aggregate portion asphalt mixture in the SGC.

8.2. Coring of the compacted sample.

8.3. Preparation of the specimen for testing (method I: in dry condition, method II: in moisture damage condition), and

8.4. Storage considerations.

The procedures for conducting each stage are as follows:

8.1. FAM preparation: in this step, the job formula for the HMA mixture, the binder properties (for determining the amount of binder, and the mixing and compacting temperatures), and the value of the theoretical maximum specific gravity of the FAM are required. The mixing and compacting temperatures should be calculated from the results of viscosity according to the AASHTO T 316 procedure.

8.1.1. Conduct a mixture preparation and compaction of a 150 mm (6 inches) specimen in the SGC, following most of the steps specified in the AASHTO T 312 – 04. A summary of the procedure is:

- According to the DMA mixture design process (section 7), weight each aggregate fraction that compose the mixture and combine them into a pan;
- Mixture the portions and extend the fine aggregate material in a pan taking special care for do not lose the finest portion (material passing in sieve No. 200) during the process;
- Leave the pan in the oven overnight at the mixing temperature;

- Introduce the binder and all the elements (spoons, can, etc.) required for mixing in the oven at the mixing temperature for two hours (or the time required for the binder to become a liquid) before the mixing process;
- Take the fine aggregate material and the mixing can out of the oven and weight the total amount of material that was estimated for the batch. Take the binder out of the oven and pour the corresponding amount of asphalt binder in the can, according the mixture formula;
- Pass the material to the mixing can, take especial care of no loosing the finest portion of the material;
- Perform the mixing process until the entire granular material seems to be homogeneously coated by binder (at least two minutes in the mechanical mixer);
- Perform a two hours short term aging process by introducing the loose mixture into the oven at the mixing temperature;
- Introduce all the elements that are going to be required during the compaction process into the oven at least 30 minutes prior the compaction (mold, spoons, etc.);
- After the two hours, remove the material from the oven and proceed to do the compaction process following the AASHTO T 312 - 04.

The following specifications should be used as inputs in the gyratory compactor:

  - Angle:1.25 ± 0.02˚
  - Pressure: 600 ± 18 kPa
  - Criteria of termination: use the percent of voids specified in the design, the mass of the batch and the maximum specific gravity of the mixture to determine a termination criterion for compaction (height or density)

- Wait to remove the sample from the mold. The time necessary to remove the sample from the mold depend on the used amount of binder. Usually from one hour to one hour and 30 minutes is necessary;

- Label the sample.

Figure A-3 presents a final sample obtained from this process:

FIGURE A-3 150 mm (6 inches) Diameter Sample.

8.1.2. Leave the sample to cool down for at least three hours.

8.1.3. Calculate the air voids content of the FAM. It is possible to use the AASHTO T 116 procedure or the Corelock® Procedure (using program number 1). Verify that the air void content is in the expected range according to the mixture design formula. If there is a difference of more than 15 percent between the expected and the actual air void content verify the compaction process (especially the termination criterion) and repeat the previous process. If the air void content is acceptable, continue with the next step.

8.2. Coring of the compacted sample

8.2.1. Proceed to saw the upper and lower part of the cylindrical sample to obtain a new cylinder with the same diameter (150 mm) but with 50 mm in height (Figure A-4);

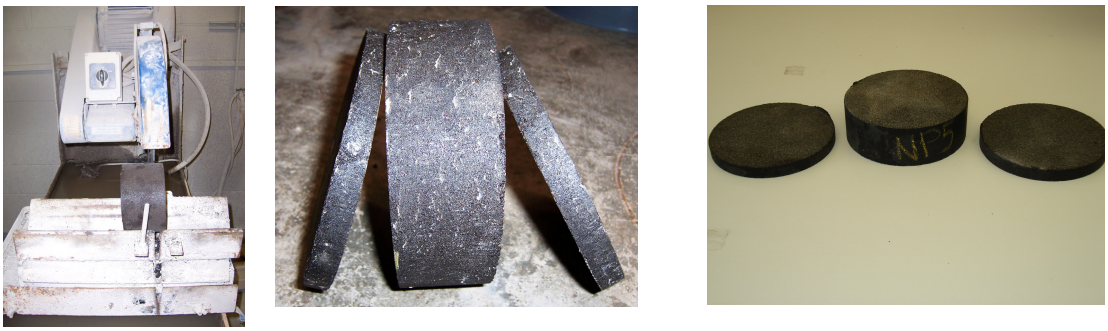

(a) (b)

FIGURE A-4 (a) Sawing Process, and (b) Final Result.

8.2.2. Leave the core to dry completely for at least four hours (it is recommended to use a fan during the process);

8.2.3. Calculate the air voids content of the core following the same procedure used in 8.1.3;

8.2.4. Proceed to core DMA cylindrical specimens of 50 mm height and 12 mm diameter. The velocity used during the coring process is a relevant parameter in determining the quality of the sample. To avoid damage in the top of the DMA sample is recommended to "sandwich" the SGC sample with the cut top and bottom parts during the coring procedure;

8.2.5. Immediately after each specimen is obtained, label it as *A*, *B*, *C*, where *A* corresponds to the inner concentric zone of the core, *B* to the intermediate and *C* to the outer zone (Figure A-5). Include also a number for each sample in each zone (i.e., *C*4 is the four sample that was obtained for the outer zone). Besides, each sample should also contain a mark indicating the border that corresponds to the upper part of the original compacted specimen. It is recommended to obtain at least 24 DMA samples in total from a 150 mm by 50 mm core. A typical value of total DMA specimens is in the order of 30 and a maximum value is approximate 32 samples;

FIGURE A-5 Coring DMA Specimens.

8.2.6. Leave the samples to completely dry for at least four hours (a fan is recommended);

8.2.7. Calculate the air voids content of at least five samples of each group (i.e., *A*, *B* and *C*). For doing this follow a procedure similar to the one indicated in AASHTO T 116 but adapting a small scale in order to measure the weight of the saturated sample under water. If the air voids in specimens belonging to the same group differ in more than 35 percent, select three new specimens and repeat the measurements. If the differences continue review the other groups. If all groups presents this differences and/or the differences among the average air void content of the three groups is higher than 35 percent repeat the experiment;

8.2.8. Select at least eight specimens corresponding to the zone having the average air void content closer to the design value. Take into account variability of the results obtained in 8.2.7 and the amount of samples available in each group.

8.3. Preparation of the specimen for testing

Method I: testing dry specimens

8.3.1. Take four specimens selected and use epoxy to glue the holders and the specimen (Figure A-6);

FIGURE A-6 Holders, Glue and Specimens in the Gluing Process.

8.3.2. Wait at least one hour (or the time specified in the glue directions) before proceed to install the sample in the DMA;

8.3.3. Proceed to test the sample.

Method II: testing moisture conditioned specimens

8.3.4. Take the other four of the specimens selected and use epoxy to apply a thin layer of glue at the borders. The goal of this step is to facilitate the gluing process after the mixtures has been subject to the conditioning process;

8.3.5. For moisture conditioning the sample it is required to count with a container that allows applying vacuum into a material submerged in water. Metallic containers as those specified in the procedures for determining the theoretical maximum specific gravity and density of bituminous paving mixtures (AASHTO T 209) can be utilized for this purpose.

- Weight the sample in dry condition, before starting the conditioning procedure;
- Place a porous stone at the bottom of the recipient;
- Fill half of the recipient with water;

- Put the sample on the porous stone. A maximum of three samples can be conditioned at the same time;
- Close the recipient and apply vacuum saturation at a pressure of 27 mmHg during one hour;
- Remove the sample, dry the surface and weight the specimen;
- Using the information collected, calculate the level of saturation of the sample;

A minimum of 85 percent saturation level should be achieved with this process. If this is not the case (e.g. in samples with a typical low air void content), modify the time of vacuum saturation until achieving the minimum required. If several mixtures are being tested for comparison purposes, use a unique time for vacuum saturation, otherwise the differences in the damage generated in the sample will produce false comparison analysis.

8.3.6. After conditioning, wait 30 minutes for gluing the specimens to the holders. Follow the same procedure specified for Method I.

8.3.7. After two hours of gluing proceed to do the test as specified for Method I.

Note: a specimen that has been conditioned should be tested in the following two days or it should be discarded.

8.4. Storage Considerations

The total testing procedure (for all selected DMA specimens in both tests fatigue and relaxation modulus) should be completed in a period of less than three weeks. After this period, all the specimens that have not being used should be stored in a cold room at 10ºC conditions in order to retard aging. If these specimens are going to be used, they should be removed from the cold room at least one night before the testing day.

9. TEST PROCEDURE

Note: Relaxation test is a non-destructive procedure. If relaxation test parameters are required, it is possible to perform this test in a specimen before performing oscillation test. This means that after finishing relaxation test, the same installed sample can be used for oscillation. This suggestion applies to both, dry and moisture conditioning specimens. For details of relaxation test procedure refer to the second part of this section.

Shear Oscillation (Fatigue)

9.1. Verify if air supply is on (30 psi).

9.2. Remove bearing lock if applicable.

9.3. Turn on power to electronics control box.

9.4. Open instrument control software on computer.

9.5. Install the correct clamp on the DMA.

9.6. If applicable, calibrate the instrument (bearing friction, clamp, and inertia).

9.7. Zero the gap.

9.8. Insert DMA specimen into holders (Figure A-7).

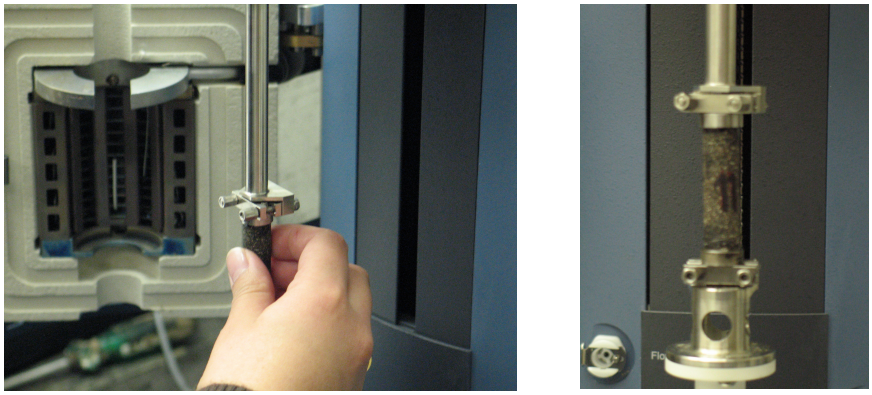

FIGURE A-7 Installation of the Specimen in the Rheometer.

9.9. Tighten screws/bolts to secure sample (do not over tighten or stripping of screws/bolts will occur).

9.10. If running a test at temperature other than room temperature, close the temperature chamber around sample. Be sure sample fits into chamber without touching.

9.11. Zero normal force. Be sure to zero actual force on sample, not force transducer.

9.12. In computer software:

9.12.1 Select DMA test geometry;

9.12.2 Input required data (height and diameter of DMA specimen, sample ID, etc) (only if required by software);

9.12.3 Go to oscillation (if running a fatigue test);

9.12.4 Two oscillation procedures are required;

9.12.5 Low strain/stress – recommended values

- Frequency – 10 Hz

- Strain (or stress) amplitude – according to the homogeneity concept, the ratio of stress response to any applied strain should be independent of the strain magnitude for the linear viscoelastic region. This strain amplitude can be found performing strain sweep test and monitoring the dynamic modulus as the strain increases. A typical value is 0.001 percent for controlled-strain tests and 3.20×10^{3} Pa for controlled-stress tests
- Duration – two minutes
- Sampling rate – sample every five cycles taking at least 128 points per cycle or as many as possible if less than 128
- Temperature (if applicable) – be sure sample has reached equilibrium with set temperature

9.12.6 High strain/stress – recommended values

- Frequency – 10 Hz
- Strain (or stress) amplitude – selected according to strain (or stress) sweep results, based on stiffness of sample and maximum torque of machine (Annex A-1). Typical values are in the order of 0.1 percent to 0.2 percent for controlled-strain tests and 9.08×10^{4} Pa to 1.65×10^{5} Pa for controlled-stress tests. The high strain/stress selected should allow achieving a fatigue life longer than 30 minutes but less than five hours
- Duration – until evident failure of sample occurs, but must meet above criteria
- Sampling rate – sample every five cycles taking at least 128 points per cycle or as many as possible if less than 128
- Temperature (if applicable) – be sure sample has reached equilibrium with set temperature
- Start test with applicable oscillation test procedure
- Verify if sine waves are smooth after a few oscillations, otherwise cancel test immediately and start over. Rough sine waves indicate machine is

not able to reach desired strain at desired frequency. If necessary modify inputs

- Stop test after failure occurs. Failure can be identified as a sharp drop in the dynamic modulus and phase angle. Wait until the dynamic modulus stabilizes at the lower value before stopping test. If failure does not occur before the maximum suggested time of eight hours, it is the operator's decision to continue the test until failure or terminate the test

9.12.7 Loosen screw/bolts and raise machine head to remove specimen (if running a test at other than room temperature, the temperature chamber will need to be opened first).

Relaxation Modulus Test

9.13. Repeat steps 9.1 to 9.11 of the shear oscillation procedure test.

9.14. In computer software:

9.14.1 Select DMA test geometry;

9.14.2 Input required data (height and diameter of DMA specimen, sample ID, etc) (only if required by software);

9.14.3 Go to oscillation (if running a fatigue test);

9.14.4 Select the option for relaxation test procedure;

9.14.5 Enter the following recommended minimum parameters:

- Frequency – 10 Hz
- Strain amplitude – according to the homogeneity concept, the ratio of stress response to any applied strain should be independent of the strain magnitude for the linear viscoelastic region. This strain amplitude can be found performing strain sweep test and monitoring the dynamic modulus as the strain increases. A typical value is 0.001 percent.
- Duration – two minutes

- Sampling rate – Sample every five cycles taking at least 128 points per cycle or as many as possible if less than 128
- Temperature (if applicable) – be sure sample has reached equilibrium with set temperature
- Review if the particular machine that is being used required more parameters and introduce them

9.14.6 Loosen screw/bolts and raise machine head to remove specimen (if running a test at other than room temperature, the temperature chamber will need to be opened first);

9.14.7 If fatigue test is going to be performed on the same specimen, follow the step 9.12 for the Oscillation Test described in the first part of this section.

---

10. DATA ANALYSIS

10.1 Relaxation Modulus Test

10.1.1 Plot relaxation modulus (E) versus time (t);

10.1.2 Fit the curve obtained on 10.1.1 using the power law relationship ($E(t) = E_\infty + E_1 t^{-n}$) (Figure A-8).

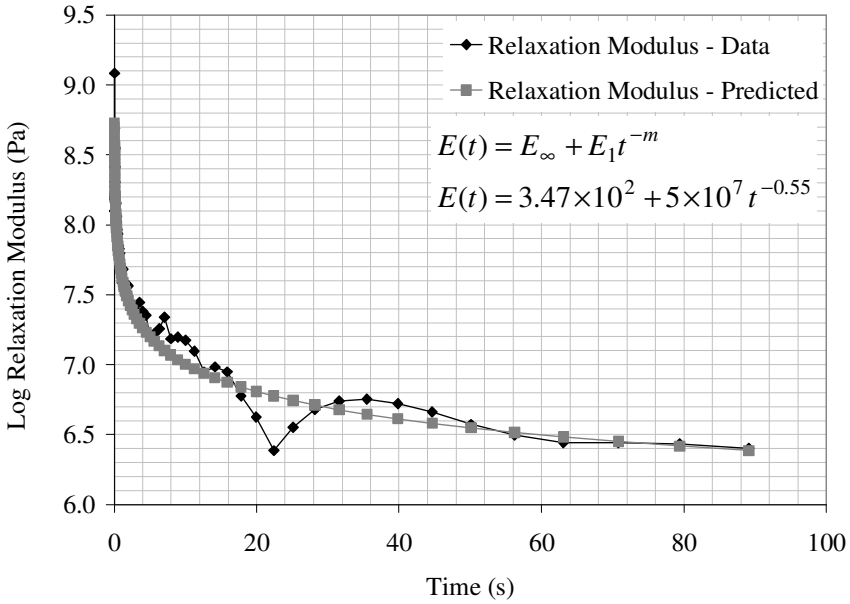

FIGURE A-8 Relaxation Modulus versus Time.

10.2 Oscillation Test

10.2.1 Pick the linear viscoelastic (LVE) material properties (dynamic modulus and phase angle) from the low amplitude test. Use average values.

10.2.2 Select specific cycles from the high amplitude test related to fatigue life (maximum point from the relationship between G^*/G_0 versus number of load cycles, where G^* is the dynamic modulus and G_0 is the initial dynamic modulus), Figure A-9. The selected cycles should be: initial, related to 5, 10, 20, 30, 40, 50, 60, 70, 80, 90, 100 and 110 percent of fatigue life (total of 13 cycles).

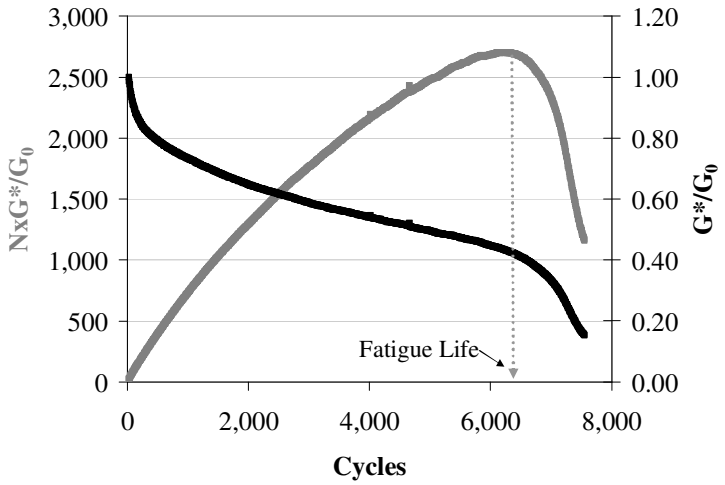

FIGURE A-9 Determination of the Fatigue Life.

10.2.3 Calculate, for each of the 13 selected cycles from the high amplitude test, pseudo strain values according to the Equations A-2 and A-3:

$$\gamma^R = \frac{G^*_{VE}\gamma_{0F}\sin(wt+\delta_{VE})}{G_R} \qquad \text{controlled-strain (A-2)}$$

$$\gamma^R = \frac{G^*_{VE}\gamma_{0NF}\sin(wt-\delta_{NF}+\delta_{VE})}{G_R} \qquad \text{controlled-stress (A-3)}$$

where, γ is the strain, w is the circular frequency ($2\pi f$), t is the time, δ is the phase angle and G_R is the reference modulus. F indicates that the labeled quantities are associated with the fatigue test, N stands for the parameter that is changing during each loading cycle, and VE stands for the material viscoelastic properties that the material would attain if it does not exhibit damage at the strain and stress levels used in the fatigue test. G_R is determined by:

$$G_R = \frac{(\max Stress - \min Stress)}{(\max Strain - \min Strain)} \qquad \text{(A-4)}$$

G_R is calculated for the cycle referred as five percent (keep the same value for the calculations of the following percentages). For each cycle it is recommended to get approximately 128 data points inside the cycle. For simplicity, G_{VE} is considered equal to G_R.

10.2.4 Plot the relationship between pseudo strain and stress for each cycle chosen from the high amplitude test (Figure A-10). The approximate 128 points collected in each cycle will make possible the construction of the areas in the Figure A-10.

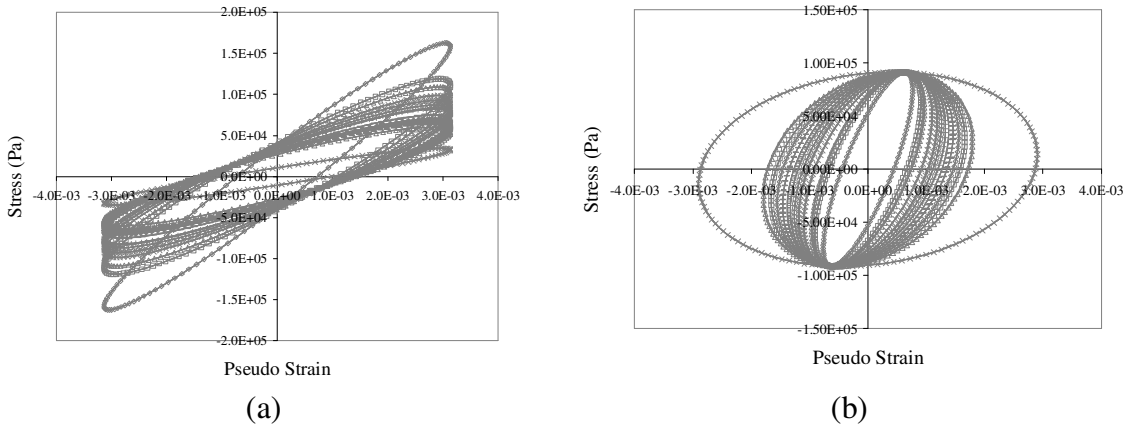

FIGURE A-10 Hysteresis Loop for: (a) Controlled-Strain, and (b) Controlled-Stress.

10.2.5 Calculate the area of the plots generated on step 10.2.4. This area is the actual hysteresis loop area, which represents the dissipated pseudo strain energy (DPSE) for each cycle.

10.2.6 Calculate W_{R1} using Equations A-5 and A-6. This DPSE component accounts for the damage that causes an increase in the apparent phase angle and

an increase in the hysteresis loop area with respect to a reference modulus that represents the intact undamaged material.

$$W_{R1} = \pi G^*_{VE} \gamma^2_{0F} \sin(\delta_{NF} - \delta_{VE}) \qquad \text{controlled-strain (A-5)}$$

$$W_{R1} = \pi \frac{\tau^2_{0F}}{G^*_{VE}} \sin(\delta_{NF} - \delta_{VE}) \qquad \text{controlled-stress (A-6)}$$

where, τ is the used stress amplitude.

10.2.7 Calculate W_{R2} using Equations A-7 and A-8. This DPSE component accounts for the non-uniform energy dissipation within the hysteresis loop (difference between the actual and the idealized hysteresis loop area). Do not consider this step if data points within each cycle are not available.

$$\left(\text{Area of Stress - Pseudo StrainLoop} / \frac{G^*_N}{G^*_{VE}} \right) - W_{R1} \qquad \text{controlled-strain (A-7)}$$

$$\left(\text{Area of Stress-Pseudo Strain Loop} \times \frac{G^*_N}{G^*_{VE}} \right) - W_{R1} \qquad \text{controlled-stress (A-8)}$$

10.2.8 Calculated W_{R3} using Equations A-9 and A-10. This DPSE component is associated with the difference between the pseudo stiffness of the undamaged material and the pseudo stiffness after damage.

$$W_{R3} = \frac{1}{2} \gamma^2_{0F} (G^*_{VE} - G^*_{NF}) \qquad \text{controlled-strain (A-9)}$$

$$W_{R3} = \frac{1}{2} \tau^2_{0F} \left(\frac{1}{G^*_{NF}} - \frac{1}{G^*_{VE}} \right) \qquad \text{controlled-stress (A-10)}$$

10.2.9 Sum W_{R1}, W_{R2} and W_{R3} calculated from steps 10.2.6, 10.2.7 and 10.2.8 If step 10.2.7 was not considered, calculate just the sum of W_{R1} and W_{R3}.

10.2.10 Plot $W_{R1}+W_{R2}+W_{R3}$ versus log of the number of load cycles (N). If you did not consider step 10.2.7, plot just $W_{R1}+W_{R3}$.

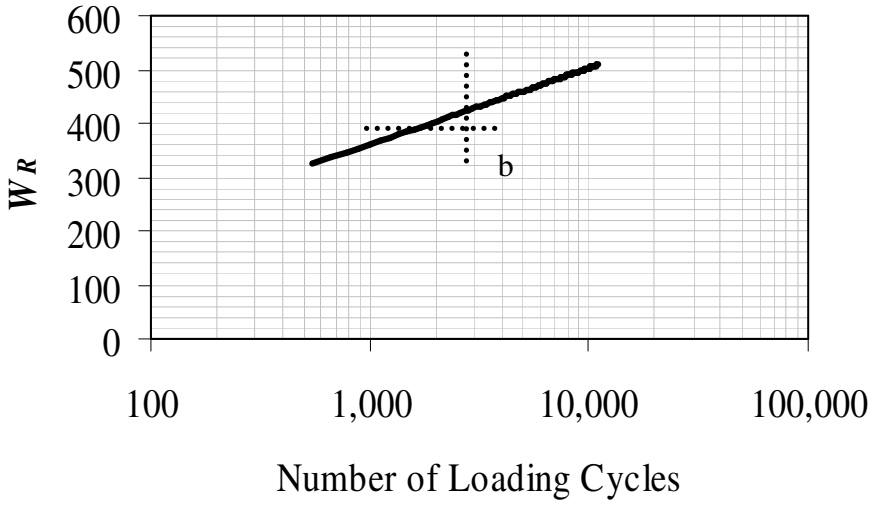

FIGURE A-11 W_R versus Number of Load Cycles.

10.2.11 Select b value from the plot on step 10.2.10. b value is the slop of the plot.

10.2.12 Calculate $R(Nf)$ values using Equation A-11.

$$R(Nf) = \left[(2n+1)^{n+1} \left(\frac{G_R b}{4\pi E_1 \Delta G f} \right)^n N \right]^{\frac{1}{2n+1}} \qquad \text{(A-11)}$$

where, n is equal to $1/m$ for controlled-strain tests and $1+1/m$ for controlled-stress tests, m is the exponent of time in the power law equation of the relaxation

modulus, E_1 is obtained from relaxation modulus-time relationship, ΔGf is the bond energy, and N is the number of cycles to failure. G_R is the reference modulus.

11. KEYWORDS

Dynamic Mechanical Analyzer (DMA), fatigue test, relaxation modulus, damage, dissipated energy.

ANNEXES

A-1. Strain/stress sweep test for determining the high strain amplitude for the oscillation test

A-1.1. In computer software:

A-1.1.1 Go to oscillation;

A-1.1.2. Select amplitude sweep test;

A-1.1.3 Strain/stress sweep test – recommended values

- Strain/stress range – strain range from 0.001 percent to 0.6 percent, and stress range from 1.1×10^3 to 2.0×10^5 Pa**.** Amplitude range should go from very low values (on the linear region) to values high enough to check nonlinear and damage behaviors;
- Delay time – 2 seconds;
- Number of samples – 25;
- Number of periods – 200;
- Number of points per period – 8,192;
- Temperature and frequency – selected by the operator.

A-1.2 Data Analysis

A-1.2.1 Monitor the strain/stress amplitude responses (slopes of strain/stress versus time plots). These slopes are determined by plotting the strain/stress amplitude for each one of the 200 load applications and fitting a linear trend line. For strain sweep tests, positive slopes represent strain hardening, slopes close to zero represent nonlinear viscoelastic behavior, and negative slopes represent damage. For stress sweep tests, negative slopes represent strain hardening, slopes close to zero represent nonlinear viscoelastic behavior and positive slopes represent damage.

A-1.2.2 Select the strain/stress amplitude that corresponds to the limit for the dynamic modulus and the phase angle that mark the end of the nonlinear viscoelastic region and the start of the damage region. This amplitude is selected fitting the data with a horizontal line ($y = \alpha_0$) connected at the point x_0 to a linear ($y = b_0 + b_1 x$) - for strain sweep case (Figure A-12) or quadratic function ($y = \beta_0 + \beta_1 x + \beta_2 x^2$) - for stress sweep case (Figure A-13). This specific strain/stress amplitude should be used for the shear oscillation test (fatigue).

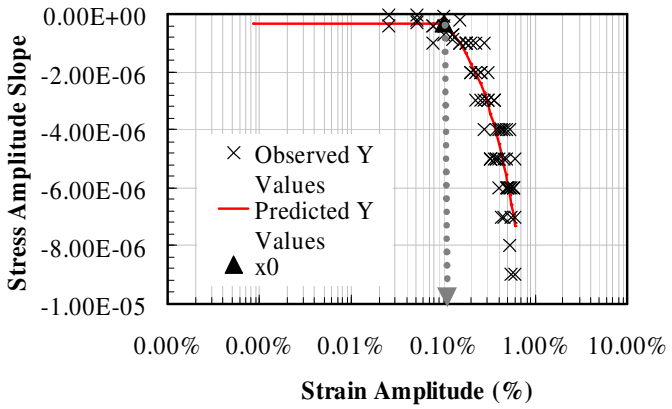

FIGURE A-12 Stress Amplitude Slope versus Strain Amplitude, Strain Sweep Test.

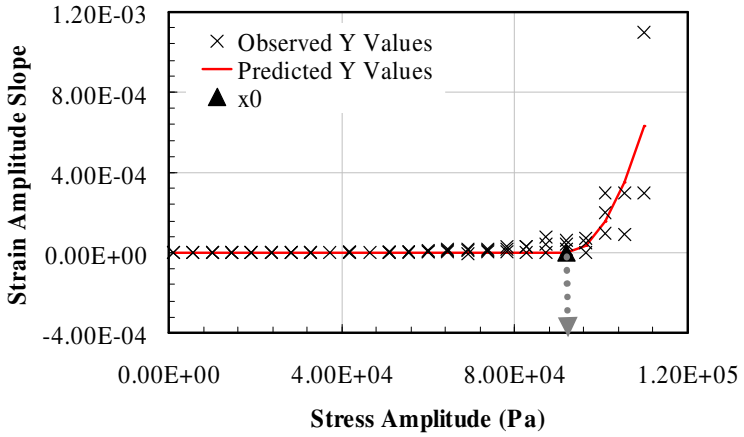

FIGURE A-13 Strain Amplitude Slope versus Stress Amplitude, Stress Sweep Test.

A-2. Fine Aggregate Matrix (FAM) Design Example

A-2.1 Consider a HMA mixture that contains: 22 percent of #8 limestone, 22 percent of #8 gravel, 10 percent of limestone sand, 26 percent of natural sand, and 20 percent of Rap. Binder percentage used was 5.4 percent by weight of the total mixture. Aggregates gradation and mixture blend are in Table A-1.

TABLE A-1 Hot Mix Asphalt (HMA) Aggregates Gradation and Mixture Blend

Sieve Size (mm)	Aggregate (% Passing)					Blend (% Passing)
	#8 Limestone	# 8 Gravel	Limestone Sand	Natural Sand	Rap	
50.80 (2")	100	100	100	100	100	100
37.50 (1 ½")	100	100	100	100	100	100
25.40 (1")	100	100	100	100	100	100
19.05 (3/4")	100	100	100	100	100	100
12.70 (1/2")	100	100	100	100	98	100
9.50 (3/8")	88	95	100	100	83	93
4.75 (#4)	18	20	100	100	55	55
2.36 (#8)	2	2	90	92	34	41
1.18 (#16)	2	2	63	67	25	30
0.60 (#30)	2	2	40	44	16	20
0.30 (#50)	2	2	20	18	12	10
0.15 (#100)	2	2	9	5	10	5
0.075 (#200)	2	2	6.4	4.3	7.6	4

A-2.2 Knowing that for the DMA mixture just aggregates smaller than 1.18 mm (passing on sieve No. 16) are used, aggregate quantities should be proportionate again. DMA mixture contains, for this example: 1.5 percent of #8 limestone, 1.5 percent of #8 gravel, 21.3 percent of limestone sand, 58.9 percent of natural sand, and 16.9 percent of Rap. These values were found multiplying the HMA aggregate contribution by the amount of each aggregate passing on sieve No. 16 and them dividing this product by the percent of the blend that is passing on sieve No. 16. For example, the amount of #8 limestone that should be used on the DMA mixture was found:

$$Ammount\ of\ \#8\ limestone\ DMA\ = \frac{0.22 \times 0.02}{0.30} = 1.5\% \qquad \text{(A-12)}$$

A-2.3 Aggregates gradation and mixture blend for DMA are in Table A-2. Note that, aggregates gradations were also proportionate again.

TABLE A-2 Fine Aggregate Matrix (FAM) Gradation and Mixture Blend

Sieve Size (mm)	Aggregate (% Passing)					Blend (% Passing)
	#8 Limestone	#8 Gravel	Limestone Sand	Natural Sand	Rap	
1.18 (#16)	100	100	100	100	100	100
0.60 (#30)	100	100	63.5	65.7	64	66
0.30 (#50)	100	100	31.8	26.9	48	34
0.15 (#100)	100	100	14.3	7.5	40	17
0.075 (#200)	100	100	10.2	6.4	30.4	14

A-2.4 In order to calculate the amount of binder by weight that should be used on the DMA mixture, HMA gradation should be considered. Assume a mixture batch size of 4,500 Kg. Calculate the mass of aggregate blend retained on each sieve (Table A-3).

TABLE A-3 Mass of Aggregate Blend Retained on each Sieve

Sieve Size (mm)	% Retained	Mass(g)
50.80 (2")	0.0	0.00
37.50 (1 ½")	0.0	0.00
25.40 (1")	0.0	0.00
19.05 (3/4")	0.0	0.00
12.70 (1/2")	0.4	17.0
9.50 (3/8")	6.7	286.9
4.75 (#4)	37.5	1596.4
2.36 (#8)	14.8	628.3
1.18 (#16)	11.0	468.3
0.60 (#30)	10.1	429.1
0.30 (#50)	9.6	407.0
0.15 (#100)	4.9	207.7
0.075 (#200)	0.9	39.3
Pan (passing on sieve #200)	4.2	177.0

A-2.5 Add mass of aggregate smaller than 1.18 mm. The mass of aggregate smaller than 1.18 mm for this example is 1260.07 g.

A-2.6 Calculate binder weight multiplying percent binder used on the HMA (5.4 percent) by the mixture batch size (4,500 g). Binder weight for this example is 243 g.

A-2.7 Calculate binder percentage that should be used on the DMA mixture. Binder percentage should be calculated dividing the binder amount (243 g) by the DMA mixture amount (1260.07+243=1503.07 g). Binder percentage for this example is 16.17 percent. Coarse aggregate absorption can be reduced by the total binder percentage if this information is available.

APPENDIX B

ANALYSIS USING CRACK GROWTH INDEX APPROACH

1. DERIVATIONS

1.1 Dissipated Pseudo Strain (DPSE) Sources

The energy dissipated (W) within a stress-strain hysteresis loop can be calculated as follows.

$$W = 4\int_{0}^{\frac{\pi}{2w}} \sigma \frac{\partial \varepsilon}{\partial t} \partial t \tag{B-1}$$

if, $\varepsilon = \varepsilon_0 \sin wt$ Equation B-1 results in Equation B-2.

$$W = \sigma_0 \varepsilon_0 \pi \sin \delta \tag{B-2}$$

Controlled-Strain

For controlled-strain mode of loading, the applied strain (ε) and the measured stress (σ) can be represented using Equations B-3 and B-4, respectively.

$$\varepsilon = \varepsilon_0 \sin(wt) \tag{B-3}$$

$$\sigma = \sigma_0 \sin(wt + \delta_{VE}) \tag{B-4}$$

Knowing that $\sigma_0 = \varepsilon_0 G^*_{VE}$, pseudo strain ($\varepsilon^R$) can be represented using Equation B-5. If G_{VE}* and G_R are assumed be the same, strain (ε) and pseudo strain (ε^R) will have the same amplitude.

$$\varepsilon^R = \frac{\varepsilon_0 G^*_{VE} \; sin(\, wt + \delta_{VE} \,)}{E_R} \tag{B-5}$$

For controlled-strain loading, the energy dissipated within the hysteresis loop in the stress-pseudo strain domain (DPSE) can be represented using Equation B-6.

$$W_{R1} = DPSE = \pi \sigma_0 \varepsilon^R \; sin(\, \delta - \delta_{VE} \,) \tag{B-6}$$

Knowing that $\varepsilon^R = \frac{\sigma_0}{G_R}$ and $\sigma_0 = G^*_N \varepsilon_0$, Equation B-6 becomes Equation B-7. *N* subscript is used to indicate that the parameter changes as a function of the number of loading cycles. For this analysis, G_{VE}* and G_R are assumed to have the same amplitude.

$$\begin{aligned} W_{R1} &= \pi \sigma_0 \frac{\sigma_0}{G_R} sin(\, \delta - \delta_{VE} \,) \\ W_{R1} &= \pi \sigma_0 \frac{G^*_{VE} \varepsilon_0}{G_R} sin(\, \delta - \delta_{VE} \,) \\ W_{R1} &= \pi \sigma_0 \varepsilon_0 \; sin(\, \delta - \delta_{VE} \,) \end{aligned} \tag{B-7}$$

To separate the effect of the decrease in the dynamic modulus (G^*_N) and the increase in the phase angle (δ), Equation B-7 is divided by the ratio of the damage stiffness (G^*_N) to the undamaged stiffness (G^*_{VE}) $\left(\frac{G^*_N}{G^*_{VE}} \right)$ and results in Equation B-8. Equation B-8 represents the first source of the DPSE, that is the dissipated energy due to increase in the apparent phase angle at a given reference undamaged modulus.

$$W_{R1} = \pi G^*_{VE} \varepsilon_0^2 \, sin(\, \delta - \delta_{VE} \,) \tag{B-8}$$

The second source of the DPSE (W_{R2}) is the difference between the hysteresis loop area calculated (W_{R1}, Equation B-8) and the real loop area.

$$W_{R2} = \left(\frac{\text{area of the stress versus pseudo strain loop}}{\frac{G^*_N}{G^*_{VE}}} \right) - W_{R1} \tag{B-9}$$

The third source of the DPSE (W_{R3}) is associated with the difference between the pseudo stiffness of the undamaged material and the pseudo stiffness after damage (Figure B-1). The energy dissipated to change the material from an undamaged stage to a damage one, can be represented using Equation B-10.

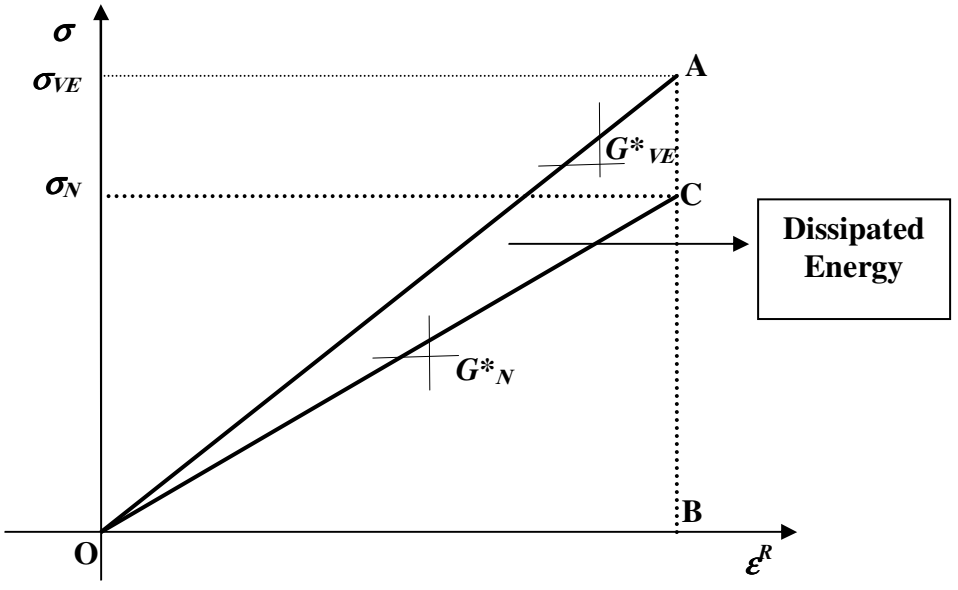

FIGURE B-1. Difference between Pseudo Stiffness of the Undamaged and the Damage Materials, Controlled-Strain Mode of Loading.

$$W_{R3} = \Delta OAB - \Delta OCB \tag{B-10}$$

Developing Equation B-10 in terms of stress and strain, we have Equation B-11 that represents W_{R3} for controlled-strain mode of loading.

$$\begin{aligned}
W_{R3} &= \frac{1}{2}\sigma_{VE}\varepsilon^{R} - \frac{1}{2}\sigma_{N}\varepsilon^{R} \\
W_{R3} &= \frac{1}{2}\sigma_{VE}\frac{\sigma_{VE}}{G^{*}_{VE}} - \frac{1}{2}\sigma_{N}\frac{\sigma_{VE}}{G^{*}_{VE}} \\
W_{R3} &= \frac{1}{2}G^{*}_{VE}\varepsilon_{0}\frac{\sigma_{VE}}{G^{*}_{VE}} - \frac{1}{2}G^{*}_{N}\varepsilon_{0}\frac{\sigma_{VE}}{G^{*}_{VE}} \\
W_{R3} &= \frac{1}{2}G^{*}_{VE}\varepsilon_{0}\frac{G^{*}_{VE}\varepsilon_{0}}{G^{*}_{VE}} - \frac{1}{2}G^{*}_{N}\varepsilon_{0}\frac{G^{*}_{VE}\varepsilon_{0}}{G^{*}_{VE}} \\
W_{R3} &= \frac{1}{2}G^{*}_{VE}\varepsilon_{0}^{2} - \frac{1}{2}G^{*}_{N}\varepsilon_{0}^{2} \\
W_{R3} &= \frac{1}{2}\varepsilon_{0}^{2}(G^{*}_{VE} - G^{*}_{N})
\end{aligned} \tag{B-11}$$

Controlled-Stress

For controlled-stress mode of loading, the applied stress (σ) and the measured strain (ε) can be represented using Equations B-12 and B-13, respectively.

$$\sigma = \sigma_{0}\, sin(\, wt\,) \tag{B-12}$$

$$\varepsilon = \varepsilon_{0}\, sin(\, wt - \delta_{N}\,) \tag{B-13}$$

The pseudo energy can be calculated using a pseudo stress-strain relationship or using a stress-pseudo strain relationship. In order to have direct comparison between controlled-strain and controlled-stress results, stress-pseudo strain relationship will be

used for both modes of loading. Applying a strain (ε) described in Equation B-14, the measured stress (σ) is the one describe in Equation B-15.

$$\varepsilon = \varepsilon_0 \, sin(\, wt - \delta_N \,) \tag{B-14}$$

$$\sigma = \sigma_0 \, sin(\, wt - \delta_N + \delta_{VE} \,) \tag{B-15}$$

Knowing that $\sigma_0 = \varepsilon_0 G^*_{VE}$, pseudo strain ($\varepsilon^R$) can be represented using Equation B-16. If G_{VE}* and G_R are assumed be the same, strain (ε) and pseudo strain (ε^R) will have the same amplitude.

$$\varepsilon^R = \frac{\varepsilon_0 G^*_{VE} \, sin(\, wt - \delta_N + \delta_{VE} \,)}{E_R} \tag{B-16}$$

For controlled-stress loading, the energy dissipated within the hysteresis loop in the stress-pseudo strain domain (DPSE) can be represented using Equation B-17.

$$W_{R1} = DPSE = \pi \sigma_0 \varepsilon^R \, sin(\, \delta - \delta_{VE} \,) \tag{B-17}$$

Knowing that $\varepsilon^R = \frac{\sigma_0}{G_R}$ and $\sigma_0 = G^*_N \varepsilon_0$, Equation B-17 becomes Equation B-18. *N* subscript is used to indicate that the parameter changes as a function of the number of loading cycles. For this analysis, G_{VE}* and G_R are assumed to have the same amplitude.

$$\begin{aligned} W_{R1} &= \pi \sigma_0 \frac{\sigma_{VE}}{G_R} sin(\, \delta - \delta_{VE} \,) \\ W_{R1} &= \pi \sigma_0 \frac{G^*_{VE} \varepsilon_0}{G_R} sin(\, \delta - \delta_{VE} \,) \\ W_{R1} &= \pi \sigma_0 \varepsilon_0 \, sin(\, \delta - \delta_{VE} \,) \end{aligned} \tag{B-18}$$

To separate the effect of the decrease in the dynamic modulus (G_N^*) and the increase in the phase angle (δ), Equation B-18 is multiplied by the ratio of the damage stiffness to the undamaged stiffness $\left(\frac{G_N^*}{G_{VE}^*}\right)$ and results in Equation B-19. Equation B-19 represents the first source of the DPSE, that is the dissipated energy due to increase in the apparent phase angle at a given reference undamaged modulus.

$$W_{R1} = \frac{\pi\sigma_0^2 \, sin(\,\delta - \delta_{VE}\,)}{G_{VE}^*} \tag{B-19}$$

The second source of the DPSE (W_{R2}) is the difference between the hysteresis loop area calculated (W_{R1}, Equation B-19) and the real loop area.

$$W_{R2} = \left(area\ of\ stress\ versus\ pseudo\ strain\ loop \times \frac{G_N^*}{G_{VE}^*} \right) - W_{R1} \tag{B-20}$$

The third source of the DPSE (W_{R3}) is associated with the difference between the pseudo stiffness of the undamaged material and the pseudo stiffness after damage (Figure B-2). The energy dissipated to change the material from an undamaged stage to a damage one, can be represented using Equation B-21.

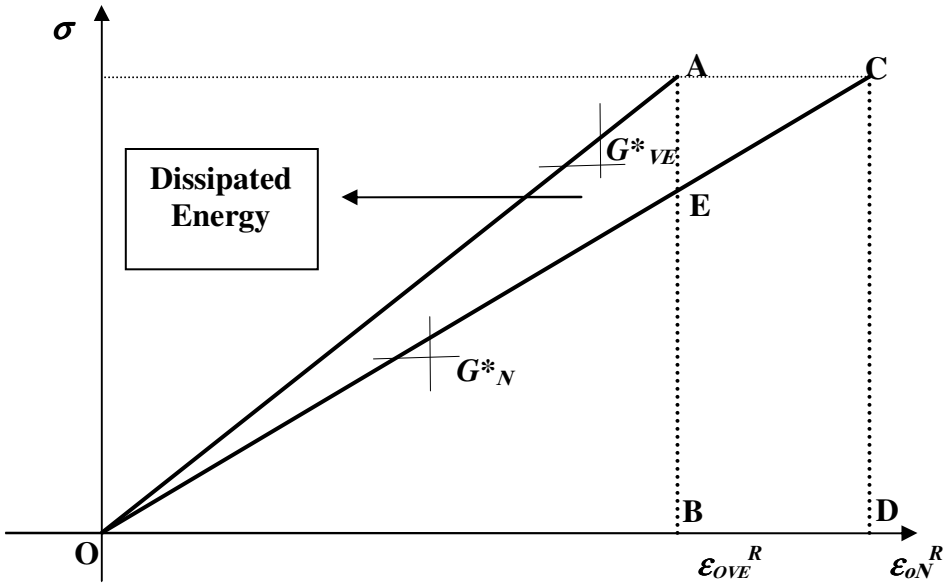

FIGURE B-2. Difference between Pseudo Stiffness of the Undamaged and the Damage Materials, Controlled-Stress Mode of Loading.

$$W_{R3} = \Delta OAB - \Delta OCD + \quad ABCD \tag{B-21}$$

Developing Equation B-21 in terms of stress and strain, we have Equation B-22 that represents W_{R3} for controlled-stress mode of loading.

$$W_{R3} = \frac{1}{2}\sigma\varepsilon_{0VE}^{R} - \frac{1}{2}\sigma\varepsilon_{0N}^{R} + \left(\varepsilon_{0N}^{R} - \varepsilon_{0VE}\right)\sigma$$

$$W_{R3} = \frac{1}{2}\sigma\frac{\sigma_0}{G_{VE}^{*}} - \frac{1}{2}\sigma\frac{\sigma_0}{G_{N}^{*}} + \left(\frac{\sigma_0}{G_{N}^{*}} - \frac{\sigma_0}{G_{VE}^{*}}\right)\sigma$$

$$W_{R3} = \frac{\sigma_0^2}{2G_{VE}^{*}} - \frac{1}{2}\frac{\sigma_0^2}{G_{N}^{*}} + \left(\sigma\varepsilon_{0N} - \sigma\varepsilon_{0VE}\right)$$

$$W_{R3} = \frac{\sigma_0}{2}\varepsilon_{0VE} - \frac{\sigma_0}{2}\varepsilon_{0N} + \sigma_0\varepsilon_{0N} - \sigma_0\varepsilon_{0VE}$$

$$W_{R3} = \sigma_0\left(\frac{\varepsilon_{0VE}}{2} - \varepsilon_{0VE}\right) + \sigma_0\left(\varepsilon_{0N} - \frac{\varepsilon_{0N}}{2}\right)$$

$$W_{R3} = -\frac{\sigma_0\varepsilon_{0VE}}{2} + \frac{\sigma_0\varepsilon_{0N}}{2}$$

$$W_{R3} = \frac{\sigma_0}{2}\left(\varepsilon_{0N} - \varepsilon_{0VE}\right)$$

$$W_{R3} = \frac{\sigma_0^2}{2}\left(\frac{1}{G_{N}^{*}} - \frac{1}{G_{VE}^{*}}\right) \qquad \text{(B-22)}$$

1.2 Crack Growth Index

From Paris' law:

$$\frac{d\bar{r}}{dN} = A\left[J_R\right]^n \qquad \text{(B-23)}$$

where, $\bar{r}$ is the average crack radius, J_R is the pseudo strain energy release rate per unit crack area, A and n are material constants.

Manipulating Equation B-23 we have Equation B-24.

$$\frac{d\bar{r}}{dN} = A\left[\frac{\frac{\partial W_R}{\partial N}}{\frac{\partial\left(M\,2\pi\bar{r}^{\,2}\right)}{\partial N}}\right]^n$$

$$\frac{d\bar{r}}{dN} = A\left[\frac{\frac{\partial W_R}{\partial N}}{4\pi M\bar{r}\,\frac{\partial\bar{r}}{\partial N}}\right]^n \qquad \text{(B-24)}$$

$$\bar{r}^{\,n}\left(\frac{\partial\bar{r}}{\partial N}\right)^{n+1} = A\left[\frac{\frac{\partial W_R}{\partial N}}{4\pi M}\right]^n$$

where, M is the number of cracks in a specimen, and $\frac{\partial}{\partial N}\left(M\,2\pi\bar{r}^{\,2}\right) = M\,4\pi\bar{r}\,\frac{d\bar{r}}{dN}$.

Taking power of $\frac{1}{(n+1)}$ in Equation B-24 and integrating in respect to $\bar{r}$, we have Equation B-25.

$$\int_{r=0}^{r=r_0} r^{\frac{n}{n+1}}\partial r = A^{\frac{1}{n+1}}\left[\frac{1}{4\pi M}\right]^{\frac{n}{n+1}}\frac{n+1}{2n+1}\left(\frac{b}{N_i}\right)^{\frac{2n+1}{n+1}} \qquad \text{(B-25)}$$

where, $W_R = a + b\,log(N)$.

Now, considering the fundamental law of fracture we have Equation B-26.

$$\Delta G_f = E_R D(t\alpha) J_R \qquad \text{(B-26)}$$

where, $t\alpha$ (Equation B-27) is the time that the crack takes to pass through the plastic zone (α).

$$t\alpha = k_1\frac{\alpha}{\dot{c}} \qquad \text{(B-27)}$$

where, k_1 is equal to 1/3 (k_1 depends on the size of m from the power law relationship between creep compliance and time), $\dot{c} = \frac{\partial c}{\partial t}$, and $D(t\alpha)$ can be represented using Equation B-28.

$$D(t\alpha) = D_0 + D_1\left(k_1 \frac{\alpha}{\dot{c}}\right)^m \tag{B-28}$$

Rewriting Equation B-26 considering Equation B-28 results in Equation B-29.

$$\Delta G_f = E_R\left[D_0 + D_1\left(k_1 \frac{\alpha}{\dot{c}}\right)^m\right] J_R \tag{B-29}$$

Solving Equation B-29 for $\frac{\partial c}{\partial t}$ results in Equation B-30.

$$\frac{dc}{dt} = \left[\frac{E_R D_1 J_R}{\Delta G_f - D_0 E_R J_R}\right]^{\frac{1}{m}} k_1 \alpha \tag{B-30}$$

Knowing that $\alpha = k_2 \frac{J_R}{D_1 \sigma_t^2 I_1}$, where $I_i = \frac{1}{n+1}$ ($n=0$ for ductile materials and $n=1$ for brittle materials), Equation B-30 becomes Equation B-31.

$$\frac{dc}{dt} = k_1 k_2 \frac{D_1^{\left(\frac{1}{m}-1\right)} E_R^{\frac{1}{m}} J_R^{\left(\frac{1}{m}+1\right)}}{\left[\Delta G_f - D_0 E_R J_R\right]^{\frac{1}{m}}} \frac{1}{\sigma_t^{\,2} I_1} \tag{B-31}$$

To be able to compare Equation B-31 with Paris' law (Equation B-23) we should change Equation B-31 from $\frac{dc}{dt}$ to $\frac{dc}{dN}$.

$$\frac{dc}{dN} = k\left[\frac{D_1^{1-m} E_R J_R^{m+1}}{\Delta G_f - D_0 E_R J_R}\right]^{\frac{1}{m}} \int_0^{\Delta t} \frac{[w(t)]^{1+\frac{1}{m}}}{\sigma_t^2 I_1} \partial t \tag{B-32}$$

where, $k=k_1k_2$, and $w(t)$ is the shape of the applied load $f(t)$.

Putting Equations B-23 and B-32 together, we have Equation B-33 or Equation B-34..

$$A = k\left[\frac{E_R}{D_1 \Delta G_f}\right]^n \int_0^{\Delta t} \frac{[w(t)]^{1+\frac{1}{m}}}{\sigma_t^2 I_1} \partial t \tag{B-33}$$

$$A = K\left[\frac{E_R}{D_1 \Delta G_f}\right]^n \tag{B-34}$$

Replacing Equation B-34 in Equation B-25 results in Equation B-35.

$$\bar{r}(N) = K^{\frac{1}{2n+1}} (2n+1)^{\frac{n+1}{2n+1}} \left(\frac{E_R}{4\pi M E_1 \Delta G_f}\right)^{\frac{n}{2n+1}} b^{\frac{n}{2n+1}} N^{\frac{1}{2n+1}} \tag{B-35}$$

Since M, which is the number of cracks, is an unknown; $\bar{r}$ in Equation B-35 is substituted by an equivalent crack radius ($R(N)$) (Equation B-36) that will represent the influence of those M cracks (Figure B-3).

$$R(N) = \frac{r(N)}{K^{\frac{1}{2n+1}}} = \left[(2n+1)^{n+1}\left(\frac{E_R b}{4\pi E_1 \Delta G_f}\right)^n N\right]^{\frac{1}{2n+1}} \tag{B-36}$$

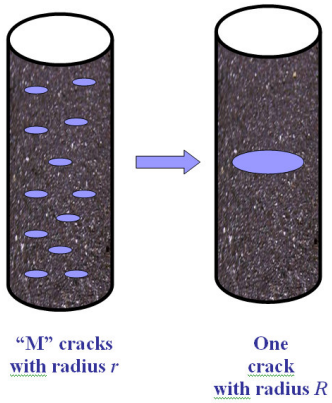

FIGURE B-3. Crack Growth Index Illustration.

2. PROTOCOL

- Run time sweep DMA test for both modes of loading: controlled-strain and controlled-stress;

- Plot $N \times \frac{G^*}{G_0}$ versus number of loading cycles. N is the number of cycles, G^* is the dynamic modulus, and G_0 is the value of G^* at the first load cycle;

- Select fatigue life from the plot on the last step. Fatigue life is determined to be the number of load cycles at which the value of $N \times \frac{G^*}{G_0}$ becomes maximum;

- Select data (strain and stress) correspondent to initial cycle, and cycles correspondent to 5, 10, 20, 30, 40, 50, 60, 70, 80, 90 and 100 percent of fatigue life;

- Calculate pseudo strain for both modes of loading using Equations B-5 and B-16;

- Plot stress versus pseudo strain hysteresis loops;

- Calculate area for the plots found on last step. Use trapezoidal rule;

- Select dynamic modulus (G^*) and phase angle (δ) for the initial cycle, and cycles correspondent to 5, 10, 20, 30, 40, 50, 60, 70, 80, 90 and 100 percent of fatigue life;

- Calculate W_R using Equations B-37 and B-38 for controlled-strain and controlled-stress modes of loading, respectively;

$$W_R = \frac{DPSE(\ from\ area\ of\ the\ stress\ versus\ pseudo\ strain\ plots\ )}{\frac{G_N^*}{G_{VE}^*}} \tag{B-37}$$

$$W_R = DPSE(\ from\ area\ of\ the\ stress\ versus\ pseudo\ strain\ plots) \times \frac{G_N^*}{G_{VE}^*} \tag{B-38}$$

where, G^*_N is the dynamic modulus at load cycle N, and G^*_{VE} is the viscoelastic dynamic modulus.

- Calculate W_{R1} using Equations B-7 and B-18 for controlled-strain and controlled-stress modes of loading, respectively;

- Calculate W_{R2} using Equations B-9 and B-20 for controlled-strain and controlled-stress modes of loading, respectively;

- Calculate W_{R3} using Equations B-11 and B-22 for controlled-strain and controlled-stress modes of loading, respectively;

- Add W_{R1}, W_{R2} and W_{R3};

- Plot $W_{R1}+W_{R2}+W_{R3}$ versus number of loading cycles (log scale). The slope of this plot represents "*b*", the rate of change in DPSE;

- Calculate $R(N)$ using Equation B-36. In Equation B-36, n is related to the exponent m in the relaxation modulus-time relationship as: $n = 1 + \frac{1}{m}$.

APPENDIX C

ANALYSIS USING NONLINEAR VISCOELASTIC MODEL APPROACH

1. DERIVATIONS

Schapery (*25*) adapted the solution for linear viscoelasticity (Boltzmann superposition integral) to represent the nonlinear viscoelastic behavior. The strain response (ε) for a given stress (σ) history can be represented using Equation C-1.

$$\varepsilon = g_0 D_0 \sigma + g_1 \int_0^t \hat{D}(t-\tau) \frac{\partial g_2 \sigma}{\partial \tau} d\tau \qquad \text{(C-1)}$$

where, $\hat{D}$ is the transient component of the creep compliance.

To account for oscillatory contributions, the function described in Equation C-1 is expanded to become as shown in Equation C-2.

$$\Delta\varepsilon = D_0(g_{0,t} + \Delta g_0)\sigma + (g_{1,t} + \Delta g_1) \int_{-\infty}^t D(t-\tau) \frac{\partial}{\partial \tau}(g_{2,t} + \Delta g_2)\sigma \partial\tau \qquad \text{(C-2)}$$

where, terms with subscript *t* indicate that the parameter is evaluated at a constant stress (σ_t) applied at *t=0*, terms with symbol Δ represent the oscillatory contribution, and *w* is the angular frequency defined as $w = 2\pi f$.

For the current study, no preload was used. Terms with subscript *t* in Equation C-2 were removed, resulting in Equation C-3.

$$\Delta\varepsilon = D_0 \Delta g_0 \sigma + \Delta g_1 \int_{-\infty}^t D(t-\tau) \frac{\partial}{\partial \tau} \Delta g_2 \sigma \partial\tau \qquad \text{(C-3)}$$

Stress (σ), Δg_0, Δg_1, and Δg_2 can be represented using Equations C-4 through C-7.

$$\sigma = \sigma_0 e^{iwt} \tag{C-4}$$

$$\Delta g_0 = 1 + H(\sigma - \bar{\sigma})k\sigma_0 e^{iwt} \tag{C-5}$$

$$\Delta g_1 = 1 + H(\sigma - \bar{\sigma})f\sigma_0 e^{iwt} \tag{C-6}$$

$$\Delta g_2 = 1 + H(\sigma - \bar{\sigma})h\sigma_0 e^{iwt} \tag{C-7}$$

where,

$$H(\sigma - \bar{\sigma}) \equiv \begin{cases} 0, \sigma < \bar{\sigma} \\ 1, \sigma > \bar{\sigma} \end{cases} \tag{C-8}$$

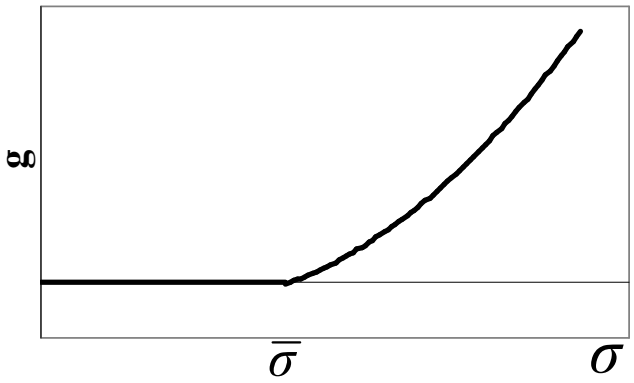

FIGURE C-1 Nonlinear Viscoelastic Parameter (*g*) versus stress (σ).

Substituting Equations C-4 through C-7 in Equation C-3, we have:

$$\Delta\varepsilon = D_0 \Delta g_0 \sigma + f\sigma_0 e^{iwt} \int_{-\infty}^{t} D(t-\tau) \frac{\partial (h\sigma_0^2 e^{2iw\tau})}{\partial \tau} \partial\tau \tag{C-9}$$

$$\Delta\varepsilon = D_0 \Delta g_0 \sigma + f\sigma_0 e^{iwt} h\sigma_0^2 (2iw) \int_{-\infty}^{t} D(t-\tau) e^{2iw\tau} \partial\tau \tag{C-10}$$

Changing variables for Equation C-10:

$$\Delta\varepsilon = D_0 \Delta g_0 \sigma + f\sigma_0 e^{iwt} h\sigma_0^2 (2iw) \int_{0}^{\infty} D(v) e^{2iwt-v} \partial v \tag{C-11}$$

$$\Delta\varepsilon = D_0 \Delta g_0 \sigma + f\sigma_0 e^{3iwt} h\sigma_0^2 (2iw) \int_{0}^{\infty} \hat{D}(v) e^{-2iwv} \partial v \tag{C-12}$$

where, $v = t-\tau$

Defining that $\bar{w} = 2w$ and knowing that $e^{-i\bar{w}v} = cos(\bar{w}v) - i\sin(\bar{w}v)$, Equation C-12 can be rewritten as:

$$\Delta\varepsilon = D_0 \Delta g_0 \sigma + fh\sigma_0 e^{iwt} e^{i\bar{w}t} \sigma_0^{\,2} (i\bar{w}) \int_{0}^{\infty} \hat{D}(v) \left[cos(\bar{w}v) - i\, sin(\bar{w}v) \right] \partial v \tag{C-13}$$

$$\Delta\varepsilon = D_0 \Delta g_0 \sigma + fh\sigma e^{i\bar{w}t} \sigma_0^2 \bar{w} \int_{0}^{\infty} \hat{D}(v) \left[sin(\bar{w}v) - i\, cos(\bar{w}v) \right] \partial v \tag{C-14}$$

$$\Delta\varepsilon = D_0 \Delta g_0 \sigma + fh\sigma h\sigma^{i\bar{w}t} \sigma_0^2 \left[\left| \hat{D} \right|_{\bar{w}} cos(\hat{\delta}_{\bar{w}}) - i \left| \hat{D} \right|_{\bar{w}} sin(\hat{\delta}_{\bar{w}}) \right] \tag{C-15}$$

Creep compliance for the nonlinear viscoelastic region (D_{NL}^{*}) can be represented using Equations C-16 though C-18.

$$D_{NL}^{*} = \frac{\Delta\varepsilon}{\sigma} = D_0 \Delta g_0 + fhe^{i\bar{w}t}\sigma_0^2\left[\left|\hat{D}\right|_{\bar{w}} \cos(\hat{\delta}_{\bar{w}}) - i\left|\hat{D}\right|_{\bar{w}} \sin(\hat{\delta}_{\bar{w}})\right] \quad \text{(C-16)}$$

$$D_{NL}^{*} = D_0 \Delta g_0 + fh\sigma_0^2\left|\hat{D}\right|_{\bar{w}} e^{i(\bar{w}t - \hat{\delta}_{\bar{w}})} \quad \text{(C-17)}$$

$$D_{NL}^{*} = D_0 \Delta g_0 + fh\sigma_0^2\left[\left|\hat{D}\right|_{\bar{w}} \cos(\bar{w}t - \hat{\delta}_{\bar{w}}) + i\left|\hat{D}\right|_{\bar{w}} \sin(\bar{w}t - \hat{\delta}_{\bar{w}})\right] \quad \text{(C-18)}$$

Separating real and imaginary parts for Equation C-18, results in Equations C-19 and C-20.

$$D_{NL}^{*\prime} = D_0 \Delta g_0 + fh\sigma_0^2\left[\left|\hat{D}\right|_{\bar{w}} \cos(\bar{w}t - \hat{\delta}_{\bar{w}})\right] \quad \text{(C-19)}$$

$$D_{NL}^{*\prime\prime} = -fh\sigma_0^2\left[\left|\hat{D}\right|_{\bar{w}} \sin(\bar{w}t - \hat{\delta}_{\bar{w}})\right] \quad \text{(C-20)}$$

Expanding Equations C-19 and C-20, results in Equations C-21 and C-22.

$$D_{NL}^{*\prime} = D_0 \Delta g_0 + fh\sigma_0^2\left|\hat{D}\right|_{\bar{w}}\left[\cos(\bar{w}t)\cos(\hat{\delta}_{\bar{w}}) - \sin(\bar{w}t)\sin(\hat{\delta}_{\bar{w}})\right] \quad \text{(C-21)}$$

$$D_{NL}^{*\prime\prime} = -fh\sigma_0^2\left|\hat{D}\right|_{\bar{w}}\left[\sin(\bar{w}t)\cos(\hat{\delta}_{\bar{w}}) - \cos(\bar{w}t)\sin(\hat{\delta}_{\bar{w}})\right] \quad \text{(C-22)}$$

Knowing that at peak, $t = \frac{1}{2}T = \frac{1}{2f} = \frac{2\pi}{2w} = \frac{2\pi}{\bar{w}}$, Equations C-21 and C-22 can be rewritten as Equations C-23 and C-24.

$$D_{NL}^{*\prime} = D_0 \Delta g_0 + fh\sigma_0^2\left|\hat{D}\right|_{\bar{w}}\left[\cos(\hat{\delta}_{\bar{w}})\right] \quad \text{(C-23)}$$

$$D_{NL}^{*\,''} = fh\sigma_0^2 \left|\hat{D}\right|_{\bar{w}} \left[sin(\hat{\delta}_{\bar{w}})\right] \tag{C-24}$$

Equations C-23 and C-24 can also be rewritten as Equations C-25 and C-26.

$$D_{NL}^{*\,'} = D_0 \Delta g_0 + fh\sigma_0^2 \left|\hat{D}\right|_{\bar{w}}^{'} \tag{C-25}$$

$$D_{NL}^{*\,''} = fh\sigma_0^2 \left|\hat{D}\right|_{\bar{w}}^{''} \tag{C-26}$$

Equations C-25 and C-26, together with Equations C-6 and C-7, results in Equation C-27.

$$\Delta\varepsilon = D_0 \Delta g_0 \Delta\sigma + \Delta g_1 \Delta g_2 \Delta\sigma(\hat{D}' + i\hat{D}'') \tag{C-27}$$

where, $\hat{D}'$ is the stored part of the transient component of the creep compliance, and $\hat{D}''$ is the dissipated one. $\hat{D}'$ and $\hat{D}''$ can be defined using Equations C-28 and C-29.

$$\left|D^*\right|_{LVE} cos\,\delta_{LVE} = D_0 + \hat{D}_{LVE}^* cos\,\hat{\delta}_{LVE} = D_0 + \hat{D}' \tag{C-28}$$

$$\left|D^*\right|_{LVE} sin\,\delta_{LVE} = \hat{D}_{LVE}^* sin\,\hat{\delta}_{LVE} = \hat{D}'' \tag{C-29}$$

where, the subscript LVE stands for the property found on the linear viscoelastic (LVE) region (using low strain/stress amplitudes), and $\hat{\delta}$ is the phase angle between the dissipated and stored parts of the transient creep compliance.

Considering that creep compliance can be represented by Equation C-30, equating expressions C-27 and C-30 and separating real and imaginary parts, we have Equations C-31 and C-32 for controlled-stress analysis.

$$D^* = \frac{\Delta\varepsilon}{\Delta\sigma} = \frac{\varepsilon_0}{\sigma_0}\cos\delta + i\frac{\varepsilon_0}{\sigma_0}\sin\delta \quad \text{(C-30)}$$

where, ε_0, σ_0, and δ are strain, stress amplitude and phase angle, respectively.

$$\frac{\varepsilon_0}{\sigma_0}\cos\delta = D_0(\Delta g_0) + (\Delta g_1)(\Delta g_2)\hat{D}' \quad \text{(C-31)}$$

$$\frac{\varepsilon_0}{\sigma_0}\sin\delta = (\Delta g_1)(\Delta g_2)\hat{D}'' \quad \text{(C-32)}$$

Δg_1 and Δg_2 are functions of stress representing the nonlinear response. Damage causes change in response with repeated loading at a given stress amplitude. In order to add damage analysis, a damage parameter was considered (V). Equations C-31 and C-32 can be rewritten as Equations C-33 and C-34. If no damage occurs (linear or nonlinear viscoelastic behaviors only), damage parameter (V) should be equal to one, and Equations C-31 and C-32 will be equal to Equations C-33 and C-34.

$$\frac{\varepsilon_0}{\sigma_0}\cos\delta = D_0(\Delta g_0) + (\Delta g_1)(\Delta g_2)(V)\hat{D}' \quad \text{(C-33)}$$

$$\frac{\varepsilon_0}{\sigma_0}\sin\delta = (\Delta g_1)(\Delta g_2)(V)\hat{D}'' \quad \text{(C-34)}$$

2. PROTOCOL

- Conduct time sweep fatigue tests using a low stress amplitude (for the linear viscoelastic region) and determine $\hat{D}'$ and $\hat{D}''$ in Equations C-28 and C-29;

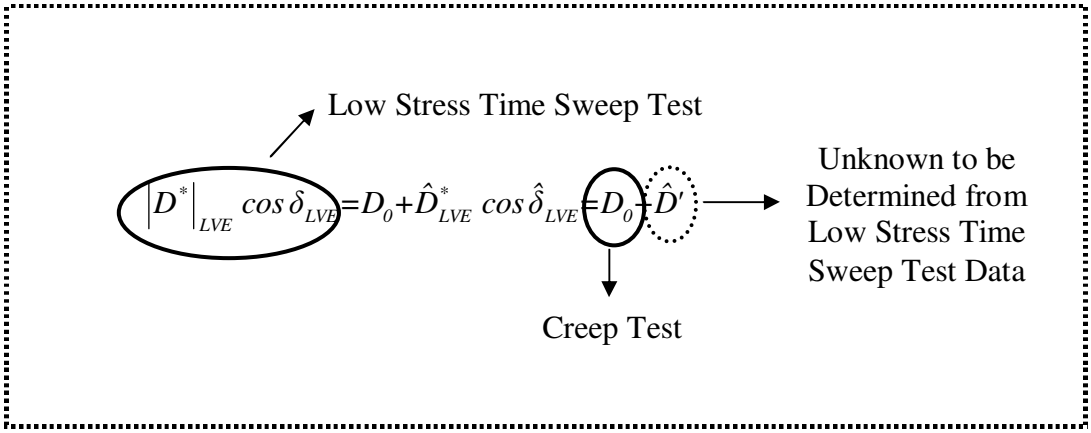

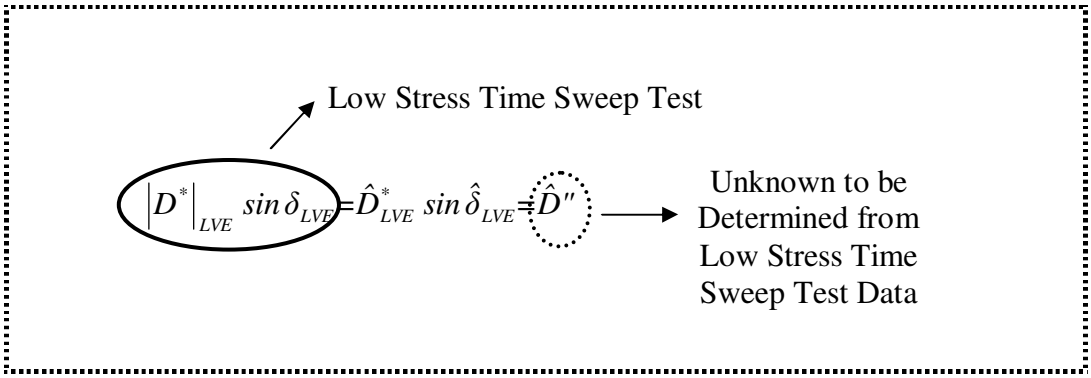

- Conduct time sweep tests at the threshold stress amplitude and determine D^* and δ for the same frequency (10 Hz);

- Calculate $\Delta g_1 \Delta g_2$ using Equations C-31 and C-32. Note that these nonlinear viscoelastic parameters will have two parts: stored and dissipated;

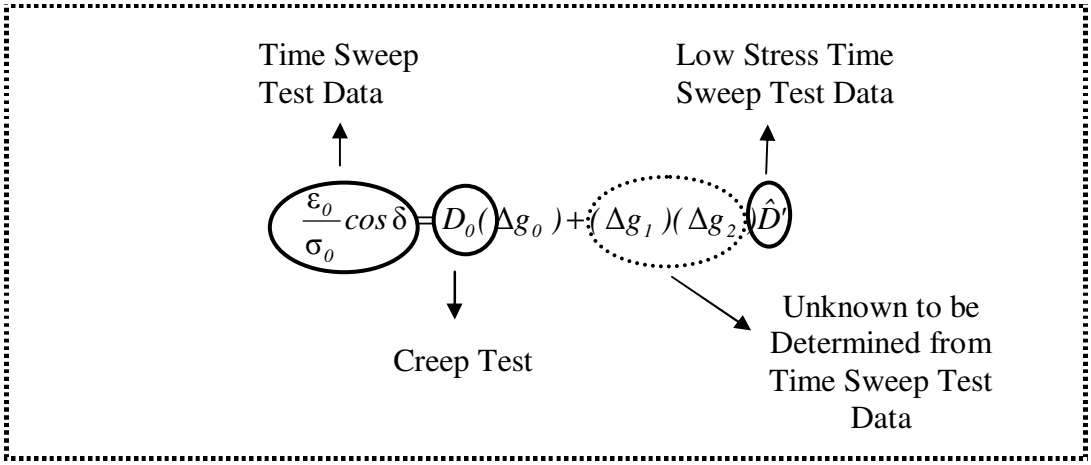

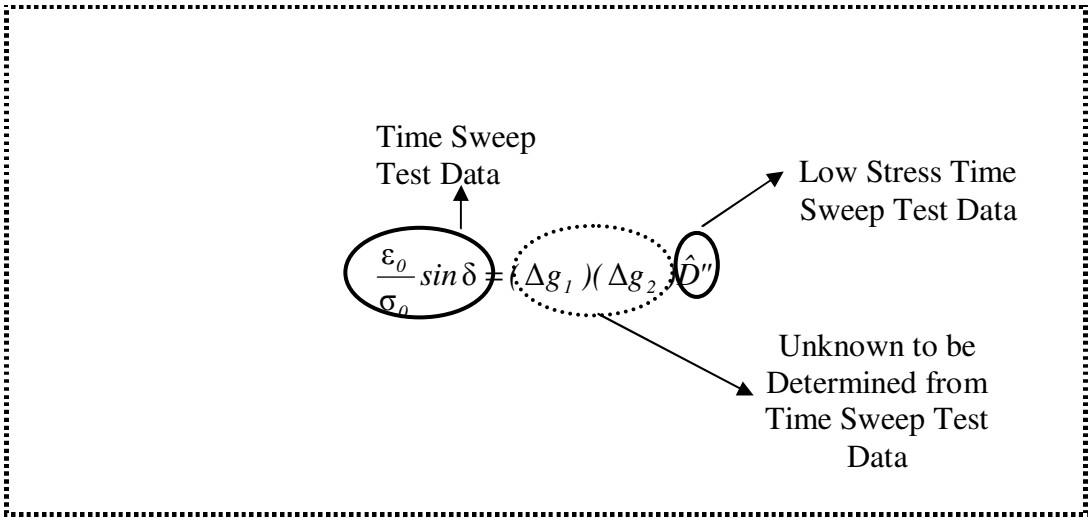

* A single value for the stress dependent nonlinear viscoelastic parameter ($\Delta g_1 \Delta g_2$) can be found minimizing the difference between the shear compliance in the constitutive model and the experimental measurements using the following error function:

$$ERR = \left(\frac{D'_{model}}{D'_{experimental}} - 1 \right)^2 + \left(\frac{D''_{model}}{D''_{experimental}} - 1 \right)^2 \quad \text{(C-35)}$$

- Conduct high stress time sweep fatigue tests using the same frequency (10 Hz), and determine D^* and δ versus time;

- Calculate V versus time using Equations C-33 and C-34. V will have two parts each: stored and dissipated.

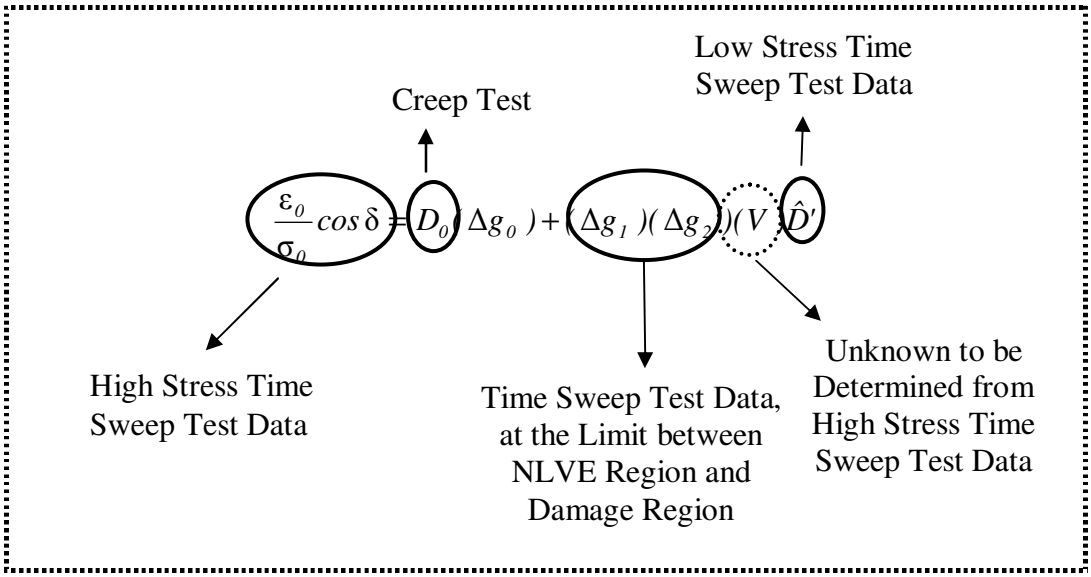

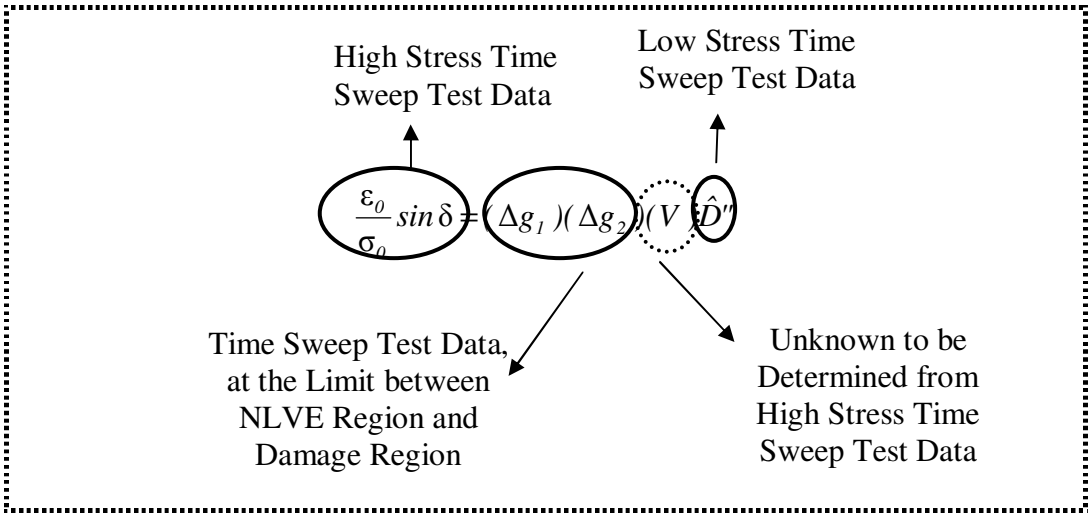

NOTE: this protocol was developed for controlled-stress tests, but the same approach can be used for controlled-strain.

VITA

Name: Veronica Teixeira Franco Castelo Branco

Address: 601A CE/TTI Building, TAMU 3135
Texas A&M University, TX 77843-3135

Email Address: vcastelobranco@hotmail.com

Education: B.A., Civil Engineering, Federal University of Ceará, Brazil, 2002
M.S., Civil Engineering, Federal University of Rio de Janeiro, Brazil, 2004
Ph.D., Civil Engineering, Texas A&M University, U.S., 2008

Work History: 2004 – Current
Graduate Research Assistant, Texas Transportation Institute (TTI), College Station, Texas, U.S.

2002 – 2004
Research Assistant, Laboratory of Pavements and Asphalt Mixtures, Federal University of Rio de Janeiro
Rio de Janeiro, Rio de Janeiro, Brazil

1999 – 2002
Research Assistant, Laboratory of Pavements Mechanics (LMP)
Federal University of Ceará
Fortaleza, Ceará, Brazil